School of Applied Geology

Some causes and consequences of lithospheric thinning in the eastern North China Craton: evidence from latest Yanshanian granitoids and dykes

Sarah Catherine Goss

This thesis is presented for the Degree of Master of Philosophy
of Curtin University of Technology

March 2010

DECLARATION

To the best of my knowledge and belief this thesis contains no material previously published by any other person except where due acknowledgment has been made. This thesis contains no material which has been accepted for the award of any other degree or diploma in any university.

Sarah Catherine Goss

31st March 2010

STATEMENT OF CONTRIBUTION OF OTHERS

Statement of contribution from my supervisor and co-author Professor Simon Wilde:

Curtin University

Faculty of Science
And Engineering

Department of Applied Geology

Telephone +61 8 9266 3580
Facsimile +61 8 9266 3153
Email s.wilde@curtin.edu.au

To Whom It May Concern

I wish to state that my contribution to the MPhil Thesis of **Sarah Catherine GOSS** titled "Some Causes and Consequences of Lithospheric Thinning in the Eastern North China Craton: evidence from latest Yanshanian Granitoids and Dykes " and the two papers that have resulted from this work, was as follows:

I formulated the project in consultation with the Student, arranged with colleagues at the Institute of Geology and Geophysics, Chinese Academy of Sciences, Beijing, China, to provide the field logistics and I attended the field trip where the samples were collected. Following this, my involvement was that normally expected of a Supervisor, i.e. throughout the project, I discussed the various issues with the Student and provided guidance as to what was required to successfully complete the project. However, the Student is entirely responsible for the results, interpretations and conclusions that were reached in the Thesis and presented in the two papers.

Sincerely,

Prof. Simon A. Wilde
Supervisor
Department of Applied Geology
CURTIN UNIVERSITY

STATEMENT OF CONTRIBUTION OF OTHERS

Statement of contribution from my co-supervisor and co-author Professor Fuyuan Wu:

CHINESE ACADEMY OF SCIENCES
Institute of Geology and Geophysics

Augest 2, 2010

To Whom It May Concern

I wish to state that my contribution to the MPhil Thesis of **Sarah Catherine GOSS** titled "Some Causes and Consequences of Lithospheric Thinning in the Eastern North China Craton: evidence from latest Yanshanian Granitoids and Dykes" and the two papers that have resulted from this work, was as follows:

I organized and took part in the initial fieldwork where the samples were collected for this project. I arranged for the Lu-Hf analyses to be undertaken at the Institute of Geology and Geophysics, Chinese Academy of Sciences, Beijing, China and monitored their quality. I had the opportunity for input into the discussion of the meaning of these results and into the final draft of the paper forwarded to *Lithos*. However, the Student is entirely responsible for the interpretation and conclusions, as presented in the Thesis and papers.

Sincerely,

Prof. Fuyuan Wu

Deputy Director
Institute of Geology and Geophysics
Chinese Academy of Sciences
Beituchengxilu 19, P. O. Box 9825, Beijing 100029, China
Tel: 86-10-82998217
Fax: 86-10-62010846
Mail: wufuyuan@mail.iggcas.ac.cn

STATEMENT OF CONTRIBUTION OF OTHERS

Statement of contribution from co-author Professor Jinhui Yang:

INSTITUTE OF GEOLOGY AND GEOPHYSICS, CHINESE ACADEMY OF SCIENCES
中国科学院地质与地球物理研究所

P.O. BOX 9825, BEIJING, 100029, CHINA
Tel.: +86-10-82998001, Fax: +86-10-62010846

To Whom It May Concern

I wish to state that my contribution to the MPhil Thesis of **Sarah Catherine GOSS** titled ""Some Causes and Consequences of Lithospheric Thinning in the Eastern North China Craton: evidence from latest Yanshanian Granitoids and Dykes" " and the two papers that have resulted from this work, was as follows.

I arranged for the geochemical analyses to be undertaken at the Institute of Geology and Geophysics, Chinese Academy of Sciences, Beijing, China and supervised their quality. I was able to have input into the discussion of the meaning of these results, but the Student is solely responsible for the conclusions as presented in the Thesis and subsequent papers.

Sincerely,

Jin-hui Yang

Prof. Jin-Hui Yang

State Key Laboratory of Lithospheric Evolution
Institute of Geology and Geophysics
Chinese Academy of Sciences
P.O. Box 9825, Beijing 100029
CHINA
Tel.: +86-10-82998510
Fax: +86-10-62010846
E-mail: jinhui@mail.igcas.ac.cn

Date: Aug. 02, 2010

TABLE OF CONTENTS

ACKNOWLEDGMENTS

This thesis could not have been completed without the support of the following organisations and individuals.

I would firstly like to thank the Department of Employment, Education and Training of Australia for their financial support in awarding me an International Postgraduate Research Scholarship (IPRS) and for Curtin University of Technology for awarding me a Curtin University Postgraduate Scholarship (CUPS). Without this financial aid none of this research would have been possible.

Field and logistical support for my project was kindly provided by the Institute of Geology and Geophysics Chinese Academy of Sciences in Beijing. I would like to thank Professor Fuyuan Wu for providing additional supervision over the duration of my research and for his expert organisation of my field work whilst I was in China.

My supervisor, Professor Simon Wilde is also to be thanked for his supervision and constructive comments over the course of my thesis. He provided me with tireless advice and thoughtful discussions.

I would also like to thank Yanbin Zhang for kindly undertaking some of the geochemical analyses associated with my research. Also Dr. Michael Wingate for his help with SHRIMP operation and performance, as well as his general support. I would also like to mention my immense gratitude to Professor Peter Cawood for all the support, encouragement and opportunities he has provided me with over the last 5 years.

Last but not least I am indebted to my mum who consistently supported me and encouraged me throughout my studies, I would not be where I am today without her love and understanding.

ABSTRACT

The lithosphere beneath the eastern part of the North China Craton (NCC) is known to have been thick (> 200 km) during the Early Palaeozoic as manifested by the presence of diamondiferous kimberlites (Menzies et al., 1993; Griffin et al., 1998; Yang et al., 2009). However, in the Cenozoic we know it was much thinner (75-80 km) as implied by the presence of spinel-facies xenoliths in the alkali basalts, as well as evidence from geophysical investigations such as seismic data and heat flow measurements (Yuan, 1996; Menzies and Xu, 1998; Gao et al., 2002; Zhou et al., 2002; Wu et al., 2005b; Yang et al., 2009). This has lead to the assumption that at some stage during the Mesozoic, part or all, of the lithospheric mantle keel was thinned or lost (Menzies et al., 1993; Wilde et al., 2003; Gao et al., 2004; Wu et al., 2005a; Liu et al., 2008d).

The exact timing and mechanism of this thinning has been a hot topic of research for some time and there is still ongoing debate. By analysing key rock units in Shandong Province in the eastern part of the NCC, this research thesis aims to establish a more accurate temporal history of the area, including how the nature and composition of the lithospheric mantle evolved during the Mesozoic. The emphasis has been on determining the differences in the geochemical signatures of selected magmatic rocks to determine the state of the lithospheric mantle at various times and depths. The granitoids that form Paper 1 (Chapter 2) were chosen because they were thought to be the youngest Late Yanshanian intrusions in the area (SBGMR, 1991; Zhao et al., 1998b; Zhou and Lu, 2000) and would provide information about the nature of the lower crust and mantle in the Early Cretaceous. The felsic, intermediate, mafic and lamprophyric dykes of Paper 2 (Chapter 3) were selected with the aim of determining if there was a spatial or temporal pattern in lithospheric evolution across the region that could be related to a distinct mechanism of thinning.

Based on the research carried out in this thesis it is confirmed that the granitoids selected are indeed younger than the more typical Late Yanshanian granitoids. The ages of the sampled intrusions range from 118 ± 1 Ma to 113 ± 2 Ma

and they represent a continuation of the extensional regime in the Early Cretaceous. The geochemistry of the granitoids suggest that they were derived from partial melting of older continental crust due to mafic magma underplating, followed by various degrees of interaction between mantle-derived mafic magma and felsic crustal magma. The dykes range in age from 114 ± 1 Ma to 105 ± 2 Ma. The geochemistry of the dykes suggests that the lithospheric mantle beneath the eastern NCC had an enriched nature during their intrusion in the Early Cretaceous. The generation of both these magmatic rock groups provide evidence of asthenospheric upwelling, lithospheric extension and interaction between the crust and mantle during the Mesozoic.

A model to explain the genesis of both the granitoids and the dykes, also consistent with the various Mesozoic tectonic events, has been developed. The conclusion is that subduction of the Pacific Plate beneath the eastern NCC, followed by slab roll-back, was the dominant driving force that led to extension, lithospheric thinning and delamination. These in turn resulted in asthenospheric upwelling and generation of basaltic magmas that were either emplaced into the lower crust as dykes (Paper 2/Chapter 3), or were underplated beneath the crust, causing partial melting and generation of the granitoids (Paper 1/Chapter 2).

The delamination of the NCC lithosphere during the Cretaceous can explain how the whole of eastern Asia, including the eastern and central NCC, the South China Craton (SCC) and the Central Asian Orogenic Belt (CAOB), were affected by extension, widespread magmatic activity and lithospheric thinning at this time (Zhou and Li, 2000; Fan et al., 2003; Zhang et al., 2003d; Wu et al., 2005a).

ORGANISATION OF THESIS

This thesis has been organised as a set of scholarly papers that have, or will be submitted to relevant international journals for publication. One paper has been submitted and is currently under review, the other will be submitted shortly. I have been the first author on both of these papers and, as stated in the declaration and statement of contribution of others, I have done the majority of the work necessary to produce them including the sample collection, geochronological and geochemical data collection, data-processing and finally the interpretation of the results.

I must also add that due to the nature of paper publishing there is some overlap and repetition between the papers, especially when defining the regional setting and background, however each of the papers has original data and provides a different contribution to the overall understanding of the problem.

Chapter 1 contains a general introduction and overview of how the research was conducted. It begins with a background section that is only a brief introduction, since much of the specific background information is already covered in the two papers forming Chapters 2 and 3. It also describes the objectives and aims of the research. It has a section on methodologies associated with the thesis; this is brief to avoid unnecessary repetition of procedures that are already described in the papers (Chapters 2 and 3). It does however provide some additional details that were not suitable for inclusion in the papers.

Chapter 2 consists of Paper 1 *The age, isotopic signature and significance of the youngest Mesozoic granitoids in Shandong Province, North China Craton* sent to Lithos (impact factor 3.303). This presents an introduction to the study area of Shandong Province which is located on the easternmost edge of the Eastern Block of the North China Craton (NCC). It also presents the problem of lithospheric thinning in NE China and the various theories proposed to explain this. It furthermore focuses on a more detailed study of the granitic rocks in the study area and what they can help clarify. The granitoids studied are interpreted to be evidence of the youngest Late Yanshanian magmatism in NE China and include the first precise U-Pb zircon

ages for these rocks, which are discussed along with their geochemical nature and significance. This is related to the larger issue of lithospheric thinning and delamination in NE China during the Late Mesozoic.

Chapter 3 consists of Paper 2 *The geochronology and geochemistry of Early Cretaceous dykes from the Jiaodong Peninsula, North China Craton*. This follows on from Chapter 2 in attempting to further clarify the nature of the lithospheric mantle beneath NE China during the time when lithospheric thinning and delamination is thought to have taken place. It discusses the role of intrusive dykes of similar age, but of varying composition and source, might have in enabling changes in the crust/mantle structure and lithospheric mantle composition to be deciphered. This in turn is again related to the regional issue of lithospheric thinning and delamination.

Chapter 4 is a short section proposing/summarising a comprehensive regional tectonic model that is consistent with the data available and based on the new geochronological and geochemical data presented in this thesis.

LIST OF PUBLICATIONS INCLUDED AS PART OF THIS THESIS

1) Goss, S.C., Wilde, S.A., Wu, F. and Yang, J., 2010. The age, isotopic signature and significance of the youngest Mesozoic granitoids in Shandong Province, North China Craton.

(has been submitted to Lithos and is currently in review)

2) Goss, S.C., Wilde, S.A., Zhang, X., Wu, F. and Yang, J., 2010. The geochronology and geochemistry of Early Cretaceous dykes from the Jiaodong Peninsula, North China Craton.

(currently being prepared for submission to Gondwana Research)

I warrant that I have obtained, where necessary, permission from the copyright owners to use any third-party copyright material reproduced in the thesis (e.g. questionnaires, artwork, unpublished letters), or to use any of my own published work (e.g. journal articles) in which the copyright is held by another party (e.g. publisher, co-author).

Sarah Catherine Goss

CHAPTER 1

1.1 BACKGROUND AND OBJECTIVES

Currently, one of the most perplexing problems in global geology is why the eastern part of the North China Craton (NCC) lost all, or part of its lithospheric mantle keel in the Mesozoic. It is unique amongst Archean cratons in showing this phenomenon since typical features of Archean cratons are that they (Kusky et al., 2007; Menzies et al., 2007):

- are geologically stable experiencing a lack of substantial tectonic or volcanic activity for the last 2500 Ma
- have thick lithospheric keels (~200 km thick) that extend into the garnet or diamond stability fields
- have low surface heat flow (~40 mW/m^2)
- have a refractory (Mg-rich and Fe-poor) sub-continental lithospheric mantle (SCLM) making them physically buoyant
- are in isostatic equilibrium
- are underlain by regions of fast P and S wave velocities that extend to 200-250 km

The evidence that this is not the case for the eastern NCC and that it has undergone reactivation since the Mesozoic includes; the presence of spinel-facies xenoliths in alkali basalts erupted in the Cenozoic (Xu, 2001; Zhou et al., 2002; Rudnick et al., 2004; Menzies et al., 2007), high heat flow data (Menzies and Xu, 1998; Menzies et al., 2007), a thin crust and lithosphere revealed through seismic data and tomographic models (Fig. 1.1) (Yuan, 1996; Menzies et al., 2007) and Re-Os isotopic systematics that show a hybrid Proterozoic and Phanerozoic lithospheric mantle signature beneath the eastern NCC (Gao et al., 2002). This is alongside the evidence of widespread tectonic activity (both compressional and extensional) and magmatism that has occurred since the Mesozoic. This large-scale tectonic activity in

the NCC during the Mesozoic was first recognised by Wong (1927) and he proposed the name of 'Yanshanian Orogeny' for these events that began in the Jurassic and extended to the Cretaceous.

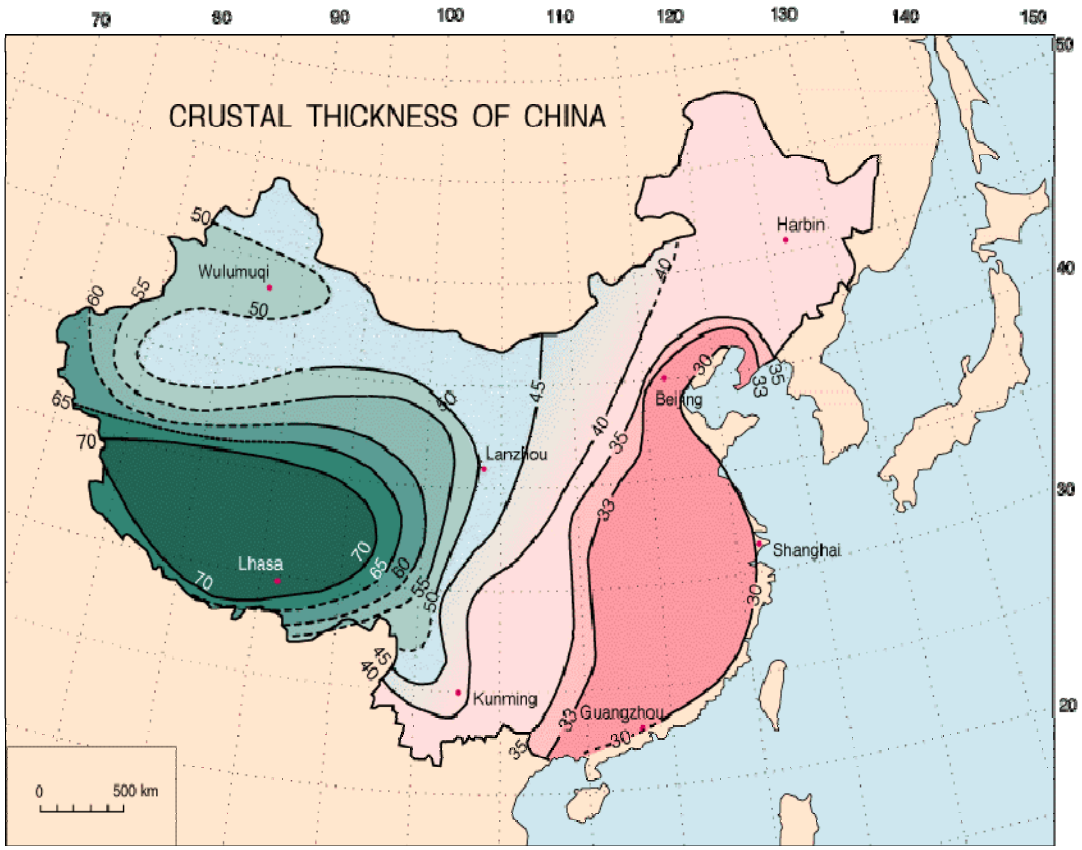

FIG. 1.1 Map of China reproduced from the United States Geological Society (USGS) showing the crustal thickness (in km). Data were obtained primarily from seismic refraction/wide-angel reflection experiments. Thick crust is displayed in green shades (to the west), and thin crust is displayed in pink shades (to the east). Solid isolines represent more reliable results while dashed lines were obtained from gravity data only.

A diverse range of suggestions has been proposed to explain lithospheric thinning and reactivation of the eastern NCC, but none of them are entirely satisfactory. In order for lithospheric thinning to take place there needs to be something that either increases the density of the SCLM to enable it to overcome its natural buoyancy and sink through the underlying asthenosphere, or there needs to be a change in the rheology or composition of the lithosphere allowing it to be removed.

Some of the mechanisms suggested include 1) thermal and chemical erosion such as hydration, or eclogisation (Griffin et al., 1998; Menzies and Xu, 1998; Xu, 2001; Zhang et al., 2004; Zhang et al., 2004a; Xu et al., 2004b; Niu, 2005; Zhang, 2005), 2) complete delamination (Zhang et al., 1998; Zhou et al., 2002), 3) partial delamination (O'Reilly et al., 2001; Wilde et al., 2003) and 4) decompressional melting (Gao et al., 1998). It is difficult to determine which of these mechanisms is involved, if it was a combination of more than one of these, or if in fact it was an entirely different mechanism.

The overall tectonic driving force for lithospheric thinning and widespread magmatic activity is likewise unknown. It has been variously linked to a) collision of the North and South China cratons (Gao et al., 1998; Yang et al., 2007a; Yang et al., 2007b), b) Pacific Ocean plate subduction (Tatsumoto et al., 1992; Fan et al., 2000; Yang et al., 2003; Wu et al., 2005a; Xu, 2007; Yang et al., 2007c), c) collision between India and Eurasia (Menzies et al., 1993), or d) a mantle plume (Deng et al., 2004).

It is the overall objective of my research to test which, if any, of these explanations for the tectonic driving force of lithospheric thinning and magmatic activity is viable. The timing of the lithospheric thinning/loss is equally controversial (Yang et al., 2003; Niu, 2005; Menzies et al., 2007) and another aim of my research was to better constrain the changes in the lithosphere to see how it evolved and changed during the Mesozoic.

My research focuses on the magmatic intrusions in the study area with the aim of using their geochemical signatures and the new precise SHRIMP U-Pb age data, to determine the state of the lithospheric mantle and lower crust during the Early Cretaceous. This is ultimately with the intention of producing a tectonic model consistent with the new geochronological and geochemical data presented as part of this thesis and that would help to clarify the geological problems described

1.2 RESEARCH DESIGN AND METHODOLOGY

The work presented in this thesis is the result of one field season of sample collection in Shandong Province in NE China. This area was specifically chosen since it contains examples of all the features that have previously been identified as reflecting lithospheric loss. For example there are Ordovician kimberlites (containing evidence of thick lithosphere) and Cenozoic alkali basalts (containing evidence of thinner lithosphere) juxtaposed together and the whole area has undergone widespread Mesozoic igneous activity. Also, seismic profiling has been undertaken here and there is evidence of changes in heat flow in the underlying mantle. Furthermore, there is evidence of uplift and later extensional basin development (Li and Mooney, 1998), strong deformation (Zhang et al., 1998; Zheng et al., 1998) and gold mineralisation (Yang et al., 2003). So information about the changes in the mantle lithosphere over time can be established.

The samples forming Paper 1 (granitoids) were selected because they were previously reported to have been younger than the surrounding Late Yanshanian granitoid intrusions dated at ~130-120 Ma (SBGMR, 1991; Zhao et al., 1998b; Zhou and Lu, 2000), although precise ages using SHRIMP U-Pb were rarely reported. The aim was to test this hypothesis and produce some precise SHRIMP U-Pb age data for the rocks. The ion microprobe U-Pb zircon dating technique has not been extensively applied to key rocks in the study area, the more common technique used had been K-Ar, Ar-Ar, or Rb-Sr methods, which do not necessarily date the actual time of emplacement.

The dykes studied as part of Paper 2 have their origins within the mantle, so they enable a ‘sample’ of the lithospheric mantle to be obtained for where and when they were intruded. The specific samples were selected in an attempt to cover before (pre-), during (syn-) and after (post-) delamination events and to determine if there was a spatial pattern in the lithospheric thinning across the region, however unfortunately due to the lack of zircons in some samples, this did not end up being possible. Instead, selected dykes of similar age, but differing compositions and

source, were analyzed in order to reveal the structure of the crust/mantle during the Cretaceous.

All samples were crushed and the ensuing powders subjected to state-of-the-art isotope systematic analytical techniques including:

a) Sensitive High-Resolution Ion Microprobe (SHRIMP II) U-Pb analyses of individual zircons
b) Lu-Hf isotopic analyses using a MC-ICP-MS on the identical sites that were analysed using the SHRIMP II
c) Precise total element whole-rock geochemical analyses. Major elements were determined using X-ray fluorescence spectrometry (XRF) and the trace element and REE concentrations were determined using ICP-MS

Furthermore, selective samples were prepared for polished thin section to allow detailed petrographic descriptions to be complied and the modal abundance of minerals was established by point counting using a Leitz microscope and a Swift point counter.

1.2.1 SHRIMP zircon U-Pb methodology and technique

The mineral zircon ($ZrSiO_2$) is very good to use for dating rocks because of its chemical and physical stability under extreme crustal conditions. The theory behind radiometric dating is that during crystallization of the zircon, radiogenic U and Th are incorporated into the crystal lattice and then they slowly decay to Pb at a known rate. Measurement of the parent isotopes (^{238}U, ^{235}U and ^{232}Th) and the stable daughter products (^{206}Pb, ^{207}Pb and ^{208}Pb respectively), along with knowledge of the half lives of the isotopes, means the time since the zircon crystal formed can be calculated. This in turn can be used to infer the age of the rock in which the zircon has been found.

There are certain events that can alter this result and "reset" the apparent age of the zircon by causing Pb loss/gain or U loss/gain; these include metamorphism, diffusion within the crystal, or recrystallization, however in general zircon U-Pb dating is considered one of the most precise dating methods available.

The methodology followed for preparing the mounts for analysis was as described in both papers (Chapters 2 and 3). The technique for overall operation of the Sensitive High-Resolution Ion Microprobe (SHRIMP II) data acquisition was as outlined in Williams (1998) and the Curtin University zircon standard CZ3 with a known U concentration of 551 ppm and conventionally-measured $^{206}Pb/^{238}U$ age of 564 Ma (Nelson, 1997) was used. The procedure was undertaken using one of the SHRIMP II machines at Curtin University of Technology, Perth. Specific operating conditions used to obtain the data for this thesis are described below.

Each spot on the zircon crystal was firstly rastered for an average of 2.5 minutes over an area of ~120 μm so that any common Pb or contamination from the gold coat was removed before analysis began. Typically each spot size was ~25 μm in diameter. Each analysis consisted of 6 scans through the run table shown below (Table 1.1) for each spot analysed. The standard CZ3 was analysed after every 3 unknowns.

TABLE 1.1 The run table used during SHRIMP U-Pb analysis for all samples in this research.

Name	Time counted (secs)	Auto centre
Zr_2O	2.0	Yes
^{204}Pb	10.0	No
Background Pb	10.0	No
^{206}Pb	20.0	Yes
^{207}Pb	30.0	No
^{208}Pb	10.0	No
^{238}U	5.0	Yes
^{248}ThO	5.0	No
^{254}UO	2.0	Yes

The counts on ^{207}Pb were for 30 seconds (i.e. longer than normal) because the count rates are typically low on younger rocks. The ^{206}Pb/^{238}U age is quoted here because the zircons are <1 Ga so the ^{207}Pb/^{206}Pb age is less sensitive or reliable, due to the low counts on ^{207}Pb.

The raw data obtained from the SHRIMP sessions were later processed using the SQUID program designed by Ludwig (2001a) and then ISOPLOT (Ludwig, 2001b) was used to plot the Concordia diagrams. The measured ^{204}Pb was used to correct the data based on the isotopic composition of Broken Hill lead.

1.2.2 MC-ICP-MS methodology and technique

A Neptune MC-ICP-MS equipped with a 193 nm UV laser was used to collect in situ zircon Lu-Hf isotopic analyses from the granitoid samples discussed in Chapter 2 (Paper 1). The analyses were undertaken at the Institute of Geology and Geophysics at the Chinese Academy of Sciences in Beijing, China. The sites on the zircon targeted were the identical sites that had been dated using the SHRIMP II. The methodology for techniques and operating conditions are described in Chapter 2 (Paper 1) and were as described in Xu et al. (2004c) and Wu et al. (2006), so will not be repeated again here. The $^{176}Hf/^{177}Hf$ and $^{176}Lu/^{177}Hf$ ratios of the standard zircon (CZ3) were used during analysis.

The ^{176}Lu decay constant from Soderlund et al. (2004) of $1.867x10^{-11}yr^{-1}$ was used to calculate the initial $^{176}Hf/^{177}Hf$ ratios. In this thesis, the T_{DM2} model ages from the analytical results were used for discussion, they represent two-stage model ages and were calculated by projecting back the initial $^{176}Hf/^{177}Hf$ of the zircon to the depleted mantle model growth curve assuming a mean $^{176}Lu/^{177}Hf$ value of 0.015 for the average continental crust (Griffin et al., 2002).

1.2.3 Geochemistry methodology

The methodology followed to prepare the rock samples for analysis was as described in both papers (Chapters 2 and 3) and the whole-rock powders were analyzed for major and trace elements at the Institute of Geology and Geophysics at the Chinese Academy of Sciences in Beijing, China.

Major element analysis was conducted using X-ray fluorescence spectrometry (XRF) following the technique of Lee (1997) and the trace element and REE concentrations were determined using ICP-MS following the solution method outlined by Yuan (2004). The USGS international standards used to calibrate trace element concentrations were AGV-1 and G-2.

The normative mineralogy of the samples was calculated from the raw data using the CIPW norm program of Kurt Hollocher, Geology Department, Union College, Schenectady, NY, 12308. The FeO and Fe_2O_3 concentrations of the samples were calculated from the total FeO raw data using the iron oxidation graph in Middlemost (1985) that was adapted from Le Maitre (1976).

1.2.4. Point counting methodology

Point counting to enable detailed petrographic descriptions of selective samples was completed using a Leitz microscope and a Swift point counter. Three thin sections of each sample were prepared and the number of counts for each mineral found were recorded from approximately 2000 equally-spaced points on each of the slides, giving a total of ~6000 points for each sample. The results of this were also used to establish the modal mineralogy.

CHAPTER 2

2.1 PAPER 1

The age, isotopic signature and significance of the youngest Mesozoic granitoids in Shandong Province, North China Craton

Sarah C. Goss[1], Simon A. Wilde[1], Fuyuan Wu[2] and Jinhui Yang[2]

[1]Department of Applied Geology, Curtin University of Technology, PO Box U1987, Perth, Western Australia 6845

[2]Institute of Geology and Geophysics, Chinese Academy of Sciences, PO Box 9825, Beijing 100029, China

Abstract

Most Cretaceous granitoids in Shandong Province, North China Craton, were typically intruded between ~130-122 Ma. However, four granitoid batholiths are younger with an average emplacement age of 116 Ma. Zircon U-Pb SHRIMP data define the emplacement ages as follows; Sanfoshan Batholith 118 ± 1 Ma, Aishan Batholith 116 ± 1 Ma, Yashan Pluton 113 ± 2 Ma and Laoshan Batholith 115 ± 2 Ma. They all contain inherited zircons with ages of ~125-120 Ma indicating interaction with previously intruded granitoids. All the samples studied are I-type granitoids with a metaluminous geochemical signature and are enriched in light rare earth elements and depleted in high-field strength elements. Paleo- to Neoarchean T_{DM2} model ages (ranging from 3900 Ma to 2491 Ma) and negative $\varepsilon_{Hf(t)}$ values imply the involvement of Archean basement and older recycled continental crustal material in the magma source region. They were likely derived from partial melting of the lower or middle crust due to mafic magma underplating followed by various degrees of interaction between mantle-derived mafic magma and felsic crustal magma and fractional crystallization. Since these granitoids post-date the proposed

delamination event in the NCC, their geochemistry provides information about the nature of the lower crust at ~116 Ma. We propose that lithospheric thinning and extension due to subduction of the Pacific Plate beneath the eastern North China Craton led to asthenospheric upwelling and basaltic magmatism. This underplating in turn led to crustal melting and the granitic intrusions described here.

Keywords: North China Craton; latest Yanshanian granitoids; SHRIMP zircon U-Pb dating; Delamination; Lithospheric thinning; Pacific Plate subduction

1. Introduction

The North China Craton (NCC) is the oldest tectonic unit in China and it contains some of the oldest rocks in the world (Liu et al., 1992; Liu et al., 2008b). It is bounded by the early Paleozoic Qilianshan orogen to the west, the Central Asian Orogenic Belt (CAOB) to the north, the Sulu ultrahigh-pressure (UHP) metamorphic belt to the east and the Mesozoic Qinling-Dabieshan metamorphic belt to the south. The Sulu belt was originally part of the Qinling-Dabieshan belt, but has been subsequently transported ~500 km northeast along the Tanlu Fault (Ames et al., 1993; Xu and Zhu, 1994; Chen et al., 2003a; Zhou et al., 2008a) (Fig. 2.1).

The basement of the NCC is divided into three main blocks; the Western Block, the Trans-North China Orogen (TNCO) and the Eastern Block (Zhao et al., 2001) (Fig. 2.1). The TNCO formed due to continent-continent collision between the Eastern and Western Blocks and this led to the amalgamation and cratonization of the NCC. There is some debate as to when exactly the collision occurred, with two main views expressed; i.e. 2.5 Ga (Gao et al., 2002; Kusky and Li, 2003; Kusky et al., 2007) or ~1.8 Ga (Wilde et al., 2003; Zhao et al., 2005; Wu et al., 2005b). Recently a third view has been proposed suggesting that there were in fact two events, one at 2.1 Ga which was a “soft” collision (possibly an arc collision) and the other at 1.8 Ga as the final “hard” collision (Trap et al., 2008; Wang, 2009).

The Western Block is separated into two smaller blocks by the Khondalite Belt, with the Ordos Block to the south and the Yinshan Block to the north (Zhao et al., 2005; Zhao et al., 2006; Santosh et al., 2007). The timing of this collision was prior to the amalgamation of the Eastern and Western Blocks (Zhao et al., 2005) and recent work by Santosh et al. (2007) suggests it occurred at ~1.92 Ga. The basement of the Yinshan Block is predominantly Archean tonalite-trondhjemite-granodiorite (TTG) gneisses, mafic granulites and granitoid-greenstone belts (Liu et al., 1993; Zhao et al., 1999b). The basement of the Ordos Block is covered by the Mesozoic-Cenozoic Ordos Basin but boreholes and aeromagnetic data reveal the existence of granulite facies basement rocks beneath (Wu et al., 1986; Wu et al., 1998; Zhao et al., 2005). The Western Block has an old cratonic lithosphere that is still stable and of average crustal thickness (Menzies et al., 1993; O'Reilly et al., 2001; Zhang et al., 2002).

The TNCO is composed of various TTG gneisses, granitoids and greenstones metamorphosed from greenschist to granulite facies during the collision of the Eastern and Western Blocks (Zhao et al., 2000).

The basement of the Eastern Block shows the greatest diversity in rock ages, with Paleoarchean-Neoarchean TTG gneisses dating back to 3.8 Ga in the Anshan area and variously intruded by granitoids at 3.3, 3.2 and 2.5 Ga (Liu et al., 1992; Song et al., 1996; Zhao et al., 1999a; Zhao et al., 2000; Wan et al., 2005; Liu et al., 2008b; Yang et al., 2008b). It also contains minor supracrustal rocks, mainly ultramafic to felsic volcanic and sedimentary rocks that have been metamorphosed from greenschist to granulite facies (Zhao et al., 1998a; Zhao et al., 1999a; Zhao et al., 2000). The Eastern Block is thought to have rifted along its easternmost margin during the Paleoproterozoic, with subsequent closure forming the Jiao-Liao-Ji Belt at ~1.9 Ga (Zhao et al., 2005).

The lithosphere beneath the Eastern Block is known to have been thick (>200 km) during the Early Paleozoic at 470 Ma, due to the presence of diamondiferous kimberlites at Mengyin and Fuxian (Menzies et al., 1993; Griffin et al., 1998; Yang et al., 2009) (Fig. 2.1). However, in the Cenozoic it underwent thinning (75-80 km), identified by the presence of spinel-facies xenoliths in alkali basalts, as well as

evidence from seismic, and other geophysical and heat flow data (Yuan, 1996; Gao et al., 2002; Zhou et al., 2002; Wu et al., 2005a; Yang et al., 2009). Seismic shear wave velocities beneath the Eastern Block are lower than would be expected if the lithosphere was cratonic and they reveal a "blobby" texture (Yuan, 1996; Zhang et al., 1998; Niu, 2005; Menzies et al., 2007; Pei et al., 2007). The lithosphere also has a higher geothermal gradient and higher heat flow than it did in the Paleozoic (Menzies and Xu, 1998; Gao et al., 2002; Zhang and Sun, 2002). This has led to the view that at some stage during the Mesozoic, part or all, the lithospheric mantle keel beneath the Eastern Block was either thinned or lost (Menzies et al., 1993; Wilde et al., 2003; Gao et al., 2004; Wu et al., 2005a; Liu et al., 2008a).

2. Geological setting of the Eastern Block

The Eastern Block of the NCC consists of TTG gneisses and nine Precambrian metamorphic domains; Western Shandong, Eastern Shandong, Eastern Hebei, Southern Liaoning, Miyun–Chengde, Western Liaoning, Anshan–Benxi, Northern Liaoning and Southern Jilin (Zhao et al., 1999a; Zhao et al., 2000; Wu et al., 2005b).

The area remained largely quiescent until the Mesozoic, when a number of major geological events occurred in the NCC. From the Triassic to Late Jurassic, the NCC was in a compressional tectonic regime (Menzies et al., 2007). The NCC and Yangtze Craton collided at ~240-220 Ma producing widespread metamorphism and the formation of the Qinling-Dabieshan UHP metamorphic belt (Fan et al., 2001; Zheng et al., 2003; Zhang, 2005; Menzies et al., 2007). There was also the generation of voluminous Jurassic (Early Yanshanian in the Chinese literature) granites at ~180-160 Ma (Wang et al., 1998; Wilde et al., 2003; Liu et al., 2004; Wu et al., 2005c).

The Late Jurassic marks the initiation of a change in tectonic regime across much of north and east China from compressional to extensional that continued into the Cretaceous (Menzies and Xu, 1998; Meng, 2003; Zhang et al., 2003a; Xu, 2007). There was lithospheric thinning (Chen et al., 2003b; Liu et al., 2004; Xu et al.,

2004b; Zhai et al., 2007), extension (Zhou and Lu, 2000; Xu, 2001), pull-apart basin formation (Zhou and Lu, 2000; Guo et al., 2001; Meng, 2003; Menzies et al., 2007; Yang et al., 2008a), changes in structural framework orientations from E-W in the Late Jurassic (Zhang et al., 2003b) to NNE-SSW in the Cretaceous (Zhai et al., 2007), reactivation and inversion of earlier thrust faults, with initiation of new normal faults (Yang et al., 2007c). In the Early Cretaceous metamorphic core complexes formed from 133 to 116 Ma (Davies et al., 2001; Darby et al., 2004; Liu et al., 2005; Yang et al., 2007c; Yang et al., 2008b) and synchronous with this was widespread emplacement of dioritic and lamprophyric dykes (125-110 Ma) and generation of the voluminous Cretaceous (Late Yanshanian in the Chinese literature) granites with contemporaneous extensive volcanism (Zhang et al., 2003b; Deng et al., 2007). Gold mineralization was also widespread at ~120 Ma (Wang et al., 1998; Zhou and Lu, 2000; Yang and Zhou, 2001; Yang et al., 2003; Zhang et al., 2003c). The extensional tectonic regime continued into the Late Cretaceous and Early Tertiary.

As alluded to above, the Mesozoic granitoids in China are traditionally divided into two groups, the Jurassic (Early Yanshanian) and Cretaceous (Late Yanshanian) plutons and batholiths. Jurassic granitoids have been variously dated at ~180-160 Ma (Wang et al., 1998; Wilde et al., 2003; Liu et al., 2004; Wu et al., 2005c), ~160-150 Ma (Zhou and Lu, 2000; Wu et al., 2005c) or 170-150 Ma (Jahn et al., 2000). The timing of the Cretaceous granitoid intrusions is variously quoted as 142-112 Ma (Kusky et al., 2007), 135-117 Ma (Yang et al., 2008a), 135-115 Ma, 130-120 Ma (Gao et al., 2004), ~120 Ma in E. Shandong (Jahn et al., 2000) and 117-85 Ma (Zhou and Lu, 2000). Some researchers consider that there was no gap in magmatic activity between the Early and Late Yanshanian (Zhou and Lu, 2000; Xu, 2001). Liu et al. (2008a) state that Luxi and Shandong recorded no magmatic activity between the intrusion of the alkaline Tongshi complex at ~185 Ma and the emplacement of mafic dyke swarms at 144 Ma and that the Late Yanshanian magmatism ended at 115 Ma, however this is not a widely held view.

Shandong Province forms the easternmost edge of the Eastern Block of the NCC and is divided by the Tanlu Fault into the eastern Jiaodong and western Luxi

segments (Ying et al., 2006). The oldest rocks in Jiaodong are metamorphosed volcanic and sedimentary rocks of the Meso-Neoarchean Jiaodong 'group' (Wang et al., 1998; Zhou and Lu, 2000). These are overlain unconformably by the Jinshan and Fenzishan 'groups' that are dated as Paleoproterozoic and consist of metamorphosed igneous and sedimentary rocks (Wang et al., 1998; Zhou and Lu, 2000). Unconformably overlying these rocks are Neoproterozoic low-grade metasedimentary units of the Penglai Group (Zhu et al., 1994; Wang et al., 1998; Zhou and Lu, 2000; Zhou et al., 2008b). Late Permo-Triassic units are mainly red beds and conglomerates (Yang et al., 2006). Molasse deposition occurred in the Early Jurassic (Qiu et al., 2002), followed by deposition of extensive volcanic and clastic sedimentary rocks in intra-continental basins that continued into the Cretaceous (Zhou and Lu, 2000; Qiu et al., 2002; Yang et al., 2006). The Cretaceous rocks are commonly divided into four units; namely the Laiyang, Qingshan, Dasheng and Wangshi groups (Zhang et al., 2003b).

Three main periods of Mesozoic magmatism are recognised in Shandong Province; Late Triassic-Early Jurassic, Middle-Late Jurassic (Early Yanshanian) and Cretaceous (Late Yanshanian). Late Mesozoic magmatic activity differs in the two regions of Shandong Province. The Jiaodong segment contains mid-Cretaceous extrusive rocks with bimodal characteristics in NE-trending rift basins, including the. Jimo basalts in the Laiyang Basin formed at 130-110 Ma (Fan et al., 2001; Ying et al., 2006) (see Fig. 2.2) and numerous mafic dykes dated at 130-120 Ma (Zhang and Sun, 2002). The basalts are considered to have originated from enriched lithospheric mantle and the felsic rocks were formed by anatexis of the lower/middle crust (Ying et al., 2006). The Luxi segment, however, consists of Cretaceous extrusive rocks in NW-trending extensional basins, e.g. Fangcheng basalts in the Pingyi Basin, dated at 125 ± 1.8 Ma, and shoshonites in the adjacent Mengyin Basin, occurring as thin layers within the Qingshan Formation, yielded an Ar-Ar age of 124-115 Ma (Zhang and Sun, 2002) (Fig. 2.1). Both regions of Shandong contain Mesozoic granitoid intrusions, however Mesozoic mafic intrusions are only found in the Luxi segment (Zhang and Sun, 2002; Zhang et al., 2007).

3. Sample selection and petrography

The granitoids selected for this study were specifically chosen because they were previously reported to be the latest Late Yanshanian intrusions in the area (SBGMR, 1991; Zhao et al., 1998a; Zhou and Lu, 2000), although precise ages were rarely reported. Since this area has been recognised as recording extensive crustal thinning since the Mesozoic (Guo et al., 2001; Xu, 2001; Zhang and Sun, 2002; Zhang et al., 2002; Wilde et al., 2003; Yang et al., 2008a), with magmatism reaching a peak at ~125 Ma (Wu et al., 2005a), such younger rocks might provide an opportunity to obtain significant information about the nature of the lower crust and mantle at this time. Samples were selected from four discrete intrusions; Sanfoshan, Aishan, Laoshan and Yashan and seven representative samples, two each from Sanfoshan, Aishan and Yashan and one from the Laoshan batholith, were selected for detailed petrographic analysis, SHRIMP U-Pb zircon dating and Lu-Hf isotopic analysis; six additional samples were selected for geochemical study (Figs. 2.2 and 2.3) and the GPS locations for all the samples are listed in Table 2.1.

The modal abundance of minerals in six of the seven samples for geochronological study were established by point counting using a Leitz microscope and Swift point counter (sample SD-12 was not counted since it was too coarse-grained). Three thin sections were prepared at right angles for most of the samples and the minerals recorded from approximately 2000 equally-spaced points on each slide, giving a total of ~6000 points for each sample (except sample SD-30 which was fine-grained and only one slide was prepared) (Table 2.2).

3.1 Sanfoshan Batholith

The Sanfoshan batholith (Tang et al., 2008) is located to the northeast of Rushan (Figs. 2.2 and 2.3a) and covers an area of ~200 km^2 (Zhou and Lu, 2000). It is a pink granitoid that consists mainly of monzogranite. It is described as either intruding into the Early/Middle Yanshanian Kunyushan suite (Zhou and Lu, 2000; Hu et al., 2004; Hu et al., 2006; Li et al., 2006), or is considered to be the youngest part of that suite (Guo et al., 2005; Tang et al., 2008). The former interpretation is

favoured here based on field observations. A sample from the western central side of the batholith had been previously dated at 113 ± 1 Ma (SHRIMP zircon U-Pb by (Guo et al., 2005). It contains microdioritic enclaves (Zhang et al., 2006).

Sample SD-11 is a medium-grained monzogranite (Fig. 2.4) with an allotriomorphic granular texture. The main minerals are plagioclase (36%), quartz (31%), alkali feldspar (28%), and biotite (2-3%). The quartz typically shows undulose extinction. The plagioclase crystals are zoned and also extensively altered to a brown aggregate of clay, epidote and sericite. The K-feldspar is microcline-perthite, with cross-hatch twinning and patchy/uneven extinction. Another distinguishing feature of the K-feldspar crystals is the granophyric intergrowth with quartz. The plagioclase and K-feldspar occur as inclusions within each other and they also locally form myrmekite when adjacent. Biotite is the only mafic mineral and it locally contains apatite inclusions; it is partially altered to chlorite. Opaque minerals are predominantly found as inclusions in biotite and quartz. Other accessory minerals are titanite and apatite, with secondary epidote.

Sample SD-12 is a pegmatitic syenogranite that was too coarse-grained to obtain meaningful modal data in thin section. It contains very large biotite flakes, plagioclase feldspar, K-feldspar and quartz.

The samples SD-13, SD-14 and SD-17 were selected for geochemical analysis only (Fig. 2.3a). Sample SD-13 is a fine-grained, pink porphyritic granite containing phenocrysts of quartz and tabular plagioclase feldspar in a fine-grained allotriomorphic-granular matrix of quartz and feldspar. All the feldspars are extensively altered to sericite and clay minerals with hematite specks abundant in the K-feldspar. Rare biotite phenocrysts are altered to white mica. Sample SD-14 is a pinkish, fine-grained syenogranite. It consists of phenocrysts of biotite, quartz and K-feldspar in an extremely fine-grained inequigranular matrix of quartz, K-feldspar and minor plagioclase feldspar. Sample SD-17 is a pink, coarse-grained monzogranite with an allotriomorphic granular texture. It is composed of quartz, plagioclase and perthitic K-feldspar with loose clusters of hornblende, green biotite, titanite and opaques. The quartz is undulose and the plagioclase is strongly zoned.

3.2 Aishan Batholith

The Aishan Batholith is located between Qixia and Penglai (Fig. 2.2) and covers an area of ~250 km^2 (Fig. 2.3b) (Zhou and Lu, 2000). It intrudes the Archean Jiaodong 'group' and the Paleoproterozoic Fenzishan 'group' and is typically reddish in colour with a porphyritic texture and predominantly monzogranitic in composition. It has yielded an extremely wide range of ages from 63.5 to 158 Ma (K-Ar) (SBGMR, 1991; Zhou and Lu, 2000).

Sample SD-27 is a coarse-grained leucocratic monzogranite and sample SD-28 is a coarse-grained porphyritic monzogranite (Fig. 2.4), both with allotriomorphic-granular textures. The main mineral assemblage for SD-27 is quartz (35%), K-feldspar (30%) and plagioclase (24%) and for SD-28 it is plagioclase (33%), K-feldspar (33%) and quartz (23%). In both rocks, the quartz typically has strain-induced undulose extinction. Quartz is commonly included in plagioclase, as well as being interstitial to the feldspars. Plagioclase crystals show albite twinning and oscillatory zoning. In general, plagioclase appears to be concentrated in specific areas that are commonly devoid of K-feldspar, although there are some areas where they are in contact and myrmekite has developed. The K-feldspar is perthite and some crystals have combined carlsbad and cross-hatch twinning. Sample SD-28 has abundant secondary pink-brown haematite alteration which is confined to the K-feldspar crystals.

The amount of biotite varies between the samples from ~1% to 5% and SD-28 also has ~2-7% green hornblende (Table 2.2). There are also a few crystals of brown hornblende present. The biotite shows evidence of deformation, since its 001 cleavage traces are locally curved. The accessory minerals are opaque oxides (~0.5%) typically found as inclusions within biotite or hornblende, euhedral titanite, long acicular crystals of apatite, as well as local patches of secondary epidote within plagioclase.

The additional sample selected for geochemical analysis was sample SD-29 (Fig. 2.3b), which is a grey-coloured monzogranite with an allotriomorphic-granular texture. It is composed of plagioclase, perthitic K-feldspar and quartz with scattered

crystals of green hornblende and biotite. The plagioclase is commonly zoned with patchy sericite alteration, particularly in the cores.

3.3 Yashan Pluton

The Yashan pluton is located to the SE of Qixia (Fig. 2.2). There is little reference to it in the published literature and there are no previously-available age data. It forms one large pluton covering an area of ~80 km^2 (Fig. 2.3c).

Sample SD-31 is a coarse-grained monzogranite (Fig. 2.4) that is weakly porphyritic with large scattered K-feldspar phenocrysts and sample SD-30 is a fine- to medium-grained monzonite enclave (Fig. 2.4) hosted by the monzogranite. Sample SD-31 consists of plagioclase (39%), K-feldspar (28%), quartz (21%) and biotite (5%). The plagioclase crystals are locally present within K-feldspar and there are areas where plagioclase is replaced by K-feldspar. Plagioclase shows strong oscillatory zoning. K-feldspar is perthitic with uneven/patchy extinction and commonly contains inclusions of all the other minerals; myrmekite is present where the two feldspars are in contact. Sample SD-30 contains no quartz and its main minerals are plagioclase (44%), K-feldspar (27%) and biotite (10%).

Both samples have approximately equal amounts of elongate hornblende and biotite, although the two samples differ in the actual amounts (Table 2.2). The hornblende and biotite are mostly enclosed within feldspar. The hornblende has minute inclusions of opaque oxides and is pleochroic from α = yellow-brown, β = green-brown, γ = green-blue, and tends to form clusters with biotite. The biotite contains inclusions of opaque oxides, epidote, apatite and titanite, and locally curved cleavages are an indication that it has undergone some strain. The accessory minerals are opaque oxides, euhedral titanite and acicular apatite, with secondary epidote and calcite.

3.4 Laoshan Batholith

The Laoshan batholith is intruded into Proterozoic rocks and covers a total area of ~600 km^2 NE of Qingdao (Figs. 2.2 and 2.3d) (Zhao et al., 1998a; Wei et al., 2000; Zhou and Lu, 2000; Wang et al., 2001; Wei et al., 2008). It is generally

described, from east to west, as consisting of A-type granite with a small area of quartz monzonite, then biotite monzogranite (oldest), followed by I-type syenogranite (Wei et al., 2000; Wei et al., 2008). It has been variously dated at 146.8 ± 0.8 Ma, 126.2 ± 0.8 Ma, 113.0 ± 0.9 Ma and 110.8 ± 0.9 Ma, depending on the rock type, in previous U-Pb zircon work (Zhao et al., 1998b).

Sample SD-59 is a medium- to coarse-grained alkali feldspar granite with an allotriomorphic texture. It consists of alkali feldspar (73%) and quartz (24%) (Fig. 2.4), with the feldspar ranging from antiperthite to perthite that could not be separated during point counting. The perthite shows haematite speckling whereas the antiperthite is a slightly darker grey colour in polarised light. The perthite also locally shows zoning or patchy extinction. The accessory minerals include opaque minerals (~2%) typically associated with biotite. The biotite ranges from 0.1% to 0.5% and occurs as small scattered flakes. There are also patches of myrmekite, grains of titanite and some larger crystals of epidote and apatite near the opaques.

Additional samples selected from the Laoshan Batholith for geochemical analysis were samples SD-56 and SD-63 (Fig. 2.3d). Sample SD-56 is a medium- to coarse-grained allotriomorphic-textured syenogranite containing perthitic K-feldspar that is various shades of pink in hand specimen. It also contains strongly zoned plagioclase and scattered flakes of biotite associated with titanite, epidote, apatite and opaques. Sample SD-63 also has an allotriomorphic texture and is a syenogranite similar to sample SD-56, but commonly with graphic intergrowth of K-feldspar and quartz. In addition, there are mafic clusters locally containing green hornblende.

4. Geochemical techniques and results

4.1 Techniques

A total of 13 granitoid samples were prepared for geochemical analysis and the sites are located on Fig. 2.3 and their co-ordinates listed in Table 2.1. Each rock was reduced to ~1cm fragments in a hydraulic press with tungsten carbide plates and then further crushed in the press to ~200 mesh. The samples were further reduced to

a fine powder in an alumina pot using a Rocklabs ring mill. The whole-rock powders were analyzed for major and trace elements at the Institute of Geology and Geophysics at the Chinese Academy of Sciences in Beijing, China. Major element analysis was conducted using X-ray fluorescence spectrometry (XRF) following the technique of Lee (1997) and the trace element and REE concentrations were determined using ICP-MS following the solution method outlined by Yuan (2004). XRF analytical precision for all major elements was better than ± 5% (most were better than ± 2%). The USGS international standards used to calibrate trace element concentrations were AGV-1 and G-2. ICP-MS analytical precision of AGV-1 for all trace elements was better than ± 5% (most were better than ± 2 %) and that of G-2 was generally better than ± 5%, although some samples showed greater variation.

The FeO and Fe_2O_3 concentrations of the samples were calculated using the iron oxidation graph in Middlemost (1985), adapted from Le Maitre (1976). The normative mineralogy was calculated using the CIPW norm program of Kurt Hollocher, Geology Department, Union College, Schenectady, NY, 12308.

4.2. Results

The geochemical data are listed in Table 2.3. Most of the batholiths and plutons contain rocks that range in composition from monzogranite, through syenogranite, to alkali feldspar granite, so in the following section the results are presented on a compositional basis, rather than being described by individual intrusions. Note that sample SD-30, a monzonitic enclave within sample SD-31, is grouped with the monzogranites; sample SD-13, which is a fine-grained aplite intrusive into SD-12, is grouped with the syenogranites; and sample SD-59, an alkali feldspar granite, is also grouped with the syenogranites for comparative purposes.

The silica content of the granitoids ranges from 56% (sample SD-30) to 77% (samples SD-13 and SD-27) making them intermediate to felsic in composition. Monzonite sample SD-30 differs in having higher abundances of total Fe_2O_3, TiO_2, Al_2O_3, MnO, MgO, CaO, P_2O_5 and lower SiO_2. All other granitoids have high total alkalis with Na_2O ranging from 2.3% to 4.6% and K_2O from 3.7 to 5.2% (except sample SD-12 which has a higher K_2O content of 7.8%). Total Fe_2O_3 contents are

low (0.6-3.2%), as are MnO (0.01-0.1%), MgO (0.02-1.9%), TiO_2 (0.1-0.4%) and P_2O_5 (0.01-0.2%). Al_2O_3 ranges between 12.5% and 17.4%.

Most samples, except for sample SD-13, are metaluminous with A/CNK molar ratios below 1.0 and A/NK molar ratios above 1.0; Na_2O/K_2O ratios are generally low (0.30-1.81 %) (Fig. 2.5). In contrast, sample SD-13 is peraluminous with an A/CNK ratio of 1.09 and A/NK molar ratio of 1.13. Overall, most major elements (Fig. 2.6) show a strong negative correlation with SiO_2 (correlation coefficient r = over - 0.9), except for K_2O which increases with SiO_2 (r = + 0.7) and Na_2O which has no strong relationship (r = - 0.3). The strong correlations indicate the rocks are co-magmatic, including the monzonite enclave.

On the classification diagram of Chappell and White (1992), most granites (not presented) plot in the I-, S- and M-type field, except for sample SD-59, which falls in the A-type field. The P_2O_5 vs. SiO_2 plot (Fig. 2.6b) reveals a negative trend, whereas the trend of Pb vs. SiO_2 is weakly positive, indicating these rocks are I- and not S-type granites (Chappell and White, 1992). Except for A-type sample SD-59, all others fall within the I-, S-, M-type field in a plot of Zr vs. 10 000 Ga/Al (Fig. 2.7) (Whalen et al., 1987) and their $Al_2O_3/(CaO + Na_2O + K_2O)$ molar ratios being below 1.0 also supports this conclusion (Maniar and Piccoli, 1989).

In the chrondrite-normalized REE diagrams (Fig. 2.8a-c), most of the granites have high total REE and are enriched in light rare earth elements (LREE) (Fig. 2.8a). They also have flat or concave upwards MREE-HREE patterns. The monzogranites (samples SD-11, SD-17, SD-27, SD-28, SD-29 and SD-31) all have a similar pattern (Fig. 2.8b). Most do not show significant Eu anomalies, although samples SD-11 and SD-17, both from the Sanfoshan Batholith, have Eu/Eu* values of 0.58 and 0.65. Sample SD-31 from the Yashan pluton also has a weak negative Eu anomaly (Eu/Eu* = 0.80). Monzonitic enclave sample SD-30 has a similar trend to the monzogranites but reveals a weak positive Eu anomaly (Eu/Eu* = 1.07). In contrast, syenogranite samples SD-13, SD-14, SD-56 and SD-63 (Fig. 2.8c) show moderate to strong negative Eu anomalies (Eu/Eu* ranging from 0.44 to 0.64) and have a similar trend, though the total REE varies. Alkali feldspar granite sample SD-59 has the most pronounced negative Eu anomaly (Eu/Eu* = 0.28) and higher HREE. Sample

SD-12 differs from the other syenogranites in having a pronounced positive Eu anomaly (Eu/Eu* = 2.33) and significantly lower total REE, implying plagioclase accumulation. Sample SD-13 is an aplite associated with sample SD-12 at Sanfoshan and it differs from the other samples in having much lower REE values. Both samples SD-12 and SD-13 have strong concave upwards HREE trends not seen in the other samples.

The Ce/Yb_{CN} ratios of all samples range from 4.86 to 29.40 with an average of 14.95. In general, the monzogranites have higher values than the syenogranites, excepting monzogranite sample SD-11, which has a lower value. The higher Ce/Yb_{CN} ratios of the monzogranites indicate relatively greater LREE enrichment and lower HREEs compared to the syenogranites, this is particularly noticeable in the Aishan samples (SD-27, SD-28, SD-29) which have values >20. The Gd/Yb_{CN} ratios, which indicate the degree of HREE fractionation, range from 0.63 to 3.29 with an average of 1.64. In general the monzogranites, with the exception of sample SD-11, again have higher values (1.49 to 3.29) than the syenogranites (0.63 to 1.42), indicating the monzogranites have undergone greater HREE fractionation. The Nb/Ta ratios of all samples range from 9.24 to 17.01 with an average of 12.98. These values are close to that of the average continental crust (Green, 1995), indicating the rocks are crustally-derived or that extensive crustal contamination has occurred.

In the primitive mantle-normalized trace element spider diagrams (Fig. 2.9), all granitoids show negative anomalies for Ti, Nb, Ta and P, so they are depleted in high-field strength elements (HFSE). The negative P anomalies are likely to be associated with apatite fractionation. The granitoids all show a strong positive anomaly in Pb. The combined depletion in Ta, Ti and Nb with the enrichment in Pb shows a crustal influence, probably generated from a source previously enriched in LILE and LREE by slab-derived hydrous fluids. The monzogranites generally show negative Ba anomalies (except for a strong positive anomaly in sample SD-31 implying feldspar accumulation), as does monzonite sample SD-30 (Fig. 2.9b), indicating feldspar fractionation. All the syenogranites, together with aplite sample SD-13 and alkali feldspar granite sample SD-59, also have negative Ba anomalies indicating feldspar fractionation. Sample SD-31 is depleted in Zr relative to the other

samples which could imply pyroxene fractionation (Nomade et al., 2002). Most samples have negative Sr anomalies implying feldspar fractionation; however monzogranite samples SD-29 and SD-31, syenogranite sample SD-12 and alkali feldspar granite sample SD-59 have positive Sr anomalies implying feldspar accumulation. Sample SD-12 also differs from the other samples in having lower total REE and lower Nb and Ta (Fig. 2.9c).

5. Geochronological techniques and results

5.1 Techniques

5.1.1. SHRIMP U-Pb

The seven samples selected for geochronology were trimmed of any weathered material before being crushed in a tungsten carbide-plated hydraulic press and then reduced to a fine powder in a tungsten carbide ring-mill. The zircon crystals were separated using heavy liquid techniques, and individual crystals were then handpicked under a binocular microscope. The crystals were placed onto double-sided adhesive tape along with pieces of the Curtin University zircon standard CZ3 and cast in epoxy resin and then polished until the crystals were sectioned in half; the mount was then cleaned and gold coated. A series of photomicrographs were taken in both reflected and transmitted light to create a 'map' of the mount prior to analysis. The grains were analysed using one of the two Sensitive High-Resolution Ion Microprobes (SHRIMP II) at Curtin University of Technology, Perth, following the techniques outlined in Williams (1998). The standard zircon CZ3 has a conventionally-measured $^{206}Pb/^{238}U$ age of 564 Ma and contains 551 ppm U (Pidgeon et al., 1994). One site on the standard zircon was analysed after every 3 unknowns and each site was rastered for an average of 2.5 minutes over an area of 120 μm to remove any common Pb or contamination from the gold coat. The average analysis spot size was 25 μm in diameter.

The $^{206}Pb/^{238}U$ age is quoted here because the zircons are <1 Ga so the $^{207}Pb/^{206}Pb$ age is less sensitive and less reliable because of the low count rates on

^{207}Pb. The measured ^{204}Pb was used to correct the data based on the isotopic composition of Broken Hill lead.

The data were processed using the SQUID program (Ludwig, 2001a) and ISOPLOT was used to produce the concordia diagrams (Ludwig, 2001b). All errors for individual analyses are given at 1σ and group ages on the concordia plots are quoted with 95% confidence (2σ).

5.1.2. MC-ICP-MS

In situ zircon Lu-Hf isotopic analyses were performed on the identical zircon sites dated using the SHRIMP II. The analyses were conducted using a Neptune MC-ICP-MS equipped with a 193 nm UV laser at the Institute of Geology and Geophysics at the Chinese Academy of Sciences in Beijing, China. Spot sizes of 32 or 63 μm were used during analysis and the laser repetition rate was 10Hz at 100mJ; the detailed analytical techniques and correction procedures are described in Xu et al. (2004a) and Wu et al. (2006). During analysis the ^{176}Hf/^{177}Hf and ^{176}Lu/^{177}Hf ratios of the standard zircon (CZ3) were 0.281707 ± 15 ($2\sigma_n$, n = 12) and 0.000032 similar to the ^{176}Hf/^{177}Hf ratio of 0.281707 ± 6 and ^{176}Lu/^{177}Hf ratio of 0.000036 quoted in Xu et al. (2004a) and also similar those from Wu et al (2006) of 0.281729 ± 21 and 0.000034. The ^{176}Lu decay constant of 1.867×10^{-11} yr^{-1} from Soderlund et al. (2004) was used to calculate the initial ^{176}Hf/^{177}Hf ratios. Both T_{DM1} and T_{DM2} model ages are listed in Table 2.5. T_{DM1} model ages reflect a single-stage model age of the magma protolith and represent a minimum age for the source of the host magma; they were calculated using the measured ^{176}Lu/^{177}Hf ratios, referred to a model depleted mantle with a present-day ^{176}Hf/ ^{177}Hf ratio of 0.28325, similar to that of average MORB (Nowell et al., 1998) and ^{176}Lu/^{177}Hf=0.0384 (Griffin et al., 2000). T_{DM2} ages are two-stage model ages and are calculated by projecting back the initial ^{176}Hf/ ^{177}Hf of the zircon to the depleted mantle model growth curve assuming a mean ^{176}Lu/ ^{177}Hf value of 0.015 for the average continental crust (Griffin et al., 2002). The T_{DM2} model ages are used in the following discussion.

5.2 U-Pb and Lu-Hf zircon isotopic results

5.2.1. Sanfoshan Batholith

The zircon crystals in samples SD-11 and SD-12 are mostly prismatic, transparent and pale yellow in colour, although those from sample SD-11 are more highly prismatic. All the zircons selected range in size from 50-100μm.

Sample SD-11: Twelve analyses were undertaken (Table 2.4) and the U content ranges from 627 to 1992 ppm and the Th content from 33 to 3881 ppm. The $^{232}Th/^{238}U$ ratios range from 0.25 to 2.01, with an average of 1.1. Eight grains have concordant ages that range from 117 Ma to 120 Ma and yield a concordia $^{206}Pb/^{238}U$ age of 118 ± 1 Ma (Fig. 2.10a), which is taken to define the crystallization age of the monzogranite. Of the four remaining grains, one yields a significantly older age of 190 ± 3 Ma and is likely an inherited Early Yanshanian granite zircon from the basement. Two other grains yield ages of 121 ± 1 Ma, with one having anomalously high U and Th. The remaining grain has a slightly younger age (115 ± 1 Ma) and this may reflect Pb loss or growth induced by emplacement of later dyke intrusions in the area.

Zircons from sample SD-11 have initial $^{176}Hf/^{177}Hf$ values that range from 0.282167 to 0.282326, with an average of 0.282257 (Table 2.5). The $\varepsilon_{Hf(t)}$ values range from -18.98 to -13.31 and T_{DM2} model ages from 2812 to 3316 Ma. The average T_{DM2} model age is 3023 Ma and the average T_{DM1} model age is 1431 Ma. The lowest initial $^{176}Hf/^{177}Hf$ value of 0.282167 and $\varepsilon_{Hf(t)}$ value of -18.98 were given by the grain with the slightly younger $^{206}Pb/^{238}U$ age of 115 Ma. The grain with the significantly older age of 190 Ma has values that do not notably differ from the rest of the grains.

Sample SD-12: Twelve analyses were undertaken on this sample and the U content ranges from 344 to 5820 ppm, the Th content from 343 to 4119 ppm and the $^{232}Th/^{238}U$ ratio from 0.31 to 1.79, with an average value of 1.0 (Table 2.4). Nine zircon grains have ages that range from 114 Ma to 119 Ma and yield a weighted mean $^{206}Pb/^{238}U$ age of 117 ± 1 Ma (Fig. 2.10b), taken to represent the crystallization age of the pegmatitic syenogranite. There are two slightly older grains with ages of

123 ± 1 Ma and 124 ± 1 Ma that have high U and Th. One zircon yielded a slightly younger age of 106 ± 2 Ma that may reflect disturbance by a later event.

Zircons from sample SD-12 all yield initial $^{176}Hf/^{177}Hf$ values over a narrow range of 0.282237 to 0.282349, with an average value of 0.282266 (Table 2.5). The $\varepsilon_{Hf(t)}$ values range from -16.50 to -12.64 and the T_{DM2} model ages from 2749 to 3098 Ma. The average T_{DM2} model age is 3007 Ma and the average T_{DM1} model age is 1431 Ma, both similar to the averages for zircons from sample SD-11.

Overall, the ages of both samples are similar within error and record an average weighted mean $^{206}Pb/^{238}U$ zircon age for the Sanfoshan Batholith of 118 ± 1 Ma and this is taken to represent the age of intrusion.

5.2.2. Aishan Batholith

The zircons from sample SD-27 are brown in colour and translucent, whereas those from sample SD-28 are pale brown in colour, transparent and clear. The zircons are prismatic in both samples and ranged in size from 50-100μm.

Sample SD-27: Twelve analyses were undertaken on this sample and the U content ranges from 202 to 1712 ppm, the Th content from 174 to 1326 ppm and the $^{232}Th/^{238}U$ ratio ranges from 0.66 to 1.33, with an average of 1.1 (Table 2.4). Eleven grains from sample SD-27 have concordant ages ranging from 121 Ma to 128 Ma and yield a $^{206}Pb/^{238}U$ concordia age of 125 ± 3 Ma (Fig. 2.10c). There is one younger grain (117 ± 3 Ma) that may have been slightly disturbed by later events in the area, as discussed above.

Eleven of the 12 zircons from sample SD-27 have initial $^{176}Hf/^{177}Hf$ values that range from 0.282182 to 0.282291, with an average value of 0.282235 (Table 2.5). The $\varepsilon_{Hf(t)}$ values of these zircons range from -18.41 to -14.44 and the T_{DM2} model ages from 2914 to 3266 Ma. The average T_{DM2} model age is 3100 Ma and the T_{DM1} model age is 1454 Ma. The remaining grain has a significantly higher initial $^{176}Hf/^{177}Hf$ value of 0.282426, an $\varepsilon_{Hf(t)}$ value of -9.70 and a T_{DM2} model age of 2491 Ma.

Sample SD-28: Twelve analyses were undertaken and the U content ranges from 207 to 1644 ppm, the Th content from 183 to 2243 ppm and the $^{232}Th/^{238}U$ ratios range from 0.80 to 1.41 with an average of 1.0 (Table 2.4). Nine grains have ages ranging from 111 Ma to 122 Ma and yield a weighted mean $^{206}Pb/^{238}U$ age of 116 ± 2 Ma (Fig. 2.10d), which is taken to record the crystallization age of the porphyritic monzogranite. The three remaining grains have slightly older ages of 123 ± 3 Ma, 124 ± 3 Ma and 130 ± 3 Ma, with the latter value from a grain with the highest U and Th contents (Table 2.4). These older grains reflect inheritance from typical Late Yanshanian granitoids in the area.

Zircons from sample SD-28 have initial $^{176}Hf/^{177}Hf$ values with a narrow range of 0.282154 to 0.282265 (Table 2.5). The $\varepsilon_{Hf(t)}$ values range from -19.49 to -15.55 and T_{DM2} model ages from 3011 to 3360 Ma. The average T_{DM2} model age is 3154 Ma and the average T_{DM1} model age is 1451 Ma.

Overall, a total of 24 SHRIMP analyses were completed on the two samples from the Aishan Batholith. In this case, it is evident that there is a real difference in age between the two samples, with sample SD-27 recording an age of 125 ± 3 Ma and sample SD-28 an age of 116 ± 2 Ma. Importantly, the two grains in SD-28 with ages of 123 ± 3 Ma and 124 ± 3 Ma are identical in age to the main population in sample SD-27, suggesting incorporation during emplacement from this slightly earlier intrusive phase.

5.2.3. Yashan Pluton

The zircons from sample SD-30 are brown in colour, translucent and tend to be stubby to rounded in shape. The zircons in sample SD-31 are euhedral, prismatic and transparent. They are pale brown in colour. All the zircons selected ranged in size from 50-100μm.

Sample SD-30: This is the monzonite enclave and fifteen analyses were undertaken. The U content ranges from 96 to 3072 ppm, the Th content from 37 to 10224 ppm and the $^{232}Th/^{238}U$ ratios range from 0.04 to 3.44, with an average value of 1.3 (Table 2.4). A total of thirteen grains have ages ranging from 111 Ma to 120 Ma and yield a $^{206}Pb/^{238}U$ concordia age of 116 ± 1 Ma (Fig. 2.10e). One grain yields

a younger age of 106 ± 2 Ma, possibly reflecting the effect of a younger intrusion, and another grain is slightly older (121 ± 2 Ma).

Fifteen out of the 16 zircons from sample SD-30 have initial $^{176}Hf/^{177}Hf$ values that range from 0.282207 to 0.282378, with an average value of 0.282296 (Table 2.5). The $e_{Hf(t)}$ values range from -17.79 to -11.55 and T_{DM2} model ages from 2652 to 3199 Ma. The average T_{DM2} model age is 2914 Ma and the T_{DM1} model age is 1356 Ma. The one remaining grain has a much higher initial $^{176}Hf/^{177}Hf$ 0.282409 and a less negative $e_{Hf(t)}$ value of -10.65 and yields a T_{DM2} model age of 2570 Ma.

Sample SD-31: Sample SD-31 is from the main granitoid body and thirteen analyses were undertaken. The U content ranges from 123 to 1177 ppm, the Th content from 115 to 1814 ppm and the $^{232}Th/^{238}U$ ratio ranges from 0.86 to 1.59, with an average value of 1.0 (Table 2.4). Nine concordant ages, ranging from 109 Ma to 117 Ma yield a $^{206}Pb/^{238}U$ concordia age of 113 ± 2 Ma (Fig. 2.10f). Three of the other grains have ages of 106 ± 1 Ma, 104 ± 2 Ma and 100 ± 7 Ma. The 106 Ma grain has high U and Th and has probably undergone Pb loss, whereas the other two show no obvious differences from the main population but could reflect the effects of a younger intrusive event or thermal disturbance. There is also a grain yielding an older age of 160 ± 3 Ma, reflecting inheritance from Early Yanshanian granites in the area (for clarity, this is not shown on the concordia plot and neither is the grain dated at 100 ± 7 Ma (Table 2.4), due to its large error and therefore unreliable age).

Zircons from sample SD-31 show a wide range of values for initial $^{176}Hf/^{177}Hf$ from 0.281978 to 0.282224, with an average of 0.282134 (Table 2.5). The $\varepsilon_{Hf(t)}$ values range from -25.52 to -16.83 and T_{DM2} model ages from 3136 to 3900 Ma. The average T_{DM2} model age is 3419 Ma and the T_{DM1} model age is 1593 Ma.

The Yashan pluton was emplaced at 113 ± 2 Ma and contains monzonite enclaves with the slightly older age of 116 ± 1 Ma, consistent with the field evidence.

5.2.4. Laoshan Batholith

Sample SD-59: Zircons are brown in colour, prismatic, euhedral and are stubby to rounded in shape. All the zircons from this sample ranged in size from 50-120μm. Twelve analyses have U contents ranging from 183 to 1114 ppm, Th

contents from 303 to 2857 ppm and the $^{232}Th/^{238}U$ ratio ranges from 1.47 to 2.65, with an average value of 1.9 (Table 2.4). Ten grains have ages ranging from 111 Ma to 119 Ma and yield a $^{206}Pb/^{238}U$ concordia age of 115 ± 2 Ma (Fig. 2.10g), taken to record the emplacement age of the alkali granite. Two other grains have slightly younger ages of 108 ± 2 Ma and 109 ± 2 Ma and could reflect disturbance due to the emplacement of younger intrusions in the area.

Zircons from sample SD-59 have initial $^{176}Hf/^{177}Hf$ values ranging from 0.282132 to 0.282242, with an average value of 0.282186 (Table 2.5). The $\varepsilon_{Hf(t)}$ values range from -20.32 to -16.53 and T_{DM2} model ages range from 3096 to 3434 Ma. The average T_{DM2} model age is 3267 Ma and the T_{DM1} model age is 1625 Ma.

6. Discussion

Since the granitoids of this study post-date the proposed lithospheric thinning/delamination event in the NCC, their geochemistry potentially provides information about the nature of the lower crust at this time and how it was influenced by magmatic underplating associated with the loss of lithosphere (Menzies et al., 1993; Gao et al., 2004; Wu et al., 2005a; Liu et al., 2008a).

6.1. Timing of granitoid magmatism in Eastern Shandong

The age of the Mesozoic granitoid intrusions in the eastern NCC is generally divided into Early Yanshanian at ~180-150 Ma (Wang et al., 1998; Jahn et al., 2000; Zhou and Lu, 2000; Wilde et al., 2003; Liu et al., 2004; Wu et al., 2005c) and Late Yanshanian at ~140-120 Ma (Jahn et al., 2000; Wilde et al., 2003; Gao et al., 2004; Kusky et al., 2007; Yang et al., 2008a) (see Fig. 2.2). The main magmatic peak or 'Giant Igneous Event' in the eastern NCC proposed by Wu et al. (2005a) is described as taking place at ~130-120 Ma, with a peak at 125 Ma. The middle-late Mesozoic granitoids in Jiaodong can likewise be divided in two main groups (Table 2.6 and Fig. 2.2), an older group that was emplaced from ~160 to 140 Ma, namely the Kunyushan, Linglong, Wendeng and Duogushan granitoids (Yang et al., 2003; Guo

et al., 2005; Liu et al., 2009; Zhao and Zheng, 2009) and a younger group emplaced at ~130 to 122 Ma, including the Guojialing (Fig. 2.2), Wulian, Junan and Rizhao (see Fig. 2.1). granitoids (Guan et al., 1998; Wang et al., 1998; Yang et al., 2003; Zhang et al., 2003c; Yang et al., 2005; Liu et al., 2009; Zhao and Zheng, 2009). The only exception to this is the Haiyang suite, where the monzogranite has been dated, using SHRIMP zircon U-Pb, at 115 ± 2 Ma (Zhao and Zheng, 2009). There was also previous age data suggesting some of the granitoids sampled in this study were similarly younger than the typical Late Yanshanian suite (see Table 2.7).

Zircon U-Pb ages in our study suggest some influence from the main Late Yanshanian event, with ages of ~125-120 Ma, represented by Aishan sample SD-27 and the inherited zircon grains from samples SD-11, SD-12, SD-28 and SD-30. The 125 ± 3 Ma granitoid from Aishan is interpreted as representing one of the main Late Yanshanian intrusives. However excluding these, all four batholiths have very similar emplacement ages, with an average of 116 ± 2 Ma (see Table 2.7). So it appears they represent a single magmatic episode that either extends or post-dates Late Yanshanian magmatism in the Jiaodong Peninsula.

Previous SHRIMP zircon U-Pb data for the Sanfoshan Batholith (Guo et al., 2005) gave an age of 113 ± 1 Ma, which is younger than that recorded here, although the range of values obtained in their study (117 ± 5 to 108 ± 4 Ma) overlaps with the average age established here (118 ± 1 Ma). Previous zircon U-Pb dating of the Laoshan alkali granite gave an age of 111 ± 1 Ma (Zhao et al., 1998b), which is also slightly younger than that determined here (115 ± 2 Ma) (see Table 2.7).

The T_{DM2} ages of the samples are Paleo- to Neoarchean, ranging from 3900 Ma to 2491 Ma (average T_{DM2} age is 3126 Ma), implying Archean basement was the protolith. The difference between the U-Pb zircon ages and the Hf model ages suggests that there was a significant crustal residence time. The $\varepsilon_{Hf(t)}$ values for all samples have a fairly narrow range from -28.07 to -12.23, with an average of -19.06. This substantiates the involvement of older lower/recycled continental crustal material in the magma source.

The granitoids in this study were sampled because they were considered, albeit on scanty data, to be younger than the surrounding Late Yanshanian granitoids

and this has been proven correct. As noted above, they either extend the duration of the Late Yanshanian granitoid magmatism into the late Early Cretaceous or represent a discrete younger magmatic event. The chemistry of the samples can be used to evaluate whether they were similar to those emplaced during the Late Yanshanian, and we investigate this below.

6.2. Petrogenesis of the late granitoids

In terms of petrography, the QAP diagram of the granitoids, based on modal data (Fig. 2.4), yields slightly different results to that based on normative data (Fig. 2.11), largely due to differences in the two feldspar proportions. Other studies (Zhao et al., 1997; Wang et al., 2001) of granitoids in close proximity to our sampling locations describe rock types that agree well with the petrographic descriptions and classification used in this study.

Most samples plot as being chemically of I-type affinity (Fig. 2.7), except SD-59 which is A-type. The granitoids are metaluminous with low A/CNK values and A/NK values above 1.0 (Table 2.3) and this agrees with previous studies of typical Late Yanshanian granitoids (Zhou and Lu, 2000; Zhao and Zheng, 2009).

Fractional crystallization has taken place during formation of the granitoids. Plagioclase fractionation is shown by the negative Sr, Eu and Ba anomalies in many samples, apatite fractionation by the negative P and fractionation of Ti-bearing phases (ilmenite, titanate, etc) by the negative Nb-Ti anomalies in all samples (Fig. 2.9). Monzogranite sample SD-31 from the Yashan pluton underwent K-feldspar accumulation, as indicated by the positive Ba anomaly. The lack of negative Eu anomalies in the monzogranites suggests plagioclase fractionation was not significant during their petrogenesis.

Previous studies have concluded that the Late Yanshanian plutons were derived from the lower crust (Yang et al., 2004a; Zhang et al., 2006). There are several factors indicating a continental crustal influence on all the rock types, including; the negative $\varepsilon_{Hf(t)}$ values; strong negative anomalies in Nb, Ta, P and Ti with a strong positive Pb anomaly; the fact they are enriched in LREE and LILE but depleted in HFSE; and the low Ce/Pb ratios (0.53-5.88, Table. 2.3). These signatures

are most likely due to partial melting of continental crust chemically affected by a previous subduction event. The NCC had an Archean lower crust that is considered to be composed of mafic to felsic granulite and it has been shown to typically have low Rb (<11.2 ppm), to be enriched in Hf and strongly depleted in Zr, Th and U (Gao et al., 1998; Tang et al., 2008). These features are not found in the granitoids studied here, which suggests that the NCC lower crust was not the source for these rocks because it had been removed by prior delamination (see Discussion) and thus the most likely source was melting at higher crustal levels.

The presence of microgranular enclaves in the Yashan monzogranite implies one of two possibilities; either there were two magmatic events and the enclaves represent xenoliths formed by the early event, or they were coeval and reflect magma mixing. The more primitive nature of the Hf isotopic data in the enclave, with lower $\varepsilon_{Hf(t)}$ values and lower model ages, may support mixing of a mantle-derived magma with crustal rocks. Additionally the ages of the two samples overlap within error thus also suggest coeval magma mingling. A comparable study of the Early Cretaceous Gudaoling granitoids in Liaoning Province gave very similar geochemical signatures to those of this study (Yang et al., 2004a). In particular, the monzogranite chrondrite-normalized REE patterns determined here are identical to those of the monzonite enclaves in the Yang et al. (2004a) study. Yang et al. (2004a) concluded that the monzogranites were derived from partial melting of a juvenile basaltic lower crust and, like those sampled here from Eastern Shandong, the lack of Eu anomalies indicates that they did not undergo significant plagioclase fractionation; the monzonitic enclaves are considered to be derived from fractional crystallization of this parental magma.

On geochemical trace element tectonic setting discrimination diagrams (Pearce et al., 1984) (Fig. 2.12a-d), with the exception of sample SD-59 (Laoshan alkali granite) which consistently plots in the within-plate granite (WPG) field, the other samples range between volcanic-arc granite (VAG) and syn-collisional granite (syn-COLG) depending on the plot. On Figs. 2.12a and 2.12b, which are based on Rb content, samples plot mainly in the VAG field; on Fig. 2.12c samples are split

equally between VAG and syn-COLG and on Fig. 2.12d all samples plot in the VAG + syn-COLG field.

On a Hf-Rb/30-Ta*3 diagram (Fig. 2.13a) of Harris et al. (1986) which is designed to discriminate between syn- and post-collisional granites and to separate them from VAG and WPG, the following is found: samples SD-29 (Aishan monzogranite) and SD-30 (Yashan monzonite enclave) plot in the VAG field, samples SD-13 (Sanfoshan porphyritic granite) and SD-31 (Yashan monzogranite) plot in the syn-COLG field and all other samples plot in the late and post-COLG field.

On the $(K_2O+Na_2O)/CaO$ vs. Zr+Nb+Ce+Y (ppm) discrimination diagram of Whalen et al. (1987) (Fig. 2.13b), 5 samples (Sanfoshan samples SD-12 and SD-13 and Laoshan samples SD-56, SD-59 and SD-63) plot in the A-type field. When plotted on the multicationic plot (Fig. 2.13c) from Batchelor and Bowden (1985), modified from de la Roche et al. (1980), all these samples, together with sample SD-14 from Sanfoshan, plot in the anorogenic field. All these samples are syenogranites from the Sanfoshan and Laoshan batholiths.

A review of previous research on Late Yanshanian Cretaceous batholiths by Zhou and Lu (2000) concluded, based on the geochemistry and low initial $^{87}Sr/^{86}Sr$ ratios, that the granitoids were formed in a subduction-related continental and island arc setting. However Yang et al. (2005) and Zhao and Zheng (2009) suggest the Late Yanshanian rocks evolved in an extensional setting that effectively reworked the Early Yanshanian granitoids. Compared to available data from other Late Yanshanian granitoids in the study area in the age range ~130-120 Ma (Yang et al., 2005) it appears that the youngest granitoids sampled here have a different tectonic setting (Fig. 2.13a).

We propose that these granitoids are a result of partial melting of lower to middle crust that has a subduction component (i.e. negative Ta and Nb) and, since alkaline igneous rocks require high melting temperatures (Clemens et al., 1986), they were likely generated by emplacement of mantle-derived mafic magmas, thus causing melting of pre-existing rocks. The slightly older, more typical Late Yanshanian granitoids from previous studies that formed between ~130-120 Ma, plot

in the volcanic arc field. However the younger samples in this study (~118-110 Ma) indicate more extensive melting of the lower and middle crust suggesting that extension was possibly becoming more significant.

It is now necessary to evaluate what tectonic process caused not only formation of the latest Late Yanshanian granitoids, but also the evolution of the A-type anorogenic granites at ~120 Ma.

6.3. Tectonic implications

The tectonic setting of the eastern NCC during the Early Cretaceous was one of extension and lithospheric thinning (Zhou and Lu, 2000; Xu, 2001; Chen et al., 2003b; Liu et al., 2004; Xu et al., 2004b; Zhai et al., 2007). This is supported by the simultaneous development of pull-apart basins (Zhou and Lu, 2000; Guo et al., 2001; Meng, 2003; Menzies et al., 2007; Yang et al., 2008a), initiation of normal faults (Yang et al., 2007c), eruption of bimodal volcanic rocks, metamorphic core complex formation (Davies et al., 2001; Darby et al., 2004; Liu et al., 2005; Yang et al., 2007c; Yang et al., 2008b) and gold mineralization (Wang et al., 1998; Zhou and Lu, 2000; Yang and Zhou, 2001; Yang et al., 2003).

Lithospheric thinning has been attributed to various mechanisms including: chemical and thermal erosion by various means (Griffin et al., 1998; Menzies and Xu, 1998; Zheng et al., 1998; Xu, 2001; Zhang et al., 2004; Xu et al., 2004b; Niu et al., 2005; Zhang, 2005), partial or complete delamination (Zhang et al., 1998; O'Reilly et al., 2001; Zhou et al., 2002; Wilde et al., 2003; Gao et al., 2004) and decompressional melting (Gao et al., 1998). It is difficult to distinguish which of these was the mechanism involved, or if it was some combination. Indeed, it might have been an entirely different mechanism such as mechanical disruption. However, whatever the driving force, lithospheric thinning and extension would have allowed the asthenosphere to rise, raising the geotherm and generating the widespread magmatic activity seen in the eastern NCC.

Previous research has attempted to explain the ultimate tectonic cause that resulted in the lithospheric thinning and generation of granitoids in eastern NCC as being linked to one of the following: a) collision between the NCC and the SCC

(South China Craton) (Gao et al., 1998; Yang et al., 2007a; Yang et al., 2007b), b) collision between India and the Eurasian plate (Menzies et al., 1993), c) subduction of the Pacific plate beneath China (Tatsumoto et al., 1992; Fan et al., 2000; Yang et al., 2003; Wu et al., 2005a; Xu, 2007; Yang et al., 2007c) or d) a mantle plume (Deng et al., 2004). Collision between the NCC and SCC at ~240-220 Ma is no longer considered a viable mechanism, since lithospheric thinning has been shown by Bouguer gravity data to extend across this boundary, indicating that thinning must post-date the collision (Xu, 2007). Also, the location of the collision zone is over 1000 km away from the eastern NCC and so it is hard to explain how it could have generated these effects (Gao et al., 1998; Liu et al., 2006). The collision between India and the Eurasian plate is also thought an unlikely mechanism for lithospheric thinning, since the collision variously dated at 52 to 34 Ma (Hodges, 2000; Aitchison et al. 2007) significantly post-dates the onset of this extensional regime (Xu, 2007; Yang et al., 2007b). There is also no evidence for a mantle plume beneath the eastern NCC during the Cretaceous (Menzies et al., 1993; Van der Voo et al., 1999), with a lack of plume-related magmatism (Tatsumoto et al., 1992; Xu, 2007; Zhang et al., 2008) and seismic tomography that shows a horizontal slab lying at the mantle transition zone (the old Pacific plate) which would prevent a plume rising up from the lower mantle (Niu et al., 2005; Menzies et al., 2007; Pei et al., 2007). Furthermore, there are other cratons that show no spatial link between mantle plume locations and lithospheric thinning; the Kaapvaal Craton is located above a major geoid high however it has retained its physical and chemical integrity and the NAIP (North Atlantic Igneous Province) is evidence of an area above a plume where the cratonic keel has not been thinned or eroded by the plume; instead it appears to have deflected the volcanism (Menzies et al., 2007). This leaves the subduction of the Pacific plate beneath China as the most likely explanation for lithospheric thinning in the eastern NCC.

In summary, our model for the generation of the latest Cretaceous granitoids in Eastern Shandong is as follows. During the Early Cretaceous lithospheric thinning and extension was taking place as a result of Pacific Plate subduction beneath the eastern NCC. Dehydration of the subducting plate would allow fluids to rise upwards

into the overlying SCLM, causing hydration and weakening (Niu, 2005; Niu et al., 2005). This would aid subsequent lithospheric thinning and partial delamination, possibly with slab break-off, allowing asthenospheric uprise and elevation of the geotherm. This in turn led to partial melting of the lithospheric mantle and the mafic magmas resulting from this were emplaced as mafic dykes (125-90 Ma) in the lower crust (Fan et al., 2005). This provided the heat source for lower crustal melting which was ultimately the source of the volcanic-arc rocks (samples SD-29 and SD-30). Continued magma mixing and mingling between the mantle-derived mafic magmas and felsic crustal magmas produced the anorogenic rocks (samples SD-12, SD-13, SD-14, SD-56, SD-59 and SD-63) of the latest Late Yanshanian granitoids. The monzonite enclave sample SD-30 is further evidence of this magma mixing. It is impossible to determine the sequence of events from the rocks sampled here because the processes were ongoing; with simultaneous melting of lower and middle crust and the subduction signature found here is due to continuation of crustal melting

Conclusions

Our study of the youngest Cretaceous (Latest Yanshanian) granitoids of Shandong Province leads to the following conclusions:

1) The granitoids sampled here are younger than the typical Late Yanshanian granitoids in Shandong Province that were emplaced between ~130-120 Ma. The SHRIMP zircon U-Pb emplacement ages are as follows: Sanfoshan Batholith 118 ± 1 Ma, Aishan Batholith 116 ± 2 Ma, Yashan Pluton 113 ± 2 Ma and Laoshan Batholith 115 ± 2 Ma. The Paleo- to Neoarchean T_{DM2} model ages of zircons range from 3900 Ma to 2491 Ma, implying the involvement of Archean basement in the protolith and the negative $\varepsilon_{Hf(t)}$ values substantiate the incorporation of older continental crustal material in the magma source region.

2) Based on the geochemical signatures, such as the enrichment in LREE and depletion in HFSE, the negative $\varepsilon_{Hf(t)}$ values, the strong negative anomalies in Nb, Ta, P and Ti with a strong positive Pb anomaly, we conclude the granitoids were derived from partial melting of older lower to middle continental crust due to mafic magma underplating and heat transfer. All granitoid types studied here can be explained by various degrees of interaction between mantle-derived mafic magma and felsic crustal magma, followed by fractional crystallization. The monzonite enclave from the Yashan Pluton provides evidence that magma mixing between mantle-derived mafic magma and felsic crustal magmas occurred.

3) We consider that the latest Late Yanshanian granitoids represent a continuation of processes resulting from Pacific Plate subduction. In the early stages, this involved melting of the lower crust with a subduction signature, a feature typical of the Late Yanshanian granitoids in the Jiaodong Peninsula. With continued subduction, mafic underplating and lithospheric thinning, with possible delamination, this led to more extensive crustal melting with the generation of anorogenic magmas. Thus granitoid magmatism continued into the late Early Cretaceous in NE China.

Acknowledgements

We thank Yanbin Zhang for kindly undertaking the geochemical analyses. This work was supported by an International Postgraduate Research Scholarship (IPRS) to S. Goss; field and logistical support were provided by the Institute of Geology and Geophysics Chinese Academy of Sciences Beijing. This is The Institute for Geosciences (TIGeR) publication number 219.

References

Aitchison, J.C., Ali, J.R., Davies, A.M., 2007. When and where did India and Asia collide? Journal of Geophysical Research 112, 1-19.

Ames, L., Tilton, G.R., Zhou, G., 1993. Timing of collision of the Sino-Korean and Yangtze cratons: U-Pb zircon dating of coesite-bearing eclogites. Geology 21, 339-342.

Batchelor, R.A., Bowden, P., 1985. Petrogenetic interpretation of granitoid rock series using multicationic parameters. Chemical Geology 48, 43-55.

Chappell, B.W., White, A.J.R., 1992. I- and S-type granites in the Lachlan Fold Belt. Transactions, Royal Society of Edinburgh Earth Science 83, 1-26.

Chen, B., Jahn, B.M., Zhai, M., 2003b. Sr-Nd isotopic characteristics of the Mesozoic magmatism in the Taihang-Yanshan orogen, North China Craton and implications for Archaean lithosphere thinning. Journal of the Geological Society, London 160, 963-970.

Chen, J.F., Xie, Z., Li, H.M., Zhou, T.X., Park, Y.S., Ahn, K.S., Chen, D.G., Zhang, X., 2003a. U-Pb zircon ages for a collision-related K-rich complex at Shidao in the Sulu ultrahigh pressure terrane, China. Geochemical Journal 37, 35-46.

Clemens, J.D., Holloway, J.R., White, A.J.R., 1986. Origin of an A-type granite; experimental constraints. American Mineralogist 71, 317-324.

Darby, B.J., Davis, G.A., Zhang, X.H., Wu, F.Y., Wilde, S.A., Yang, J.H., 2004. The newly discovered Waziyu metamorphic core complex, YiwuluShan, western Liaoning Province, northwest China. Earth Science Frontiers 11, 145-155.

Davies, G.S., Zhang, Y.D., Wang, C., B.J., D., Zhang, C., Gehrels, G., 2001. Mesozoic tectonic evolution of the Yanshan fold and thrust belt, with emphasis on Hebei and Liaoning Provinces northern China. Geological Society of America Memoir 194, 171-197.

de la Roche, H., Leterrier, J., Grandclaude, P., Marchal, M., 1980. A classification of volcanic and plutonic rocks using R1-R2 diagram and major element analyses, its relationship with current nomenclature. Chemical Geology 29, 183-210.

Deng, J.F., Mo, X.X., Zhao, Z.D., Wu, Z.X., Luo, Z.H., Su, S.G., 2004. A new model for the dynamic evolution of Chinese lithosphere: 'continental roots-plume tectonics'. Earth Science Reviews 65, 223-275.

Deng, J.F., Su, S.G., Niu, Y., Liu, C., Zhao, G.C., Zhao, X., Zhou, S., Wu, Z.X., 2007. A possible model for the lithospheric thinning of North China Craton: evidence from the Yanshanian (Jura-Cretaceous) magmatism and tectonism. Lithos 96, 22-35.

Fan, Q., Zhang, H.F., Sui, J., Zhai, M., Sun, Q., Li, N., 2005. Magma underplating and Hannuoba present crust-mantle transitional zone composition: Xenolith petrological and geochemical evidence. Science in China, Series D Earth Sciences 48, 1089-1105.

Fan, W.M., Guo, F., Wang, Y.J., Lin, G., Zhang, M., 2001. Post-orogenic bimodal volcanism along the Sulu Orogenic Belt in Eastern China. Physics and Chemistry of the Earth, Part A: Solid Earth and Geodesy 26, 733-746.

Fan, W.M., Zhang, H.F., Baker, J., Jarvis, K.E., Mason, P.R.D., Menzies, M.A., 2000. On and Off the North China Craton: Where is the Archaean Keel? Journal of Petrology 41, 933-950.

Gao, S., Luo, T.C., Zhang, B.R., Zhang, H.F., Han, Y.W., Zhao, Z.D., Hu, Y.K., 1998. Chemical composition of the continental crust as revealed by studies in East China. Geochimica et Cosmochimia Acta 62, 1959-1975.

Gao, S., Rudnick, R.L., Carlson, R.W., McDonough, W.F., Liu, Y.S., 2002. Re-Os evidence for replacement of ancient mantle lithosphere beneath the North China craton. Earth and Planetary Science Letters 198, 307-322.

Gao, S., Rudnick, R.L., Yuan, H.L., Liu, X.M., Liu, Y.S., Xu, W.L., Ling, W.L., Ayers, J., Wang, X.C., Wang, Q.H., 2004. Recycling lower continental crust in the North China Craton. Nature 432, 892-897.

Green, T.H., 1995. Significance of Nb/Ta as an indicator of geochemical processes in the crust-mantle system. Chemical Geology 120, 347-359.

Griffin, W.L., Pearson, N.J., Belousova, E., Jackson, S.E., O'Reilly, S.Y., van Achterberg, E., Shee, S.R., 2000. The Hf isotope composition of cratonic

mantle: LAM-MC-ICPMS analysis of zircon megacrysts in kimberlites. Geochimica et Cosmochimia Acta 64, 133-147.

Griffin, W.L., Wang, X., Jackson, S.E., Pearson, N.J., O'Reilly, S.Y., Xu, X., Zhou, X., 2002. Zircon chemistry and magma mixing, SE China: In-situ analysis of Hf isotopes, Tonglu and Pingtan igneous complexes. Lithos 61, 237-269.

Griffin, W.L., Zhang, A., O'Reilly, S.Y., Ryan, C.G., 1998. Phanerozoic evolution of the lithosphere beneath the Sino-Korean Craton. In: Flower, M.F.J., Chung, S.L., Lo, C.H., Lee, T.Y. (Editors), Mantle Dynamics and Plate Interactions in East Asia. American Geophysics Union Geodynamics, pp. 107-126.

Guan, K., Luo, Z.K., Miao, L.C., Huang, J.Z., 1998. SHRIMP in zircon chronology for Guojialing suite granite in Jiaodong district. Scientia Geologica Sinica 33, 318-328.

Guo, F., Fan, W.M., Wang, Y.J., Lin, G., 2001. Late Mesozoic mafic intrusive complexes in North China Block: constraints on the nature of subcontinental lithospheric mantle. Physics and Chemistry of the Earth, Part A: Solid Earth and Geodesy 26, 759-771.

Guo, J.H., Chen, F.K., Zhang, X.M., Siebel, W., Zhai, M.G., 2005. Evolution of syn- to post-collisional magmatism from north Sulu UHP belt, eastern China: zircon U-Pb geochronology. Acta Petrologica Sinica 21, 1281-1301.

Harris, N.B.W., Pearce, J.A., Tindle, A.G., 1986. Geochemical characteristics of collision-zone magmatism. In: Coward, M.P., Reis, A.C. (Editors), Collision tectonics. Special Publication of Geological Society, pp. 67-81.

Hodges, K.V. 2000. Tectonics of the Himalaya and southern Tibet from two perspectives. Geological Society of America Bulletin 112, 324-350.

Hu, F., Fan, H., Yang, J.H., Wan, Y., Liu, D., Zhai, M.G., Jin, C., 2004. Mineralizing age of the Rushan lode gold deposit in the Jiaodong Peninsula: SHRIMP U-Pb dating on hydrothermal zircon. Chinese Science Bulletin 49, 1629-1636.

Hu, F.F., Fan, H.R., Zhai, M.G., Jin, C.W., 2006. Fluid evolution in the Rushan lode gold deposit of Jiaodong Peninsula, eastern China. Journal of Geochemical Exploration 89, 161-164.

Jahn, B.M., Wu, F.Y., Chen, B., 2000. Massive granitoid generation in Central Asia: Nd isotope evidence and implication for continental growth in the Phanerozoic. Episodes 23, 82-92.

Kusky, T.M., Li, J., 2003. Paleoproterozoic tectonic evolution of the North China Craton. Journal of Asian Earth Sciences 22, 383-397.

Kusky, T.M., Windley, B.F., Zhai, M., 2007. Tectonic evolution of the North China Block: from orogen to craton to orogen. Geological Society of London, Special Publication 280, 1-34.

Le Maitre, R.W., 1976. Some problems of the projection of chemical data into mineralogical classifications. Contributions to Mineral Petrology 56, 181-189.

Lee, C.Y., Tsai, J.H., Ho, H.H., Yang, T.F., Chung, S.L., Chen, C.H., 1997. Quantative analysis in rock samples by an X-ray fluorescence spectrometer, (I) major elements. Annual Meetings of the Geological Society of China 418-420.

Li, J.W., Paulo, V., Zhou, M.F., Zhao, X.F., Ma, C., 2006. Geochronology of the Pengjiakuang and Rushan Gold Deposits, Eastern Jiaodong Gold Province, Northeastern China: implications for regional mineralization and geodynamic setting. Economic Geology 101, 1023-1038.

Liu, D., Wilde, S.A., Wan, Y., Wu, J.S., Zhou, H., Dong, C., Yin, X., 2008b. New U-Pb and Hf isotopic data confirm Anshan as the oldest preserved segment of the North China Craton. American Journal of Science 308, 200-231.

Liu, D.Y., Nutman, A.P., Compston, W., Wu, J.S., Shen, Q.H., 1992. Remnants of ≥ 3800 Ma crust in the Chinese part of the Sino-Korean craton. Geology 20, 339-342.

Liu, J., Davis, G.A., Lin, Z., Wu, F.Y., 2005. The Liaonan metamorphic core complex, Southeastern Liaoning Province, North China: A likely contributor to Cretaceous rotation of Eastern Liaoning, Korea and contiguous areas. Tectonophysics 407, 65-80.

Liu, J., Zhang, H.F., Sun, J., Ye, J., 2004. Geochemical research on C-O and Sr-Nd isotopes of mantle-derived rocks from Shandong Province, China. Science in China, Series D Earth Sciences 47, 171-180.

Liu, S., Hu, R., Gao, S., Feng, C.X., Yu, B., Feng, G., Qi, Y.Q., Wang, T., Coulson, I.M., 2009. Petrogenesis of Late Mesozoic mafic dykes in the Jiaodong Peninsula, eastern North China Craton and implications for the foundering of lower crust. Lithos 13, 621-639.

Liu, S., Hu, R.Z., Gao, S., Feng, C.X., Qi, L., Zhong, H., Xiao, T.F., Qi, Y.Q., Wang, T., Coulson, I.M., 2008a. Zircon U-Pb geochronology and major, trace elemental and Sr-Nd-Pb isotopic geochemistry of mafic dykes in western Shandong Province, east China: constraints on their petrogenesis and geodynamic significance. Chemical Geology 255, 329-345.

Liu, S., Zou, H., Hu, R.Z., Zhao, J., Feng, C.X., 2006. Mesozoic mafic dikes from the Shandong Peninsula, North China Craton: petrogenesis and the tectonic implications. Geochemical Journal 40, 181-195.

Liu, X.S., Jin, W., Li, S.X., Xu, X.C., 1993. Two types of Precambrian high-grade metamorphism, Inner Mongolia, China. Journal of Metamorphic Geology 11, 499-510.

Ludwig, K.R., 2001a. SQUID 1.02: A user's manual. Special Publication, volume 2. Berkeley Geochronology Centre, Berkeley.

Ludwig, K.R., 2001b. Users manual for Isoplot/Ex (rev. 2.49): a geochronological toolkit for Microsoft Excel, Special Publication 1a. Berkeley Geochronology Center, Berkeley, CA (2001).

Maniar, P.D., Piccoli, P.M., 1989. Tectonic discrimination of granitoids. Geological Society of America Bulletin 101, 635-643.

Meng, Q.R., 2003. What drove late Mesozoic extension of the northern China-Mongolia tract? Tectonophysics 369, 155-174.

Menzies, M.A., Fan, W., Zhang, M., 1993. Palaeozoic and Cenozoic lithoprobes and the loss of >120 km of Archaean lithosphere, Sino-Korean craton, China. Geological Society of London, Special Publication 76, 71-81.

Menzies, M.A., Xu, Y.G., 1998. Geodynamics of the North China Craton. In: Flower, M.F.J., Chung, S.L., Lo, C.H., Lee, T.Y. (Editors), Mantle Dynamics and Plate Interactions in East Asia. American Geophysical Union, pp. 155-165.

Menzies, M.A., Xu, Y.G., Zhang, H.F., Fan, W.M., 2007. Integration of geology, geophysics and geochemistry: A key to understanding the North China Craton. Lithos 96, 1-21.

Middlemost, E.A.K., 1985. Magmas and magmatic rocks: an introduction to igneous petrology. Longman, New York.

Niu, Y., 2005. Generation and evolution of basaltic magmas: some basic concepts and a new view on the origin of Mesozoic-Cenozoic basaltic volcanism in Eastern China. Geological Journal of China Universities 11, 9-46.

Niu, Y., Song, S., Zhang, L., Deng, J.F., Mo, X.X., Su, S.G., Guo, Z., Liu, J., 2005. Slab dehydration, subcontinental lithospheric thinning and Mesozoic/Cenozoic volcanism in eastern China: A special consequence of plate tectonics, IUGS-SECE Conference, Peking University, Beijing, pp. 27-29.

Nomade, S., Pouclet, A., Chen, Y., 2002. The French Guyana doleritic dykes: geochemical evidence of three populations and new data for the Jurassic Central Atlantic Magmatic Province. Journal of Geodynamics 34, 595-614.

Nowell, G.M., Kempton, P.D., Noble, S.R., Fitton, J.G., Saunders, A.D., Mahoney, J.J., Taylor, R.N., 1998. High precision Hf isotope measurements of MORB and OIB by thermal ionisation mass spectrometry: insights into the depleted mantle. Chemical Geology 149, 211-233.

O'Reilly, S.Y., Griffin, W.L., Poudjom Djomani, Y.H., Morgan, P., 2001. Are lithospheres forever? Tracking changes in subcontinental lithospheric mantle through time. Geological Society of America Today 11, 4-10.

Pearce, J.A., Harris, N.B.W., Tindle, A.G., 1984. Trace element discrimination diagrams for the tectonic interpretation of granitic rocks. Journal of Petrology 25, 956-983.

Pei, S., Zhao, J., Sun, Y., Xu, Z., Wang, S., Liu, H., Rowe, C.A., Toksoz, M.N., Gao, X., 2007. Upper mantle seismic velocities and anisotropy in China determined through Pn and Sn tomography. Journal of Geophysical Research 112.

Pidgeon, R.T., Furfaro, D., Kennedy, A.K., Nemchin, A.A., van Bronswijk, W., Todt, W.A., 1994. Calibration of zircon standards for the Curtin SHRIMP II (abstract), Eighth International Conference on Geochronology, Cosmochronology and Isotope Geology, Berkeley, University of California, pp. 251.

Qiu, Y.M., Groves, D.I., McNaughton, N.J., Wang, L.G., Zhou, T., 2002. Nature, age and tectonic setting of granitoid-hosted, orogenic gold deposits of the Jiaodong Peninsula, eastern North China craton, China. Mineralium Deposita 37, 283-305.

Santosh, M., Wilde, S.A., Li, J.H., 2007. Timing of Paleoproterozoic ultrahigh-temperature metamorphism in the North China Craton: evidence from SHRIMP U-Pb zircon geochronology. Precambrian Research 159, 178-196.

SBGMR, 1991. Regional Geology of the Shandong Province, Geological Memories. Series 1 (in Chinese) 26. Geological Publishing House, Beijing, 699 pp.

Soderlund, U., Patchett, P.J., Vervoort, J.D., Isachsen, C.E., 2004. The 176Lu decay constant determined by Lu–Hf and U–Pb isotope systematics of Precambrian mafic intrusions. Earth and Planetary Science Letters 219, 311-324.

Song, B., Nutman, A.P., Liu, D.Y., Wu, J.S., 1996. 3800-2500 Ma crustal evolution in the Anshan area of Liaoning Province, northeastern China. Precambrian Research 78, 79-94.

Streckeisen, A.L., 1974. Classification and nomenclature of plutonic rocks. Geologische Rundschau 63 (2), 773-786.

Sun, S.S., McDonough, W.F., 1989. Chemical and isotopic systematics of oceanic basalts: implication for mantle composition and processes. In: A.D. Saunders, A.D., Norry, M.J. (Editors), Magmatism in the Ocean Basins Geological Society London, pp. 313-345.

Tang, H.Y., Zheng, J.P., Yu, C.M., 2008. Age and composition of the Rushan intrusive complex in the northern Sulu orogen, eastern China: petrogenesis and lithospheric mantle evolution. Geological Magazine 1, 1-17.

Tatsumoto, M., Basu, A.R., Wankang, H., Junwen, W., Guanghong, X., 1992. Sr, Nd and Pb isotopes of ultramafic xenoliths in volcanic rocks of Eastern China: enriched components EM1 and EM11 in subcontinental lithosphere. Earth and Planetary Science Letters 113, 107-128.

Trap, P., Faure, M., Lin, W., Bruguier, O., Monie, P., 2008. Contrasted tectonic styles for the Paleoproterozoic evolution of the North China Craton: evidence for a ~2.1 Ga thermal and tectonic event in the Fuping Massif. Journal of Structural Geology 30, 1109-1125.

Van der Voo, R., Spakman, W., Bijwaard, H., 1999. Mesozoic subducted slabs under Siberia. Nature 397, 246-249.

Wan, Y.S., Liu, D.Y., Song, B., Wu, J.S., Yang, C.H., Zhang, Z.Q., Geng, Y.S., 2005. Geochemical and Nd isotopic compositions of 3.8 Ga meta-quartz dioritic and trondhjemitic rocks from the Anshan area and their geological significance. Journal of Asian Earth Sciences 4, 563-575.

Wang, L.G., Qiu, Y.M., McNaughton, N.J., Groves, D.I., Luo, Z.K., Huang, J.Z., Miao, L.C., Liu, Y.K., 1998. Constraints on crustal evolution and gold metallogeny in the Northwestern Jiaodong Peninsula, China, from SHRIMP U-Pb zircon studies of granitoids. Ore Geology Reviews 13, 275-291.

Wang, R.C., Wang, D.Z., Zhao, G.T., Lu, J.J., Chen, X.M., Xu, S.J., 2001. Accessory mineral record of magma-fluid interaction in the Laoshan I- and A-type granitic complex, Eastern China. Physics and Chemistry of the Earth, Part A: Solid Earth and Geodesy 26, 835-849.

Wang, Z., 2009. Tectonic evolution of the Hengshan-Wutai-Fuping complexes and its implication for the Trans-North China Orogen. Precambrian Research 170, 73-87.

Wei, C.S., Zhao, Z.F., Spicuzza, M.J., 2008. Zircon oxygen isotopic constraint on the sources of Late Mesozoic A-type granites in eastern China. Chemical Geology 250, 1-15.

Wei, C.S., Zheng, Y.F., Zhao, Z.F., 2000. Hydrogen and oxygen isotope geochemistry of A-type granites in the continental margins of eastern China. Tectonophysics 328, 205-227.

Whalen, J.B., Currie, K.L., Chappell, B.W., 1987. A-type granites: geochemical characteristics, discrimination and petrogenesis. Contributions to Mineral Petrology 95, 407-419.

Wilde, S.A., Zhou, X., Nemchin, A.A., 2003. Mesozoic crust-mantle interaction beneath the North China craton: A consequence of the dispersal of Gondwanaland and accretion of Asia. Geology 31, 817-820.

Williams, I.S., 1998. U-Th-Pb geochronology by ion microprobe. In: McKibben, M.A., Shanks III, W.C., Ridley, W.I. (Editors), Applications of Microanalytical Techniques to Understanding Mineralizing Processes. Reviews in Economic Geoleogy, vol. 7, pp. 1-35.

Wu, C.H., Li, S.X., Gao, J.F., 1986. Archean and Paleoproterozoic metamorphic regions in the North China Craton. In: Dong, S.B. (Editor), Metamorphism and Crustal Evolution of China. Geological Publishing House, Beijing, pp. 53-89.

Wu, F.Y., Lin, J.Q., Wilde, S.A., Zhang, X.O., Yang, J.H., 2005a. Nature and significance of the Early Cretaceous giant igneous event in eastern China. Earth and Planetary Science Letters 233, 103-119.

Wu, F.Y., Yang, J.H., Wilde, S.A., Zhang, X.O., 2005c. Geochronology, petrogenesis and tectonic implications of Jurassic granites in the Liaodong Peninsula, NE China. Chemical Geology 221, 127-156.

Wu, F.Y., Yang, Y.H., Xie, L.W., Yang, J.H., Xu, P., 2006. Hf isotopic compositions of the standard zircons and baddeleyites used in U-Pb geochronology. Chemical Geology 234, 105-126.

Wu, F.Y., Zhao, G.C., Wilde, S.A., Sun, D.Y., 2005b. Nd constraints on crustal formation in the North China Craton. Journal of Asian Earth Sciences 24, 523-545.

Wu, J.S., Geng, Y.S., Shen, Q.H., Wan, Y.S., Liu, D.Y., Song, B., 1998. Archean geological characteristics and tectonic evolution of China-Korea Paleo-continent. Geological Publishing House, Beijing.

Xu, J.W., Zhu, G., 1994. Tectonic models of the Tan-Lu fault zone, eastern China. Geological Review 36, 771-784.

Xu, P., Wu, F.Y., Xie, L.W., Yang, Y.H., 2004a. Hf isotopic compositions of the standard zircons for U-Pb dating. Chinese Science Bulletin 49, 1642-1648.

Xu, Y.G., 2001. Thermo-tectonic destruction of the Archaean lithospheric keel beneath the Sino-Korean craton in China: evidence, timing and mechanism. Physics and Chemistry of the Earth, Part A: Solid Earth and Geodesy 26, 747-757.

Xu, Y.G., 2007. Diachronous lithospheric thinning of the North China Craton and formation of the Daxin'anling-Taihangshan gravity lineament. Lithos 96, 281-298.

Xu, Y.G., Huang, X.L., Ma, J.L., Wang, Y.B., Iizuka, Y., Xu, J.F., Wang, Q., Wu, X.Y., 2004b. Crust-mantle interaction during the tectono-thermal reactivation of the North China Craton: constraints from SHRIMP zircon U-Pb chronology and geochemistry of Mesozoic plutons from Western Shandong. Contributions to Mineral Petrology 147, 750-767.

Yang, J.H., Sun, J.F., Chen, F., Wilde, S.A., Wu, F.Y., 2007a. Sources and petrogenesis of Late Triassic dolerite dykes in the Liaodong Peninsula: implications for post-collisional lithosphere thinning of the Eastern North China Craton. Journal of Petrology 48, 1973-1997.

Yang, J.H., Wu, F.Y., Chung, S.L., Lo, C.H., Wilde, S.A., Davis, G.A., 2007c. Rapid exhumation and cooling of the Liaonan metamorphic core complex: Inferences from $^{40}Ar/^{39}Ar$ thermochronology and implications for Late Mesozoic extension in the eastern North China Craton. Geological Society of America Bulletin 119, 1405-1414.

Yang, J.H., Wu, F.Y., Chung, S.L., Wilde, S.A., Chu, M.F., 2004a. Multiple sources for the origin of granites: Geochemical and Nd/Sr isotopic evidence from the

Gudaoling granite and its mafic enclaves, northeast China. Geochimica et Cosmochimia Acta 68, 4469-4483.

Yang, J.H., Wu, F.Y., Chung, S.L., Wilde, S.A., Chu, M.F., Lo, C.H., Song, B., 2005. Petrogenesis of Early Cretaceous intrusions in the Sulu ultrahigh-pressure orogenic belt, east China and their relationship to lithospheric thinning. Chemical Geology 222, 200-231.

Yang, J.H., Wu, F.Y., Shao, J.A., Wilde, S.A., Xie, L.W., Liu, X.M., 2006. Constraints on the timing of uplift of the Yanshan Fold and Thrust Belt, North China. Earth and Planetary Science Letters 246, 336-352.

Yang, J.H., Wu, F.Y., Wilde, S.A., 2003. A review of the geodynamic setting of large-scale Late Mesozoic gold mineralization in the North China Craton: an association with lithospheric thinning. Ore Geology Reviews 23, 125-152.

Yang, J.H., Wu, F.Y., Wilde, S.A., Belousova, E., Griffin, W.L., 2008a. Mesozoic decratonization of the North China Block. Geology 36, 467-470.

Yang, J.H., Wu, F.Y., Wilde, S.A., Chen, F., Liu, X.M., Xie, L.W., 2008b. Petrogenesis of an alkali syenite-granite-rhyolite suite in the Yanshan Fold and Thrust Belt, Eastern North China Craton: geochronological, geochemical and Nd-Sr-Hf isotopic evidence. Journal of Petrology 49, 315-351.

Yang, J.H., Wu, F.Y., Wilde, S.A., Liu, X.M., 2007b. Petrogenesis of late Triassic granitoids and their enclaves with implications for post-collisional lithospheric thinning of the Liaodong Peninsula, North China Craton. Chemical Geology 242, 155-175.

Yang, J.H., Zhou, X.H., 2001. Rb-Sr, Sm-Nd and Pb isotopic systematics of pyrite: Implications for the age and genesis of lode gold deposits. Geology 29, 711-714.

Yang, Y.H., Wu, F.Y., Wilde, S.A., Liu, X.M., Zhang, Y.B., Xie, L.W., Yang, J.H., 2009. *In situ* perovskite Sr-Nd isotopic constraints on the petrogenesis of the Ordovician Mengyin kimberlites in the North China Craton. Chemical Geology 264, 24-42.

Ying, J., Zhou, X., Zhang, H., 2006. The geochemical variations of mid-Cretaceous lavas across western Shandong Province, China and their tectonic implications. International Journal of Earth Sciences 95, 68-79.

Yuan, H.L., Gao, S., Liu, X.M., Li, H.M., Gunther, D., Wu, F.Y., 2004. Accurate U-Pb age and trace element determinations of zircon by laser ablation-inductively coupled plasma mass spectrometry. Geostandards and Geoanalytical Research 28, 353-370.

Yuan, X.Y., 1996. Velocity structure of the Qinling lithosphere and mushroom cloud model. Science in China, Series D Earth Sciences 39, 233-244.

Zhai, M., Fan, Q., Zhang, H., Sui, J., Shao, J.A., 2007. Lower crustal processes leading to Mesozoic lithospheric thinning beneath eastern North China: underplating, replacement and delamination. Lithos 96, 36-54.

Zhang, H., Zhai, M., Tong, Y., Peng, P., Xu, B., Guo, J., 2006. Petrogenesis of the Sanfoshan High Ba-Sr granite, Jiaodong Peninsula, East China. Geological Review 52, 43-53.

Zhang, H.F., 2005. Transformation of lithospheric mantle through peridotite-melt reaction: A case of Sino-Korean craton. Earth and Planetary Science Letters 237, 768-780.

Zhang, H.F., Goldstein, S.L., Zhou, X.H., Sun, M., Zheng, J.P., Cai, Y., 2008. Evolution of subcontinental lithospheric mantle beneath eastern China: Re-Os isotopic evidence from mantle xenoliths in Paleozoic kimberlites and Mesozoic basalts. Contributions to Mineral Petrology 155, 271-293.

Zhang, H.F., Sun, M., 2002. Geochemistry of Mesozoic basalts and mafic dykes, southeastern North China Craton, and tectonic implications. International Geology Review 44, 370-382.

Zhang, H.F., Sun, M., Zhou, X.H., Fan, W.M., Zhai, M.G., Yin, J.F., 2002. Mesozoic lithosphere destruction beneath the North China Craton: evidence from major-, trace-element and Sr-Nd-Pb isotope studies of Fancheng basalts. Contributions to Mineral Petrology 144, 241-253.

Zhang, H.F., Sun, M., Zhou, X.H., Zhou, M.F., Fan, W.M., Zheng, J.P., 2003a. Secular evolution of the lithosphere beneath the eastern North China Craton:

evidence from Mesozoic basalts and high-Mg andesites. Geochimica et Cosmochimia Acta 67, 4373-4387.

Zhang, H.F., Ying, J.F., Shimoda, G., Kita, N.T., Morishita, Y., Shao, J.A., Tang, Y.J., 2007. Importance of melt circulation and crust-mantle interaction in the lithospheric evolution beneath the North China Craton: evidence from Mesozoic basalt-borne clinopyroxene xenocrysts and pyroxenite xenoliths. Lithos 96, 67-89.

Zhang, H.F., Ying, J.F., Xu, P., Ma, Y.G., 2004. Mantle olivine xenocrysts entrained in Mesozoic basalts from the North China craton: Implication for replacement process of lithospheric mantle. Chinese Science Bulletin 49, 961-966.

Zhang, M., Zhou, X.H., Zhang, J.B., 1998. Nature of the lithospheric mantle beneath NE China: evidence from potassic volcanic rocks and mantle xenoliths In: Flower, M.F.J., Chung, S.L., Lo, C.H., Lee, T.Y. (Editors), Mantle Dynamics and Plate Interactions in East Asia. American Geophysical Union, Washington, D.C., pp. 197-219.

Zhang, X., Cawood, P.A., Wilde, S.A., Liu, R., Song, H., Li, W., Snee, L.W., 2003c. Geology and timing of mineralization at the Cangshang gold deposit, north-western Jiaodong Peninsula, China. Mineralium Deposita 38, 141-153.

Zhang, Y., Dong, S., Shi, W., 2003b. Cretaceous deformation history of the middle Tan-Lu fault zone in Shandong Province, eastern China. Tectonophysics 363, 243-258.

Zhao, G.C., Cao, Q.C., Wang, D., Li, H., 1997. Zirconic U-Pb dating on the Laoshan granitoids and it's significance. Journal of Ocean University of Qingdao 27, 382-387.

Zhao, G.C., Cawood, P.A., Wilde, S.A., Sun, M., Lu, L., 2000. Metamorphism of basement rocks in the Central Zone of the North China Craton: implications for Paleoproterozoic tectonic evolution. Precambrian Research 103, 55-88.

Zhao, G.C., Sun, M., Wilde, S.A., Li, S.H., Liu, S., 2006. Composite nature of the North China Granulite-facies Belt: tectonothermal and geochronological constraints. Gondwana Research 9, 337-348.

Zhao, G.C., Sun, M., Wilde, S.A., Li, S.Z., 2005. Late Archean to Paleoproterozoic evolution of the North China Craton: key issues revisited. Precambrian Research 136, 177-202.

Zhao, G.C., Wilde, S.A., Cawood, P.A., Lu, L., 1998a. Thermal evolution of Archaean basement rocks from the Eastern part of the North China Craton and it's bearing on tectonic setting. International Geology Review 40, 706-721.

Zhao, G.C., Wilde, S.A., Cawood, P.A., Lu, L., 1999a. Thermal evolution of two textural types of mafic granulites in the North China craton: evidence for both mantle plume and collisional tectonics. Geological Magazine 136, 223-240.

Zhao, G.C., Wilde, S.A., Cawood, P.A., Lu, L., 1999b. Tectonothermal history of the basement rocks in the western zone of the North China Craton and it's tectonic implications. Tectonophysics 310, 37-53.

Zhao, G.C., Wilde, S.A., Cawood, P.A., Sun, M., 2001. Archean blocks and their boundaries in the North China Craton: lithological, geochemical, structural and *P-T* path constraints and tectonic evolution. Precambrian Research 107, 45-73.

Zhao, G.T., Wang, D.Z., Cao, Q.C., Yu, L.S., 1998b. Thermal evolution and it's significance of I-A type granitoid complex: The Laoshan granitoid as an example. Science in China, Series D Earth Sciences 41, 529-536.

Zhao, Z.F., Zheng, Y.F., 2009. Remelting of subducted continental lithosphere: petrogenesis of Mesozoic magmatic rocks in the Dabie-Sulu orogenic belt. Science in China, Series D Earth Sciences 52, 1295-1318.

Zheng, J., O'Reilly, S.Y., Griffin, W.L., Lu, F., Zhang, M., 1998. Nature and evolution of Cenozoic lithospheric mantle beneath Shandong Peninsula, Sino-Korean Craton, Eastern China. International Geology Review 40, 471-499.

Zheng, J., Sun, M., Lu, F., Pearson, N., 2003. Mesozoic lower crustal xenoliths and their significance in lithospheric evolution beneath the Sino-Korean Craton. Tectonophysics 361, 37-60.

Zhou, J.B., Wilde, S.A., Zhao, G.C., Zheng, C.Q., Jin, W., Zhang, X.Z., Cheng, H., 2008a. Detrital zircon U-Pb dating of low-grade metamorphic rocks in the

Sulu UHP belt: evidence for overthrusting of the North China Craton onto the South China Craton during continental subduction. Journal of the Geological Society, London 165, 423-433.

Zhou, J.B., Wilde, S.A., Zhao, G.C., Zheng, C.Q., Jin, W., Zhang, X.Z., Cheng, H., 2008b. SHRIMP U-Pb zircon dating of the Neoproterozoic Penglai Group and Archaean gneisses from the Jiaobei Terrane, North China, and their tectonic implications. Precambrian Research 160, 323-340.

Zhou, T., Lu, G., 2000. Tectonics, granitoids and Mesozoic gold deposits in East Shandong, China. Ore Geology Reviews 16, 71-90.

Zhou, X., Sun, M., Zhang, G., Chen, S., 2002. Continental crust and lithospheric mantle interaction beneath North China: isotopic evidence from granulite xenoliths in Hannuoba, Sino-Korean craton. Lithos 62, 111-124.

Zhu, G., Evans, J.A., Fitches, W.R., Fletcher, C.J.N., Rundle, C.R., Xu, J., 1994. Isotopic constraints on the Palaeozoic evolution of the Shandong Peninsula, N.E. China. Journal of Southeast Asian Earth Sciences 9, 241a-248.

2.2 FIGURE CAPTIONS FOR PAPER 1

Fig. 2.1 Simplified geological map showing the tectonic subdivision of the North China Craton, with distribution of the basement rocks (modified from Zhao et al., 2005). 1 = Mengyin kimberlite, 2 = Fuxian kimberlite.

Fig. 2.2 Simplified geological map showing the distribution of Early and Late Yanshanian plutonic rocks in Shandong Province (modified from the Shandong Bureau of Geology and Mineral Resources, 1991).

Fig. 2.3 Geological maps of the various plutons selected for study, showing sample locations. a) Aishan Batholith, b) Laoshan Batholith, c) Yashan Pluton and d) Sanfoshan Batholith.

Fig. 2.4 Modal QAP diagram classifying analyzed Shandong granitoids, after Streckeisen (1974).

Fig. 2.5 A/NK [molar ratio $Al_2O_3/(Na_2O+K_2O)$] vs. A/CNK [molar ratio $Al_2O_3/(CaO+Na_2O+K_2O)$] plot (Shand's Index) for the young Shandong granitoids, after Maniar and Piccoli (1989).

Fig. 2.6 Harker diagrams for the young Shandong granitoids. Plots of CaO, P_2O_5, Al_2O_3, Na_2O, K_2O, TiO, TFe_2O_3, MgO and Pb vs. SiO_2 (wt. %). Also plot of Sr vs. MgO.

Fig. 2.7 Zr vs. 10^4Ga/Al classification diagram for the young Shandong granitoids after Whalen et al. (1987). Symbols as on Fig. 2.5.

Fig. 2.8 Chrondrite-normalized REE diagrams of the young Shandong granitoids. Normalization values from Sun and McDonough (1989). a) All granitoids, b)

Monzogranites & Monzonite, c) Syenogranites and Alkali feldspar granite. Symbols as on Fig. 2.5.

Fig. 2.9 Primitive-mantle normalized REE diagrams of the young Shandong granitoids. Normalization values from Sun and McDonough (1989). a) All granitoids, b) Monzogranites & Monzonite, c) Syenogranites and Alkali feldspar granite. Symbols as on Fig. 2.5.

Fig. 2.10 SHRIMP zircon U-Pb concordia diagrams for the young Shandong granitoids a) Sanfoshan monzogranite sample SD-11, b) Sanfoshan syenogranite sample SD-12, c) Aishan monzogranite sample SD-27, d) Aishan monzogranite sample SD-28, e) Yashan monzonite sample SD-30, f) Yashan monzogranite sample SD-31 and g) Laoshan alkali feldspar granite sample SD-59.

Fig. 2.11 Normative QAP diagram used to classify the young Shandong granitoids geochemically analyzed in this study. After Streckeisen (1974). Symbols as on Fig. 2.5.

Fig. 2.12 Trace element tectonic discrimination diagrams from Pearce et al. (1984). a) Rb vs. Y+Nb, b) Rb vs. Yb+Ta, c) Ta vs. Yb and d) Nb vs. Y. Granite fields are as follows: WPG = within-plate, VAG = volcanic-arc, syn-COLG = syn-collisional and ORG = ocean-ridge granites. Symbols as on Fig. 2.5.

Fig. 2.13 Tectonic setting discrimination diagrams for the young Shandong granitoids a) Hf-Rb/30-Ta x 3 diagram for granites after Harris et al. (1986), b) multicationic plot after Batchelor and Bowden (1985) modified from de la Roche et al. (1980) and c) (K_2O+Na_2O)/CaO vs. Zr+Nb+Ce+Y (ppm) discrimination diagram after Whalen et al. (1987) where FG = Fractionated felsic granites, OGT = unfractionated M-, I- and S-type granites. The other Late Yanshanian monzogranite (+) data plotted in a) are from Yang et al. (2005), other symbols as on Fig. 2.5.

2.3 TABLES FOR PAPER 1

TABLE 2.1

Granitoid sample locations in this study, with GPS locations

PLUTON NAME	SAMPLE ID	GPS LOCATION
Sanfoshan	SD-11*	36° 58' 34.7" (N) 121° 43' 29.1" (E)
	SD-12*	36° 58' 34.7" (N) 121° 43' 29.1" (E)
	SD-13	36° 55' 17.7" (N) 121° 39' 17.4" (E)
	SD-14	36° 55' 40.9" (N) 121° 39' 50.6" (E)
	SD-17	36° 55' 57.2" (N) 121° 43' 53.7" (E)
Aishan	SD-27*	37° 24' 47.8" (N) 120° 46' 33.5" (E)
	SD-28*	37° 24' 46.7" (N) 120° 46' 33.3" (E)
	SD-29	37° 25' 56.9" (N) 120° 48' 29.8" (E)
Yashan	SD-30*	37° 12' 08.5" (N) 120° 59' 54.0" (E)
	SD-31*	37° 12' 08.5" (N) 120 59' 54.0" (E)
Laoshan	SD-56*	36° 16' 02.4" (N) 120° 35' 11.0" (E)
	SD-59	36° 16' 02.4" (N) 120° 35' 11.0" (E)
	SD-63	36° 04' 49.1" (N) 120° 26' 01.3" (E)

* denotes samples selected for detailed petrographic analysis, SHRIMP U-Pb zircon dating and Lu-Hf isotopic analysis in addition to geochemical study

TABLE 2.2

Modal mineral abundances for Shandong granitoids determined from point counting

Pluton name	**Sanfoshan**	**Aishan**	**Aishan**	**Yashan**	**Yashan**	**Laoshan**
Rock type	Monzo-granite	Monzo-granite	Monzo-granite	Monzonite	Monzo-granite	Alkali feldspar granite
Sample ID	SD-11	SD-27	SD-28	SD-30	SD-31	SD-59
Number of slides counted	3	3	3	1	3	3
Total number of counts	6097	5603	5712	1886	6066	6152
Total approx area counted (mm^2)	2616	2506	2509	782	2565	2456
Quartz	31.3	34.5	23.4	0.0	20.5	24.2
Plagioclase feldspar	36.1	32.4	33.3	44.0	38.8	
K-feldspar	28.4	29.9	33.2	27.0	27.7	
Alkali feldspar						73.4
Biotite	2.5	1.2	4.9	10.2	5.5	0.3
Myrmekite	0.2	1.1	0.1	0.5	0.7	0.1
Hornblende (Green)			4.0	10.6	4.6	
Hornblende (Brown)			0.1			
Opaque oxides	0.6	0.4	0.5	1.4	0.8	1.9
Titanite	0.4	0.3	0.3	1.3	0.3	<0.1
Chlorite	0.3			2.7	0.6	
Epidote	0.1	<0.1	0.1	1.0	0.3	1.0
Apatite	0.1	<0.1	<0.1	0.5	<0.1	<0.1
Calcite				0.8	0.1	
Calculated values [1]						
Q	31	35	23	0	21	24
A	44	48	50	38	42	73
P [2]	56	52	50	62	58	0

[1] QAP represent quartz, plagioclase and alkali feldspar, respectively (with P and A proportioned to the nearest whole number); [2] indicates inclusion of mymekite

TABLE 2.3 Major oxide (wt. %), CIPW norms, trace element and REE (ppm) geochemistry for Shandong granitoids. Monzo = monzogranite, syeno = syenogranite, alk. felds. granite = alkali feldspar granite

Sample ID	**SD-11**	**SD-12**	**SD-13**	**SD-14**	**SD-17**	**SD-27**	**SD-28**	**SD-29**	**SD-30**	**SD-31**	**SD-56**	**SD-59**	**SD-63**
Pluton Name	Sanfoshan	Sanfoshan	Sanfoshan	Sanfoshan	Sanfoshan	Aishan	Aishan	Aishan	Yashan	Yashan	Laoshan	Laoshan	Laoshan
Rock Type	monzo	aplitic syeno	porphyry	syeno	monzo	monzo	monzo	monzo	monzonite	monzo	syeno	alk. felds. granite	syeno
Major Elements (wt. %)													
SiO_2	76.02	74.65	76.52	76.07	72.81	76.51	70.08	70.99	56.09	67.49	74.09	75.29	73.51
TiO_2	0.16	0.11	0.07	0.18	0.23	0.12	0.42	0.32	0.81	0.41	0.27	0.18	0.34
Al_2O_3	12.61	12.70	13.31	12.52	13.91	12.57	13.93	14.55	17.42	15.52	13.23	12.87	13.67
TFe_2O_3	1.17	1.01	0.63	1.07	1.75	0.90	2.87	2.19	6.73	3.25	1.60	1.25	1.63
FeO	0.50	0.39	0.27	0.45	0.74	0.39	1.29	1.02	3.37	1.53	0.68	0.51	0.70
Fe_2O_3	0.67	0.62	0.36	0.62	1.01	0.51	1.58	1.17	3.36	1.72	0.92	0.74	0.93
FeOT	1.06	0.91	0.57	0.96	1.57	0.81	2.58	1.97	6.06	2.93	1.44	1.13	1.47
MnO	0.03	0.01	0.03	0.02	0.05	0.01	0.06	0.04	0.12	0.06	0.05	0.11	0.06
MgO	0.24	0.20	0.05	0.20	0.45	0.17	1.67	1.16	3.87	1.83	0.39	0.02	0.37
CaO	0.90	0.22	0.19	0.70	1.33	0.92	2.67	2.42	6.21	3.41	0.96	0.15	1.07
Na_2O	3.62	2.29	4.24	3.50	3.95	3.49	3.65	4.08	4.58	4.04	4.04	4.64	4.21
K_2O	4.89	7.75	4.56	5.24	4.97	4.90	4.36	3.71	2.53	3.70	4.85	4.83	4.92
P_2O_5	0.05	0.01	0.02	0.04	0.08	0.03	0.20	0.14	0.49	0.17	0.07	0.01	0.08
LOI	0.14	0.30	0.48	0.28	0.20	0.10	0.28	0.26	1.30	0.38	0.36	0.34	0.22
TOTAL	99.84	99.27	100.09	99.83	99.73	99.72	100.19	99.86	100.15	100.27	99.92	99.68	100.07
CIPW norms													
Quartz	34.21	31.13	34.00	34.09	27.57	35.44	24.94	26.49	2.71	20.36	29.74	29.70	27.68
Plagioclase	34.47	20.85	36.88	32.75	39.18	33.78	39.66	45.17	58.91	47.52	38.01	39.53	39.56

Orthoclase	28.96	46.27	27.07	31.08	29.49	29.08	25.77	21.98	15.13	21.87	28.78	28.72	29.13
Corundum		0.08	1.09										
Diopside	0.37			0.30	0.66	0.21	2.76	0.81	6.81	2.47	0.64	0.54	0.88
Hypersthene	0.58	0.54	0.26	0.44	1.05	0.44	3.36	2.96	8.85	4.23	0.80		0.60
Wollastonite												0.02	
Ilmenite	0.30	0.23	0.13	0.34	0.44	0.23	0.80	0.61	1.56	0.78	0.51	0.34	0.65
Magnetite	0.97	0.91	0.52	0.90	1.46	0.74	2.29	1.70	4.93	2.49	1.33	1.07	1.35
Apatite	0.12	0.02	0.05	0.09	0.19	0.07	0.46	0.32	1.16	0.39	0.16	0.02	0.19
Zircon	0.03	0.01	0.01	0.03	0.03	0.01	0.03	0.03	0.04		0.04	0.06	0.04
Chromite										0.01			
Trace Elements & REE (ppm)													
Li	17.4	8.0	4.4	4.4	17.0	23.3	21.8	16.3	37.9	18.9	22.2	10.8	20.0
Be	2.6	0.6	5.0	3.4	3.3	2.3	2.3	1.9	3.4	1.8	3.4	5.4	3.5
Sc	1.3	0.4	2.5	1.1	2.4	0.6	5.2	3.9	12.5	5.1	2.9	1.8	2.9
V	11	5	2	10	19	10	46	34	120	54	21	4	18
Cr	4	1	1	2	5	6	34	24	25	38	3	1	2
Co	1	4	0	1	2	1	7	5	18	8	2	0	2
Ni	3	1	1	1	3	3	40	10	22	15	2	1	53
Cu	3	54	2	13	2	3	22	5	11	3	3	2	4
Zn	20	10	21	11	28	15	47	43	66	42	28	61	34
Ga	13	11	19	14	15	12	17	16	22	17	15	20	16
Rb	177	113	305	234	149	152	126	125	114	92	145	186	143
Sr	119	270	34	87	302	114	541	532	750	796	141	21	154
Y	11.2	2.5	7.0	15.7	16.7	4.5	12.9	6.9	23.7	11.2	19.5	29.4	26.6
Zr	126	42	67	139	177	83	150	149	203	14	225	290	242
Nb	15.0	8.9	21.1	22.3	19.8	10.0	15.0	7.8	14.4	8.4	25.5	43.0	26.9
Cs	2.3	1.3	5.2	3.8	1.8	1.1	1.5	2.3	3.6	1.4	1.2	0.6	0.9

Ba	237	713	83	229	927	158	898	960	822	1792	554	80	613
La	28.45	9.75	12.25	46.00	64.77	28.20	66.54	33.65	49.13	47.28	50.11	36.18	58.56
Ce	48.37	14.13	19.15	77.58	107.97	46.26	115.77	58.27	100.30	79.60	85.55	71.51	103.55
Pr	5.30	1.54	2.27	7.63	10.56	4.63	13.45	6.12	13.69	9.21	9.56	6.71	11.03
Nd	15.48	4.44	6.56	22.34	31.54	12.81	42.75	20.04	49.14	28.16	27.67	18.43	32.90
Sm	2.21	0.61	0.96	3.55	4.88	1.45	5.63	3.19	7.95	4.05	4.14	3.29	5.95
Eu	0.44	0.41	0.13	0.41	0.85	0.34	1.45	0.83	1.84	1.27	0.76	0.29	0.84
Gd	1.80	0.45	0.75	2.58	3.48	1.07	4.03	2.19	6.07	3.18	3.43	3.13	4.49
Tb	0.23	0.06	0.11	0.37	0.46	0.12	0.44	0.27	0.75	0.35	0.45	0.53	0.70
Dy	1.41	0.32	0.68	2.07	2.42	0.64	2.24	1.25	4.08	1.92	2.82	3.89	3.83
Ho	0.33	0.07	0.16	0.45	0.51	0.14	0.45	0.23	0.85	0.38	0.63	0.95	0.88
Er	0.93	0.22	0.56	1.33	1.45	0.39	1.10	0.57	2.08	0.96	1.70	2.81	2.50
Tm	0.18	0.04	0.11	0.23	0.24	0.07	0.18	0.09	0.34	0.14	0.29	0.51	0.42
Yb	1.49	0.30	0.98	1.65	1.68	0.60	1.31	0.55	2.25	1.02	2.29	4.06	2.62
Lu	0.24	0.05	0.18	0.27	0.28	0.10	0.19	0.09	0.36	0.13	0.33	0.59	0.44
Hf	3.9	1.8	3.5	4.2	5.0	2.8	3.9	3.7	5.1	0.7	6.0	8.8	7.1
Ta	1.28	0.96	1.61	1.77	1.54	1.07	1.45	0.60	0.87	0.64	1.67	2.53	1.85
Pb	29	25	36	17	22	27	22	21	17	19	19	21	24
Th	37.5	14.4	26.1	43.5	28.8	38.3	33.5	13.5	9.3	14.7	15.5	20.7	16.2
U	4.9	13.9	4.2	8.2	8.5	4.9	5.6	2.6	6.4	1.7	2.0	3.3	2.9
Eu/Eu*	0.58	2.33	0.48	0.44	0.65	0.09	0.98	0.97	0.80	1.07	0.64	0.28	0.52
Ce/Yb_{CN}	9.04	13.26	5.44	13.02	17.85	21.56	24.57	29.40	12.39	21.58	10.37	4.89	10.99
Gd/Yb_{CN}	1.00	1.26	0.63	1.29	1.71	1.49	2.55	3.29	2.23	2.57	1.24	0.64	1.42
Nb/Ta	11.74	9.24	13.10	12.59	12.92	9.40	10.31	12.96	16.56	13.15	15.27	17.01	14.50
Ce/Pb	9.32	25.47	29.29	13.98	6.18	11.58	8.18	26.06	10.14	10.62	3.70	0.97	2.02

TABLE 2.4 SHRIMP U-Pb geochronology results for Shandong granitoids

Spot	% $^{206}Pb_c$	ppm U	ppm Th	$^{232}Th/^{238}U$	ppm $^{206}Pb^*$	$^{207}Pb^*/^{206}Pb^*$	±%	$^{207}Pb^*/^{235}U$	±%	$^{206}Pb^*/^{238}U$	±%	err corr	$^{207}Pb^*/^{206}Pb^*$ Age		$^{206}Pb^*/^{238}U$ Age	
Sanfoshan Monzogranite (SD-11)																
1	3.31	753	664	0.91	12	0.0525	19.0	0.1342	19.1	0.0185	1.2	0.064	308	±433	118.4	±1
2	0.32	863	1135	1.36	14	0.0465	3.1	0.1192	3.2	0.0186	0.7	0.214	24	±74	118.8	±1
3	0.22	876	805	0.95	14	0.0459	3.4	0.1183	3.5	0.0187	0.7	0.192	-7	±83	119.4	±1
4	0.44	888	608	0.71	14	0.0452	3.5	0.1158	3.6	0.0186	0.7	0.188	-42	±85	118.6	±1
5	0.22	1313	1326	1.04	21	0.0473	2.0	0.1211	2.1	0.0186	0.5	0.257	65	±48	118.6	±1
6	0.16	1192	1488	1.29	19	0.0461	3.2	0.1203	3.3	0.0189	0.6	0.197	3	±77	120.9	±1
7	0.16	1992	3881	2.01	32	0.0470	1.7	0.1226	1.7	0.0189	0.4	0.251	47	±40	121.0	±1
8	0.25	1095	1160	1.09	17	0.0470	3.3	0.1187	3.3	0.0183	0.6	0.181	47	±78	117.1	±1
9	3.30	137	33	0.25	4	0.0260	32.3	0.1070	32.3	0.0299	1.7	0.052			189.9	±3
10	1.16	760	910	1.24	12	0.0444	6.3	0.1119	6.3	0.0183	0.8	0.121	-86	±154	116.7	±1
11	0.44	917	732	0.82	14	0.0455	4.3	0.1147	4.4	0.0183	0.7	0.154	-29	±104	116.8	±1
12	0.64	627	739	1.22	10	0.0440	6.7	0.1091	6.8	0.0180	0.9	0.126	-113	±166	115.0	±1
Sanfoshan Syenogranite (SD-12)																
1	0.38	793	727	0.95	12	0.0450	5.0	0.1119	5.2	0.0180	1.1	0.211	-55	±120	115.2	±1
2	0.65	892	623	0.72	14	0.0434	5.5	0.1099	5.6	0.0184	0.7	0.127	-145	±140	117.4	±1
3	0.64	1145	1211	1.09	18	0.0424	4.0	0.1073	4.0	0.0184	0.7	0.162	-204	±100	117.3	±1
4	3.58	782	1358	1.79	13	0.0485	10.6	0.1200	11.0	0.0180	0.9	0.083	122	±250	114.9	±1
5	0.84	700	475	0.70	10	0.0425	5.8	0.0974	6.2	0.0166	2.2	0.353	-196	±150	106.3	±2
6	0.60	890	752	0.87	14	0.0442	4.1	0.1125	4.2	0.0184	0.7	0.174	-99	±100	117.8	±1
7	0.32	853	1009	1.22	14	0.0499	4.5	0.1281	4.6	0.0186	0.7	0.155	189	±110	119.0	±1

8	0.59	511	390	0.79	8	0.0426	5.3	0.1047	5.4	0.0178	1.2	0.230	-189	±130	113.8	±1
9	1.13	344	343	1.03	5	0.0435	9.2	0.1100	9.3	0.0183	1.1	0.122	-140	±230	116.9	±1
10	0.93	1399	1700	1.26	22	0.0465	4.5	0.1176	4.6	0.0183	0.6	0.125	23	±110	117.2	±1
11	2.21	5820	1753	0.31	99	0.0476	3.2	0.1268	3.2	0.0193	0.3	0.091	81	±77	123.3	±0
12	1.18	2482	4119	1.71	42	0.0512	3.3	0.1374	3.3	0.0195	0.4	0.129	249	±75	124.3	±1
Aishan Monzogranite (SD-27)																
1	1.16	318	362	1.18	5	0.0416	13.5	0.1138	13.7	0.0199	2.2	0.161	-253	±343	126.7	±3
2	2.76	205	174	0.88	3	0.0291	30.8	0.0764	30.9	0.0190	2.8	0.091			121.6	±3
3	0.47	214	275	1.33	4	0.0481	9.0	0.1320	9.4	0.0199	2.9	0.311	103	±212	127.1	±4
4	0.92	206	193	0.97	4	0.0455	14.3	0.1258	14.5	0.0201	2.4	0.163	-29	±346	128.0	±3
5	0.84	369	434	1.21	6	0.0418	9.4	0.1152	9.7	0.0200	2.2	0.225	-236	±238	127.5	±3
6	2.76	334	381	1.18	6	0.0280	21.0	0.0729	21.1	0.0189	2.2	0.104			120.6	±3
7	0.85	1361	1326	1.01	23	0.0473	4.0	0.1251	4.5	0.0192	2.0	0.442	63	±96	122.5	±2
8	0.53	390	491	1.30	7	0.0436	7.0	0.1204	7.3	0.0200	2.1	0.288	-134	±172	127.9	±3
9	0.00	1712	1098	0.66	29	0.0496	1.4	0.1340	2.4	0.0196	2.0	0.817	177	±32	125.0	±2
10	1.68	409	261	0.66	7	0.0369	15.3	0.0932	15.5	0.0183	2.2	0.140	-566	±413	117.0	±3
11	2.40	202	227	1.16	3	0.0295	42.7	0.0774	42.8	0.0190	2.7	0.063			121.6	±3
12	1.28	343	421	1.27	6	0.0381	14.7	0.1009	14.8	0.0192	2.2	0.146	-476	±389	122.5	±3
Aishan Monzogranite (SD-28)																
1	3.49	321	308	0.99	5	0.0223	31.0	0.0560	31.0	0.0183	2.2	0.072	0	0	116.8	±3
2	1.55	215	183	0.88	4	0.0374	15.0	0.0980	15.0	0.0190	2.2	0.148	-526	±400	121	±3
3	2.21	319	375	1.21	5	0.0305	20.0	0.0800	20.0	0.0190	2.2	0.111	-1104	±600	121.5	±3
4	1.86	254	228	0.93	4	0.0334	25.0	0.0820	26.0	0.0178	2.4	0.093	-839	±730	113.8	±3
5	0.00	270	219	0.84	4	0.0544	4.8	0.1455	5.3	0.0194	2.1	0.401	387	±110	123.9	±3
6	0.79	561	634	1.17	9	0.0414	6.2	0.1015	6.5	0.0178	2.0	0.316	-265	±160	113.7	±2
7	2.67	244	200	0.84	4	0.0292	24.0	0.0740	24.0	0.0184	2.3	0.095	0	0	117.2	±3
8	2.19	207	211	1.06	3	0.0324	27.0	0.0810	27.0	0.0182	2.4	0.089	-926	±790	116	±3

9	3.43	249	192	0.80	4	0.0200	65.0	0.0490	65.0	0.0174	2.6	0.041	0	0	111.1	±3
10	1.36	261	216	0.85	4	0.0363	15.0	0.0960	15.0	0.0192	2.2	0.145	-607	±410	122.6	±3
11	0.23	1644	2243	1.41	29	0.0467	2.3	0.1314	3.0	0.0204	2.0	0.650	34	±55	130.2	±3
12	2.28	303	279	0.95	5	0.0311	22.0	0.0780	22.0	0.0182	2.2	0.102	-1050	±660	116.1	±3
Yashan Monzonite (SD-30)																
1	0.70	1278	2597	2.10	20	0.0453	4.6	0.1133	6.9	0.0181	5.2	0.747	-37	±110	115.8	±6
2	2.50	96	48	0.52	2	0.0430	29.0	0.1070	29.0	0.0183	2.5	0.084	-193	±730	116.7	±3
3	0.46	576	700	1.25	9	0.0457	4.3	0.1148	4.5	0.0182	1.3	0.299	-18	±100	116.4	±2
4	0.64	2279	3856	1.75	35	0.0487	2.7	0.1179	3.0	0.0176	1.2	0.411	135	±63	112.1	±1
5	0.65	1544	2854	1.91	24	0.0468	3.1	0.1160	3.3	0.0180	1.2	0.368	39	±74	114.9	±1
6	3.34	165	119	0.75	3	0.0350	27.0	0.0840	27.0	0.0174	2.1	0.078	-705	±740	111	±2
7	0.88	308	249	0.83	5	0.0445	8.3	0.1147	8.4	0.0187	1.5	0.183	-85	±200	119.5	±2
8	2.30	465	571	1.27	7	0.0391	14.0	0.0900	14.0	0.0166	1.5	0.112	-411	±360	106.4	±2
9	1.81	462	642	1.44	7	0.0409	11.0	0.1020	11.0	0.0181	1.5	0.132	-292	±290	115.7	±2
10	0.69	1091	1748	1.66	17	0.0432	4.5	0.1079	4.7	0.0181	1.3	0.273	-153	±110	115.6	±2
11	0.55	1048	51	0.05	17	0.0443	3.8	0.1160	4.0	0.0190	1.3	0.317	-96	±94	121.4	±2
12	0.31	1227	863	0.73	20	0.0484	2.5	0.1235	2.8	0.0185	1.3	0.471	121	±59	118.1	±2
13	0.52	3072	10224	3.44	47	0.0503	2.5	0.1237	6.6	0.0178	6.1	0.924	210	±59	113.9	±7
14	0.84	397	406	1.06	6	0.0456	7.7	0.1136	7.8	0.0181	1.5	0.188	-25	±190	115.5	±2
15	0.48	902	37	0.04	15	0.0459	4.1	0.1184	4.3	0.0187	1.3	0.308	-10	±99	119.6	±2
Yashan Monzogranite (SD-31)																
1	1.36	226	210	0.96	3	0.0412	12.0	0.0920	12.0	0.0162	1.6	0.135	-275	±300	103.7	±2
2	0.07	1177	1814	1.59	17	0.0497	2.1	0.1137	2.4	0.0166	1.2	0.512	180	±48	106.2	±1
3	0.53	275	230	0.86	4	0.0506	5.8	0.1224	6.0	0.0175	1.5	0.248	225	±130	112	±2
4	1.58	201	177	0.91	3	0.0441	12.0	0.1080	12.0	0.0178	1.7	0.137	-106	±300	113.9	±2
5	2.06	218	115	0.55	3	0.0418	15.0	0.1050	15.0	0.0182	1.7	0.112	-238	±380	116.5	±2
6	1.10	245	195	0.82	4	0.0431	11.0	0.1020	11.0	0.0171	1.6	0.147	-161	±270	109.2	±2

7	2.51	187	198	1.10	3	0.0325	23.0	0.0770	23.0	0.0171	1.8	0.081	-917	±660	109.4	±2
8	0.04	195	170	0.90	3	0.0506	4.3	0.1252	4.6	0.0179	1.6	0.346	225	±99	114.6	±2
9	1.95	144	144	1.03	2	0.0434	17.0	0.1040	17.0	0.0173	1.9	0.112	-146	±420	110.8	±2
10	1.45	241	237	1.02	4	0.0452	12.0	0.1130	12.0	0.0181	1.6	0.131	-44	±300	115.7	±2
11	1.49	381	560	1.52	6	0.0402	11.0	0.0990	11.0	0.0179	1.5	0.133	-338	±280	114.3	±2
12	1.25	308	294	0.99	4	0.1960	51.0	0.4200	51.0	0.0156	7.0	0.136	2790	±830	99.8	±7
13	1.57	123	115	0.97	3	0.3988	2.0	1.3790	2.6	0.0251	1.8	0.674	3905	±29	159.7	±3
Laoshan Alkali Granite (SD-59)																
1	0.10	808	1636	2.09	13	0.0491	2.1	0.1240	2.4	0.0183	1.2	0.488	154	±50	117	±1
2	0.71	710	1591	2.32	11	0.0448	4.7	0.1123	5.0	0.0182	1.7	0.333	-65	±120	116.1	±2
3	0.12	467	864	1.91	7	0.0488	3.1	0.1222	3.4	0.0182	1.3	0.395	140	±73	115.9	±2
4	3.02	183	303	1.71	3	0.0284	31.0	0.0690	31.0	0.0175	1.9	0.062	0	0	111.9	±2
5	1.34	497	918	1.91	8	0.0470	22.0	0.1190	22.0	0.0183	1.6	0.073	52	±520	116.9	±2
6	0.33	1114	2857	2.65	17	0.0494	3.2	0.1238	3.5	0.0182	1.3	0.372	168	±76	116.1	±2
7	0.60	840	1450	1.78	14	0.0476	5.3	0.1222	5.4	0.0186	1.3	0.232	80	±130	118.9	±2
8	2.97	378	603	1.65	6	0.0383	25.0	0.0890	25.0	0.0169	1.8	0.073	-462	±660	107.7	±2
9	1.02	324	460	1.47	5	0.0611	9.7	0.1490	9.9	0.0177	1.7	0.168	641	±210	113.1	±2
10	0.48	441	681	1.60	7	0.0480	7.1	0.1152	7.3	0.0174	1.4	0.192	101	±170	111.1	±2
11	1.61	249	378	1.57	4	0.0385	15.0	0.0910	15.0	0.0171	1.7	0.111	-447	±390	109.3	±2
12	0.53	516	782	1.57	8	0.0452	4.5	0.1112	4.7	0.0178	1.3	0.280	-45	±110	114	±2

Errors are 1-sigma; Pb_c and Pb^* indicate the common and radiogenic portions, respectively
Error in Standard calibration was 0.39%

TABLE 2.5 In situ Lu-Hf zircon results for Shandong granitoids

Spot No.	t (Ma)	$^{176}Yb/^{177}Hf$	$^{176}Lu/^{177}Hf$	$^{176}Hf/^{177}Hf$	$2\sigma_m$	$\varepsilon_{Hf}(0)$	$\varepsilon_{Hf}(t)$	$T_{DM1}(Hf)$	$T_{DM2}(Hf)$	$f_{Lu/Hf}$
SD-11 (Sanfoshan monzogranite)										
1	120	0.046593	0.001747	0.282258	0.000025	-18.16	-15.67	1431	3024	-0.95
2	118	0.055431	0.002000	0.282278	0.000023	-17.46	-15.04	1413	2966	-0.94
3	119	0.043263	0.001665	0.282242	0.000023	-18.74	-16.26	1451	3076	-0.95
4	118	0.042956	0.001694	0.282326	0.000021	-15.76	-13.31	1333	2812	-0.95
5	118	0.037791	0.001438	0.282252	0.000021	-18.39	-15.92	1429	3045	-0.96
6	118	0.072209	0.002511	0.282282	0.000026	-17.33	-14.95	1427	2957	-0.92
7	119	0.049484	0.001659	0.282302	0.000029	-16.62	-14.14	1366	2887	-0.95
8	117	0.046129	0.001815	0.282259	0.000026	-18.14	-15.72	1433	3026	-0.95
9	190	0.021662	0.000848	0.282214	0.000028	-19.74	-15.68	1459	3070	-0.97
10	117	0.043028	0.001575	0.282292	0.000025	-16.97	-14.53	1377	2920	-0.95
11	117	0.045715	0.001759	0.282210	0.000022	-19.88	-17.46	1501	3181	-0.95
12	116	0.042542	0.001492	0.282167	0.000024	-21.40	-18.98	1551	3316	-0.96
SD-12 (Sanfoshan syenogranite)										
1	114	0.049271	0.001965	0.282265	0.000030	-17.94	-15.59	1431	3013	-0.94
2	117	0.027509	0.001164	0.282266	0.000024	-17.90	-15.43	1399	3001	-0.96
3	117	0.046122	0.001928	0.282260	0.000030	-18.12	-15.70	1436	3025	-0.94
4	115	0.076657	0.002932	0.282258	0.000041	-18.16	-15.87	1479	3038	-0.91
5	104	0.047721	0.001858	0.282254	0.000027	-18.31	-16.17	1442	3058	-0.94
6	117	0.043836	0.001773	0.282242	0.000026	-18.74	-16.31	1455	3079	-0.95
7	118	0.057767	0.002104	0.282301	0.000027	-16.64	-14.23	1383	2893	-0.94
8	113	0.054164	0.001986	0.282349	0.000035	-14.97	-12.64	1311	2749	-0.94
9	116	0.058074	0.002249	0.282239	0.000033	-18.86	-16.50	1480	3095	-0.93
10	117	0.049117	0.002004	0.282267	0.000034	-17.88	-15.47	1430	3004	-0.94

11	123	0.018659	0.001029	0.282255	0.000022	-18.28	-15.67	1409	3026	-0.97
12	123	0.071938	0.003178	0.282237	0.000036	-18.93	-16.50	1521	3098	-0.90
SD-27 (Aishan monzogranite)										
1	120	0.022751	0.000845	0.282291	0.000027	-17.00	-14.44	1352	2914	-0.97
2	117	0.045732	0.001724	0.282226	0.000029	-19.30	-16.87	1476	3129	-0.95
3	120	0.016781	0.000645	0.282237	0.000031	-18.93	-16.35	1420	3086	-0.98
4	122	0.130342	0.005037	0.282224	0.000032	-19.38	-17.12	1624	3151	-0.85
5	122	0.042930	0.001711	0.282426	0.000038	-12.23	-9.70	1191	2491	-0.95
6	116	0.036654	0.001231	0.282182	0.000027	-20.86	-18.41	1519	3266	-0.96
7	115	0.069134	0.002630	0.282269	0.000024	-17.79	-15.47	1451	3002	-0.92
8	121	0.019285	0.000731	0.282201	0.000031	-20.19	-17.60	1473	3197	-0.98
9	119	0.016657	0.000591	0.282269	0.000026	-17.78	-15.22	1373	2984	-0.98
10	108	0.019008	0.000730	0.282198	0.000026	-20.31	-18.00	1477	3224	-0.98
11	109	0.022191	0.000819	0.282272	0.000024	-17.68	-15.36	1378	2990	-0.98
12	116	0.018199	0.000688	0.282217	0.000025	-19.61	-17.12	1448	3152	-0.98
SD-28 (Aishan monzogranite)										
1	112	0.027532	0.001122	0.282154	0.000025	-21.86	-19.49	1554	3360	-0.97
2	114	0.019245	0.000758	0.282201	0.000026	-20.20	-17.76	1474	3207	-0.98
3	115	0.024447	0.000938	0.282263	0.000024	-18.00	-15.55	1394	3011	-0.97
4	112	0.018341	0.000721	0.282253	0.000027	-18.34	-15.94	1400	3044	-0.98
5	114	0.019001	0.000743	0.282200	0.000027	-20.22	-17.78	1474	3209	-0.98
6	108	0.020139	0.000771	0.282180	0.000024	-20.92	-18.62	1503	3279	-0.98
7	112	0.030791	0.001147	0.282250	0.000031	-18.46	-16.09	1420	3057	-0.97
8	110	0.018091	0.000688	0.282217	0.000027	-19.62	-17.26	1449	3160	-0.98
9	107	0.014254	0.000557	0.282214	0.000027	-19.73	-17.42	1448	3173	-0.98
10	116	0.012907	0.000454	0.282212	0.000024	-19.81	-17.31	1447	3168	-0.99
11	123	0.022146	0.000847	0.282207	0.000027	-19.96	-17.34	1468	3175	-0.97

12	109	0.017921	0.000677	0.282265	0.000025	-17.93	-15.59	1382	3011	-0.98
SD-30 (Yashan monzonite)										
1	97	0.010322	0.000415	0.282210	0.000023	-19.89	-17.79	1449	3199	-0.99
2	117	0.035135	0.001440	0.282374	0.000034	-14.06	-11.61	1256	2660	-0.96
3	118	0.039211	0.001508	0.282371	0.000039	-14.18	-11.71	1262	2669	-0.95
4	113	0.110773	0.004073	0.282409	0.000037	-12.82	-10.65	1297	2570	-0.88
5	115	0.050329	0.001847	0.282332	0.000035	-15.58	-13.20	1331	2800	-0.94
6	113	0.015282	0.000600	0.282291	0.000029	-17.01	-14.59	1343	2923	-0.98
7	121	0.022034	0.000826	0.282345	0.000030	-15.09	-12.51	1276	2743	-0.98
8	108	0.036560	0.001339	0.282346	0.000029	-15.06	-12.79	1292	2759	-0.96
9	113	0.040210	0.001464	0.282378	0.000035	-13.92	-11.55	1251	2652	-0.96
10	117	0.010021	0.000400	0.282271	0.000026	-17.73	-15.20	1364	2980	-0.99
11	122	0.003970	0.000196	0.282267	0.000025	-17.87	-15.21	1363	2985	-0.99
12	119	0.008016	0.000363	0.282269	0.000029	-17.79	-15.21	1365	2983	-0.99
13	159	0.124801	0.004330	0.282233	0.000036	-19.05	-16.02	1576	3078	-0.87
14	117	0.018567	0.000773	0.282207	0.000030	-19.99	-17.49	1466	3185	-0.98
15	120	0.014455	0.000557	0.282263	0.000029	-18.02	-15.44	1381	3004	-0.98
SD-31 (Yashan monzogranite)										
1	105	0.026337	0.000951	0.282131	0.000027	-22.67	-20.44	1579	3440	-0.97
2	107	0.210427	0.007118	0.282020	0.000040	-26.58	-24.74	2067	3814	-0.79
3	113	0.016438	0.000592	0.282149	0.000025	-22.04	-19.61	1539	3371	-0.98
4	115	0.023591	0.000856	0.282130	0.000027	-22.70	-20.24	1576	3429	-0.97
5	118	0.011829	0.000424	0.281978	0.000031	-28.07	-25.52	1766	3900	-0.99
6	110	0.020765	0.000753	0.282081	0.000025	-24.43	-22.07	1639	3588	-0.98
7	113	0.025892	0.000918	0.282148	0.000025	-22.06	-19.66	1554	3375	-0.97
8	116	0.026204	0.000948	0.282172	0.000026	-21.22	-18.75	1521	3296	-0.97
9	113	0.025806	0.000941	0.282224	0.000026	-19.37	-16.97	1449	3136	-0.97

10	117	0.017769	0.000655	0.282180	0.000026	-20.95	-18.44	1500	3270	-0.98
11	118	0.030466	0.001053	0.282156	0.000025	-21.80	-19.30	1549	3346	-0.97
12	80	0.018034	0.000653	0.282178	0.000027	-21.01	-19.29	1502	3322	-0.98
13	159	0.012961	0.000467	0.282199	0.000025	-20.27	-16.83	1466	3153	-0.99
SD-59 (Laoshan alkali granite)										
1	124	0.193732	0.006229	0.282159	0.000033	-21.68	-19.47	1788	3360	-0.81
2	121	0.093454	0.003137	0.282189	0.000029	-20.62	-18.22	1589	3250	-0.91
3	119	0.104411	0.003340	0.282165	0.000025	-21.47	-19.13	1634	3330	-0.90
4	116	0.097610	0.003034	0.282132	0.000030	-22.62	-20.32	1668	3434	-0.91
5	118	0.085221	0.002695	0.282149	0.000033	-22.02	-19.65	1628	3376	-0.92
6	118	0.130038	0.004346	0.282188	0.000028	-20.66	-18.42	1647	3265	-0.87
7	120	0.135959	0.004419	0.282207	0.000026	-19.98	-17.70	1621	3202	-0.87
8	111	0.114186	0.003575	0.282188	0.000031	-20.64	-18.47	1610	3266	-0.89
9	115	0.117918	0.003663	0.282171	0.000030	-21.27	-19.03	1641	3318	-0.89
10	113	0.134756	0.004138	0.282229	0.000029	-19.21	-17.05	1575	3140	-0.88
11	114	0.088810	0.002842	0.282217	0.000028	-19.61	-17.33	1535	3167	-0.91
12	117	0.131672	0.004333	0.282242	0.000032	-18.76	-16.53	1564	3096	-0.87

TABLE 2.6

Previously published SHRIMP U-Pb ages of mid-late Mesozoic granitoids

Granitoid Suite Name	SHRIMP U-Pb age	Reference
Duogushan	161 ± 1 Ma	(Guo et al., 2005; Zhao and Zheng, 2009)
Wendeng	160 ± 3 Ma	(Guo et al., 2005; Zhao and Zheng, 2009)
Linglong	160-156 Ma	(Liu et al., 2009)
Kunyushan	165-142 Ma 135-130 Ma	(Zhang et al., 1995; Qiu et al., 2002b; Yang et al., 2004b; Guo et al., 2005; Liu et al., 2009; Zhao and Zheng, 2009)
Guojialing	130-126 Ma	(Guan et al., 1998; Wang et al., 1998; Zhang et al., 2003c)
Rizhou	127 ± 2 Ma	(Yang et al., 2005; Zhao and Zheng, 2009)
Junan	123 ± 2 Ma	(Liu et al., 2009; Zhao and Zheng, 2009)
Wulian	125-122 Ma	(Yang et al., 2005; Liu et al., 2009; Zhao and Zheng, 2009)
Haiyang	115 ± 2 Ma	(Zhao and Zheng, 2009)

TABLE 2.7

Comparison of SHRIMP U-Pb age data with previously published ages for the latest Yanshanian granitoids

	Method	Sanfoshan	Aishan	Yashan	Laoshan
This study	**U-Pb**	**118 ± 1 Ma**	**116 ± 2 Ma** **125 ± 3 Ma**	**113 ± 2 Ma**	**115 ± 2 Ma**
Guo et al., 2005	U-Pb	113 ± 1 Ma			
Zhao et al., 1998b	U-Pb				111 ± 1 Ma
Zhou & Lu, 2005	K-Ar		158-64 Ma		

2.4 FIGURES FOR PAPER 1

FIG. 2.1

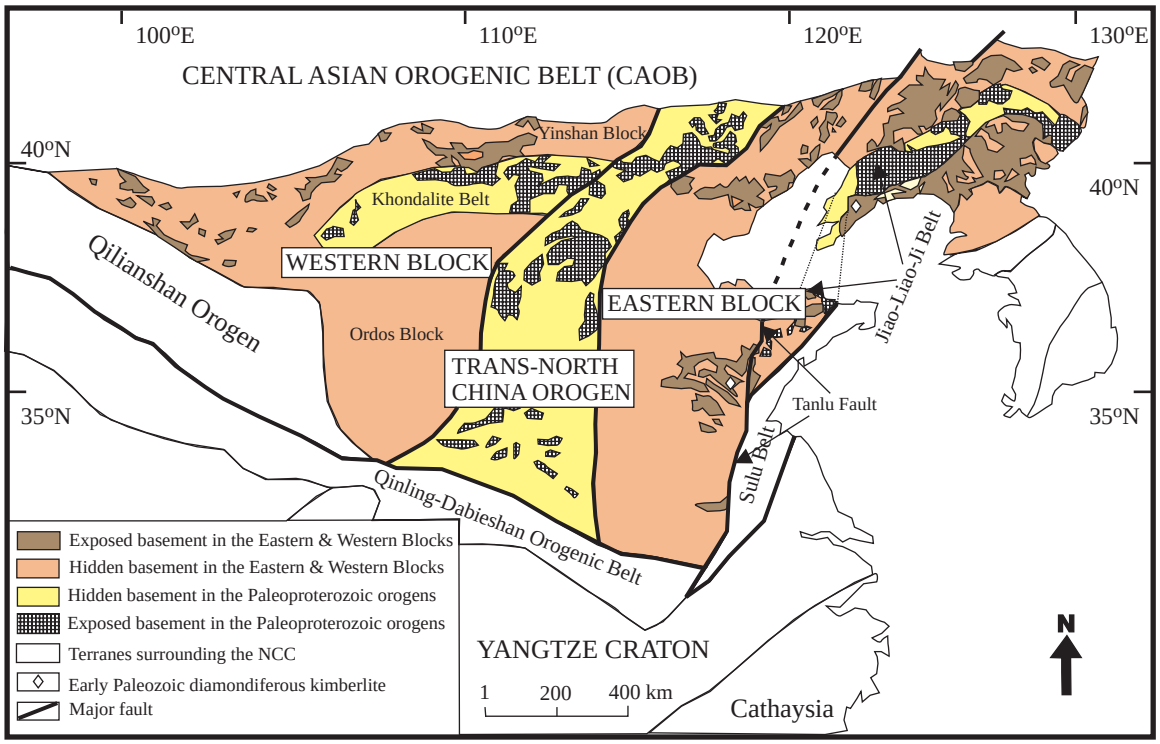

FIG. 2.2

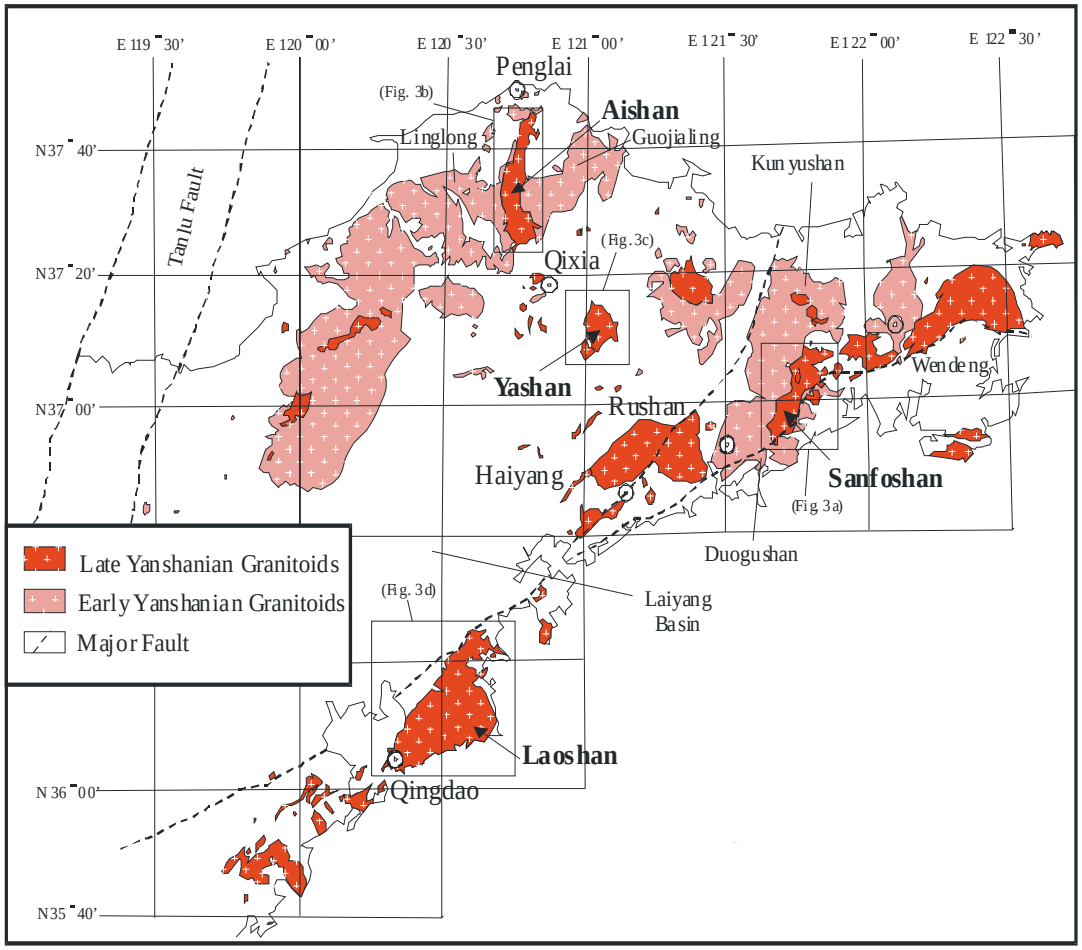
E 119°30'
E 120°00'
E 120°30'
E 121°00'
E 121°30'
E 122°00'
E 122°30'
N37°40'
N37°20'
N37°00'
N36°00'
N35°40'
Penglai
(Fig. 3b)
Aishan
Linglong
Guojialing
Kunyushan
Tanlu Fault
(Fig. 3c)
Qixia
Yashan
Rushan
Wendeng
Haiyang
Sanfoshan
(Fig 3a)
Duogushan
Laiyang
Basin
(Fig. 3d)
Laoshan
Qingdao
Late Yanshanian Granitoids
Early Yanshanian Granitoids
Major Fault

FIG. 2.3

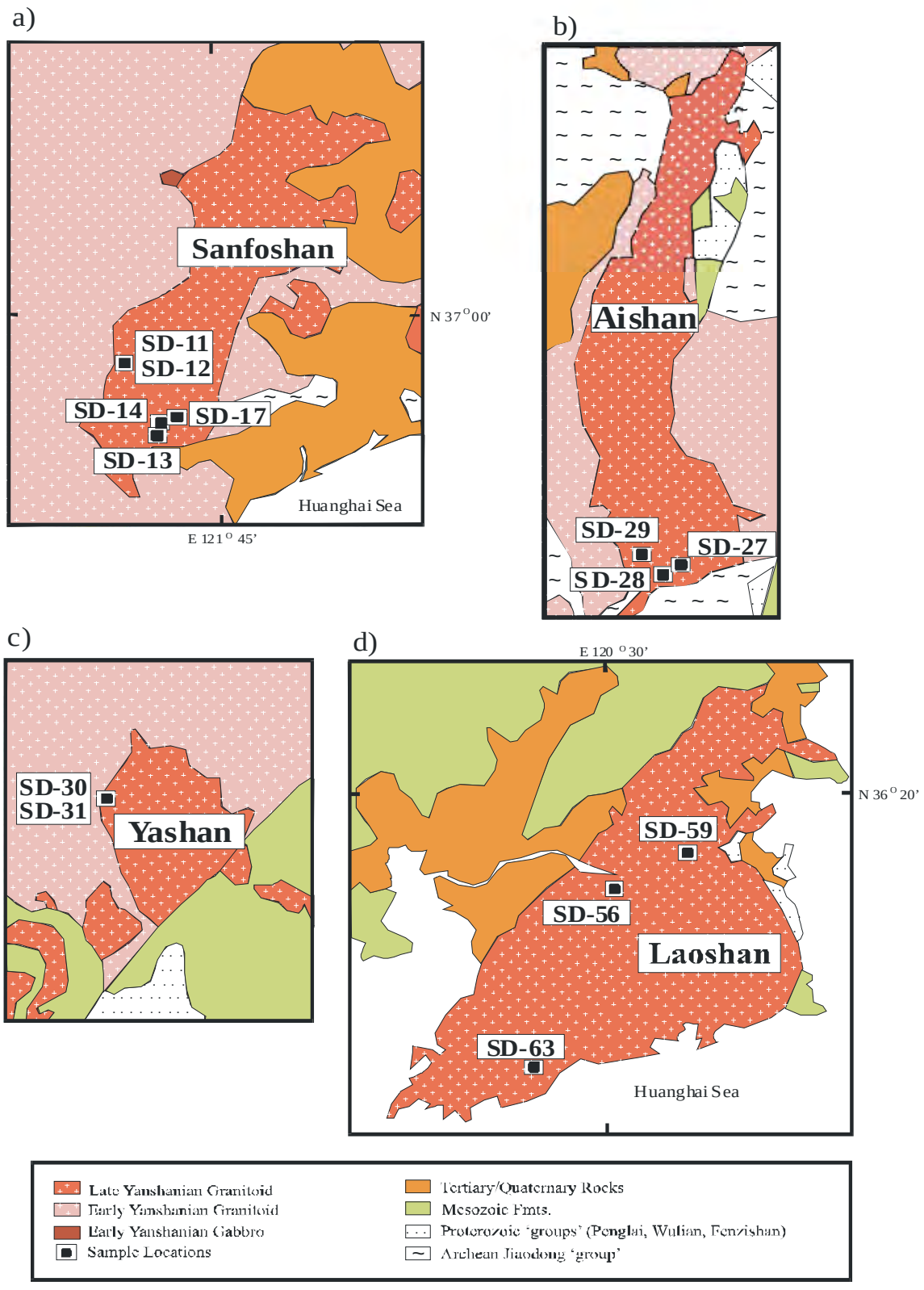
a)
Sanfoshan
SD-11
SD-12
SD-14
SD-17
SD-13
Huanghai Sea
N 37° 00'
E 121° 45'
b)
Aishan
SD-29
SD-27
SD-28
c)
SD-30
SD-31
Yashan
d)
E 120° 30'
N 36° 20'
SD-59
SD-56
Laoshan
SD-63
Huanghai Sea
Late Yanshanian Granitoid
Early Yanshanian Granitoid
Early Yanshanian Gabbro
Sample Locations
Tertiary/Quaternary Rocks
Mesozoic Fmts.
Proterozoic 'groups' (Penglai, Wulian, Fenzishan)
Archean Jiaodong 'group'

FIG. 2.4

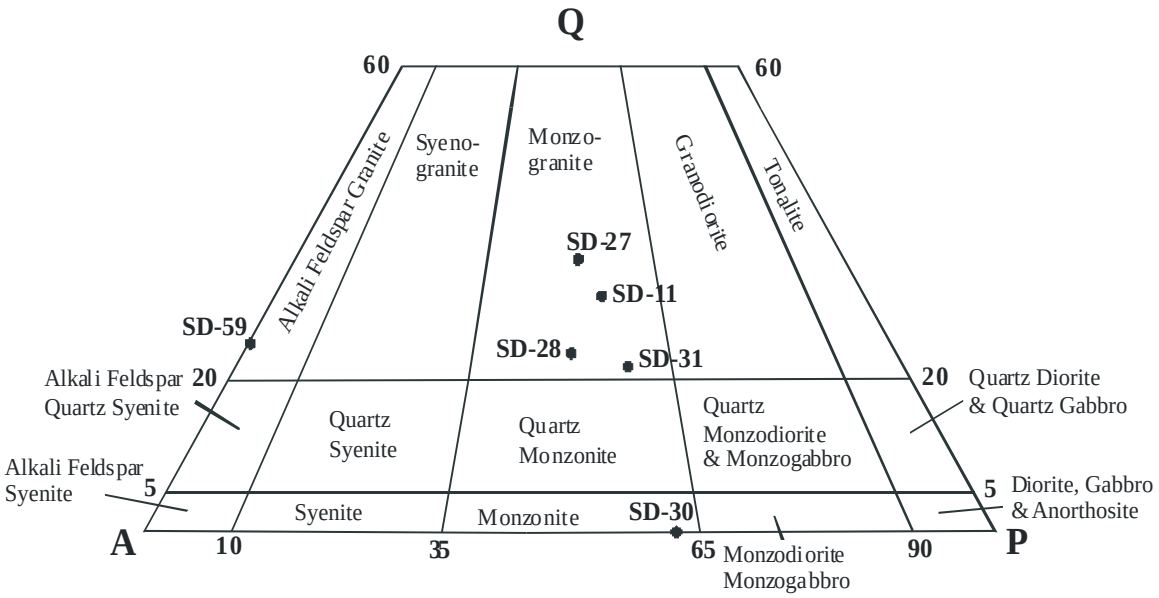
Q
60
60
Alkali Feldspar Granite
Syeno-granite
Monzo-granite
Granodiorite
Tonalite
SD-27
SD-11
SD-59
SD-28
SD-31
Alkali Feldspar Quartz Syenite
20
20
Quartz Diorite & Quartz Gabbro
Quartz Syenite
Quartz Monzonite
Quartz Monzodiorite & Monzogabbro
Alkali Feldspar Syenite
5
5
Diorite, Gabbro & Anorthosite
Syenite
Monzonite
SD-30
A
10
35
65
90
P
Monzodiorite Monzogabbro

FIG. 2.5

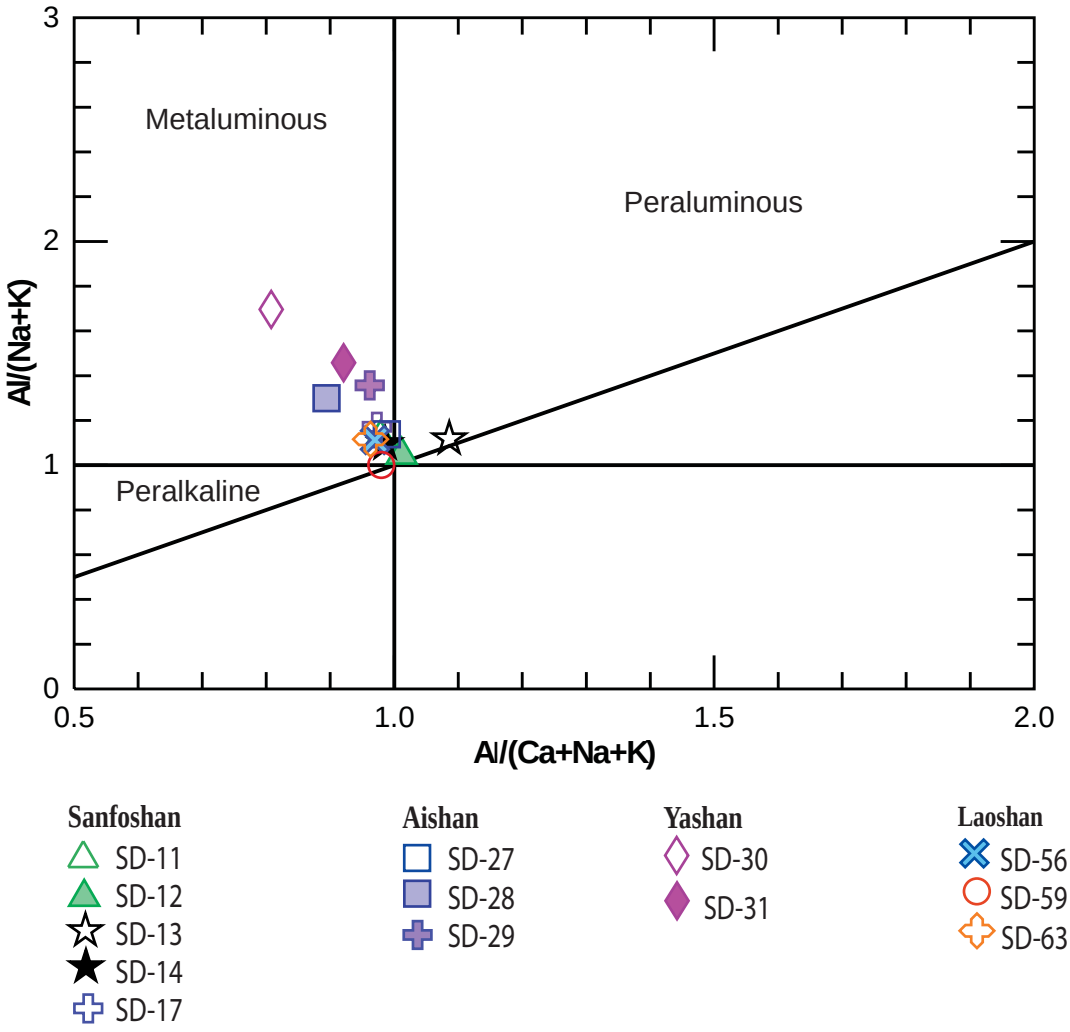
Metaluminous
Peraluminous
Peralkaline
Al/(Na+K)
Al/(Ca+Na+K)
0
1
2
3
0.5
1.0
1.5
2.0
Sanfoshan
SD-11
SD-12
SD-13
SD-14
SD-17
Aishan
SD-27
SD-28
SD-29
Yashan
SD-30
SD-31
Laoshan
SD-56
SD-59
SD-63

FIG. 2.6

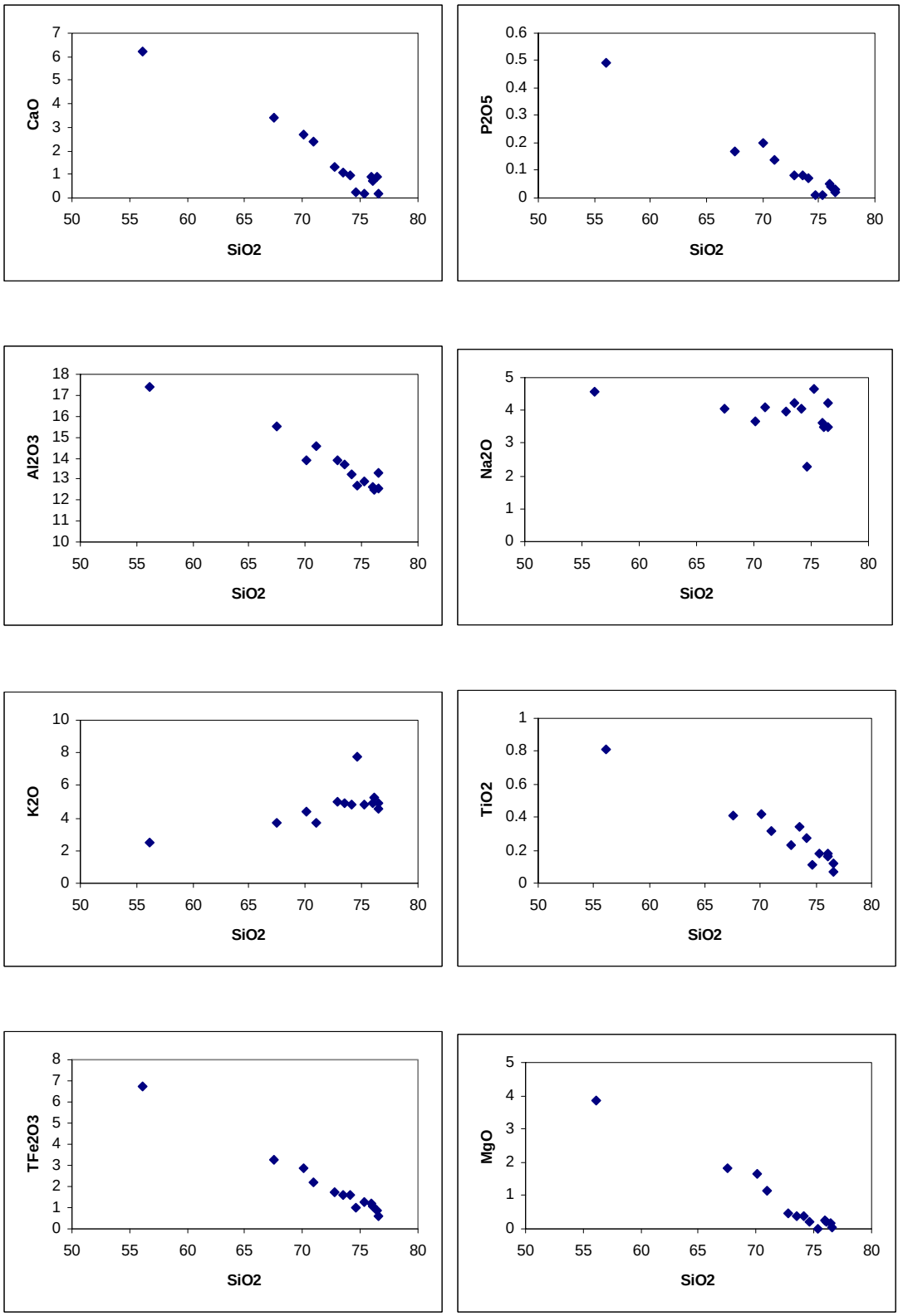
CaO
SiO2
P2O5
SiO2
Al2O3
SiO2
Na2O
SiO2
K2O
SiO2
TiO2
SiO2
TFe2O3
SiO2
MgO
SiO2

FIG. 2.6 (continued)

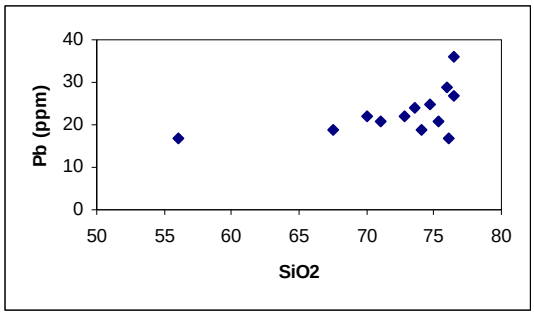

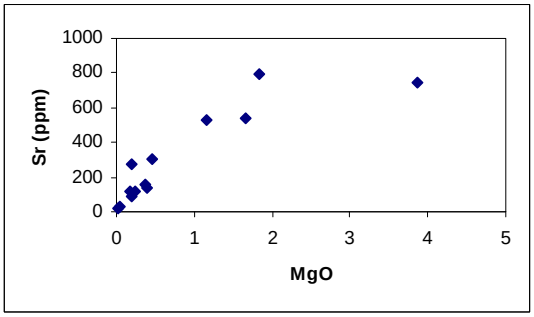

FIG. 2.7

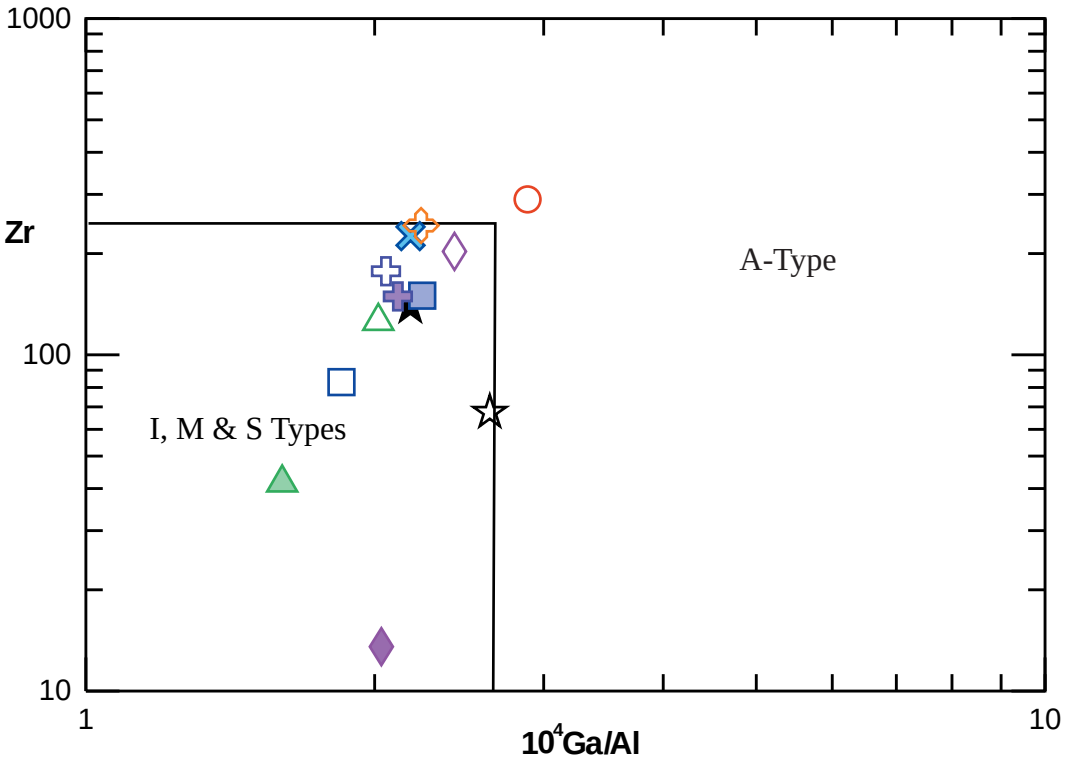

FIG. 2.8

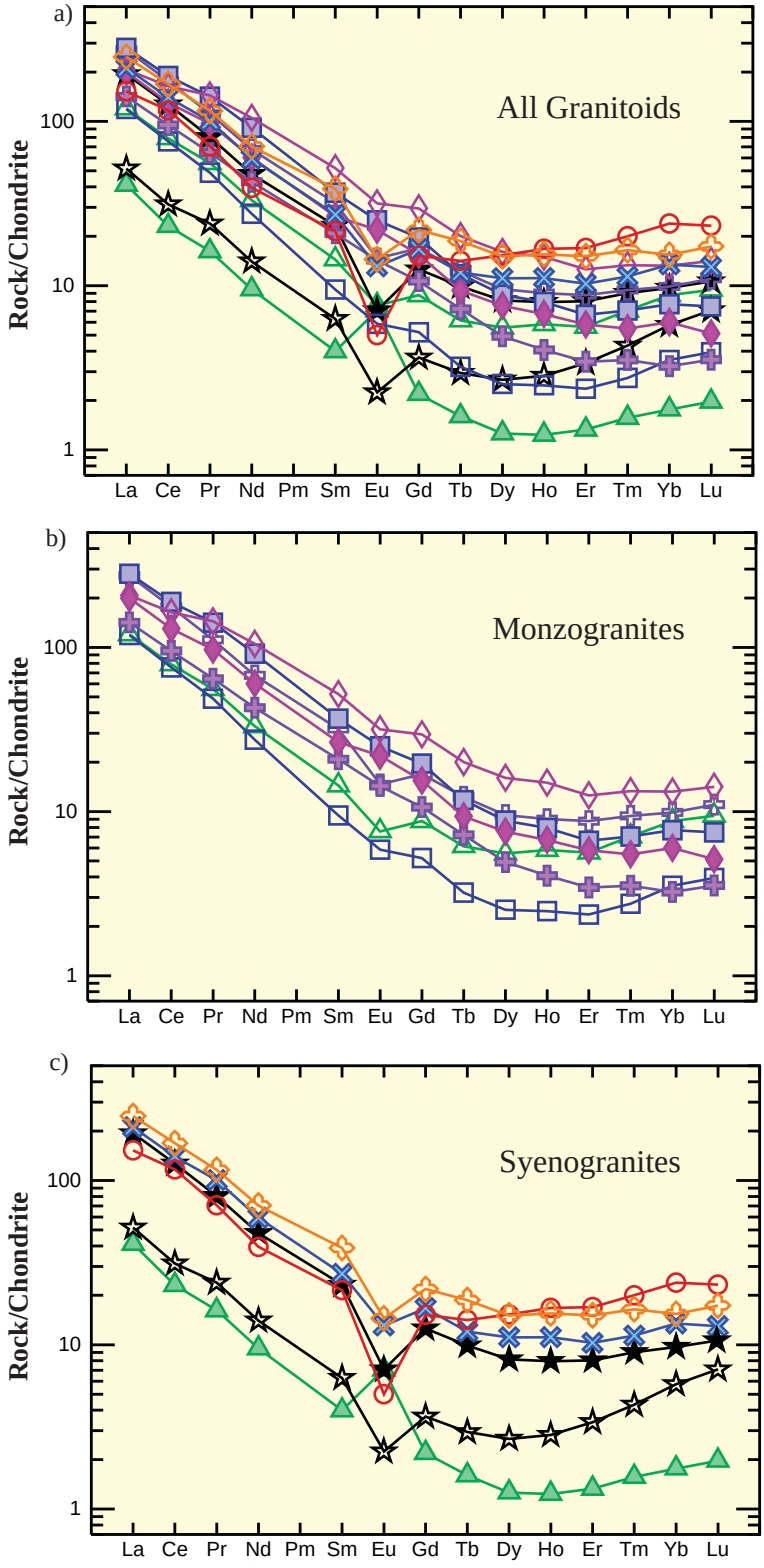
a)
All Granitoids
Rock/Chondrite
100
10
1
La Ce Pr Nd Pm Sm Eu Gd Tb Dy Ho Er Tm Yb Lu
b)
Monzogranites
Rock/Chondrite
100
10
1
La Ce Pr Nd Pm Sm Eu Gd Tb Dy Ho Er Tm Yb Lu
c)
Syenogranites
Rock/Chondrite
100
10
1
La Ce Pr Nd Pm Sm Eu Gd Tb Dy Ho Er Tm Yb Lu

FIG. 2.9

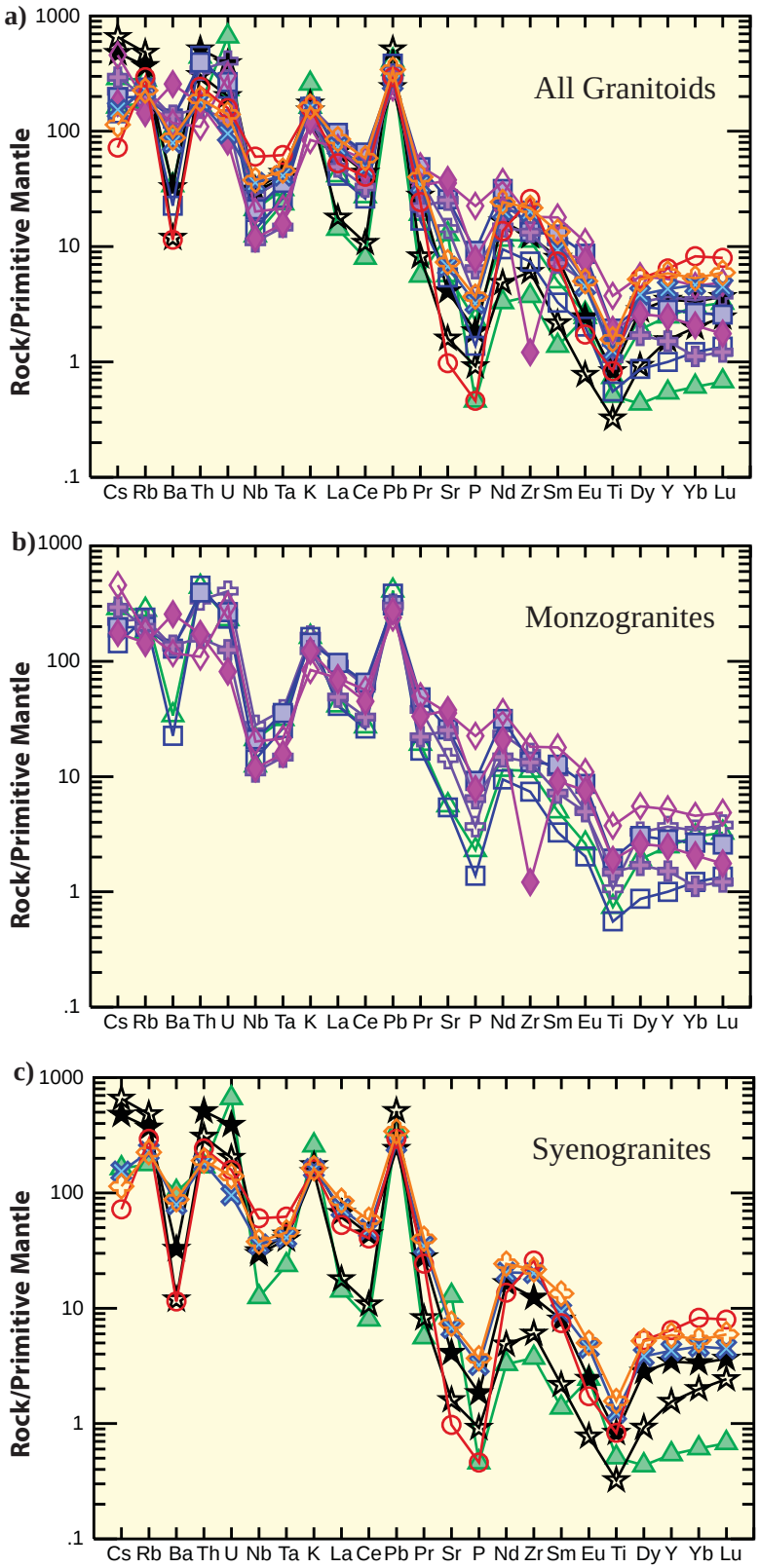
a)
All Granitoids
Rock/Primitive Mantle
1000
100
10
1
.1
Cs Rb Ba Th U Nb Ta K La Ce Pb Pr Sr P Nd Zr Sm Eu Ti Dy Y Yb Lu
b)
Monzogranites
Rock/Primitive Mantle
1000
100
10
1
.1
Cs Rb Ba Th U Nb Ta K La Ce Pb Pr Sr P Nd Zr Sm Eu Ti Dy Y Yb Lu
c)
Syenogranites
Rock/Primitive Mantle
1000
100
10
1
.1
Cs Rb Ba Th U Nb Ta K La Ce Pb Pr Sr P Nd Zr Sm Eu Ti Dy Y Yb Lu

FIG. 2.10

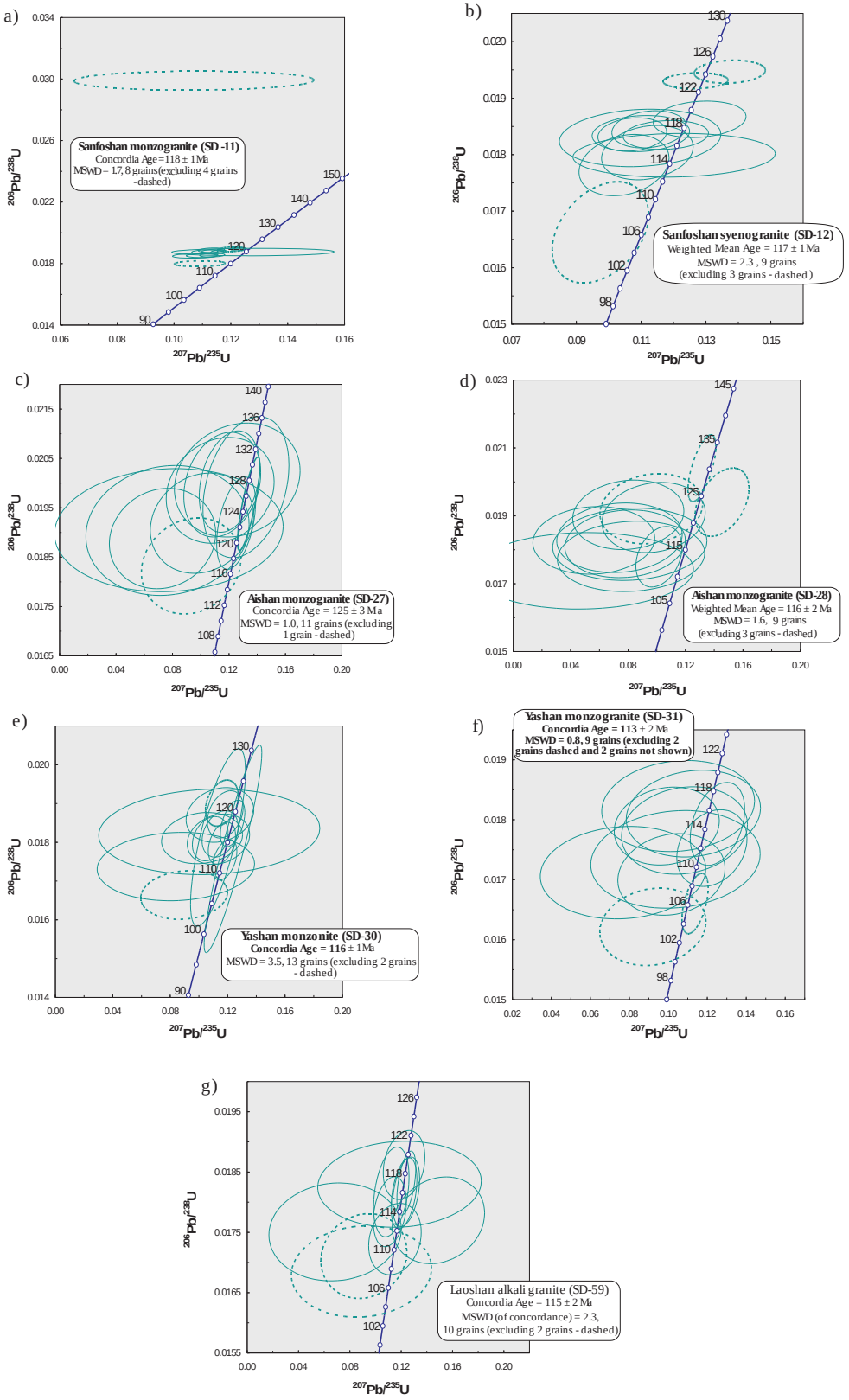
a)
Sanfoshan monzogranite (SD -11)
Concordia Age = 118 ± 1Ma
MSWD = 1.7, 8 grains(excluding 4 grains - dashed)
b)
Sanfoshan syenogranite (SD-12)
Weighted Mean Age = 117 ± 1Ma
MSWD = 2.3 , 9 grains
(excluding 3 grains - dashed)
c)
Aishan monzogranite (SD-27)
Concordia Age = 125 ± 3 Ma
MSWD = 1.0, 11 grains (excluding 1 grain - dashed)
d)
Aishan monzogranite (SD-28)
Weighted Mean Age = 116 ± 2 Ma
MSWD = 1.6, 9 grains
(excluding 3 grains - dashed)
e)
Yashan monzonite (SD-30)
Concordia Age = 116 ± 1Ma
MSWD = 3.5, 13 grains (excluding 2 grains - dashed)
f)
Yashan monzogranite (SD-31)
Concordia Age = 113 ± 2 Ma
MSWD = 0.8, 9 grains (excluding 2 grains dashed and 2 grains not shown)
g)
Laoshan alkali granite (SD-59)
Concordia Age = 115 ± 2 Ma
MSWD (of concordance) = 2.3,
10 grains (excluding 2 grains - dashed)
206Pb/238U
207Pb/235U

FIG. 2.11

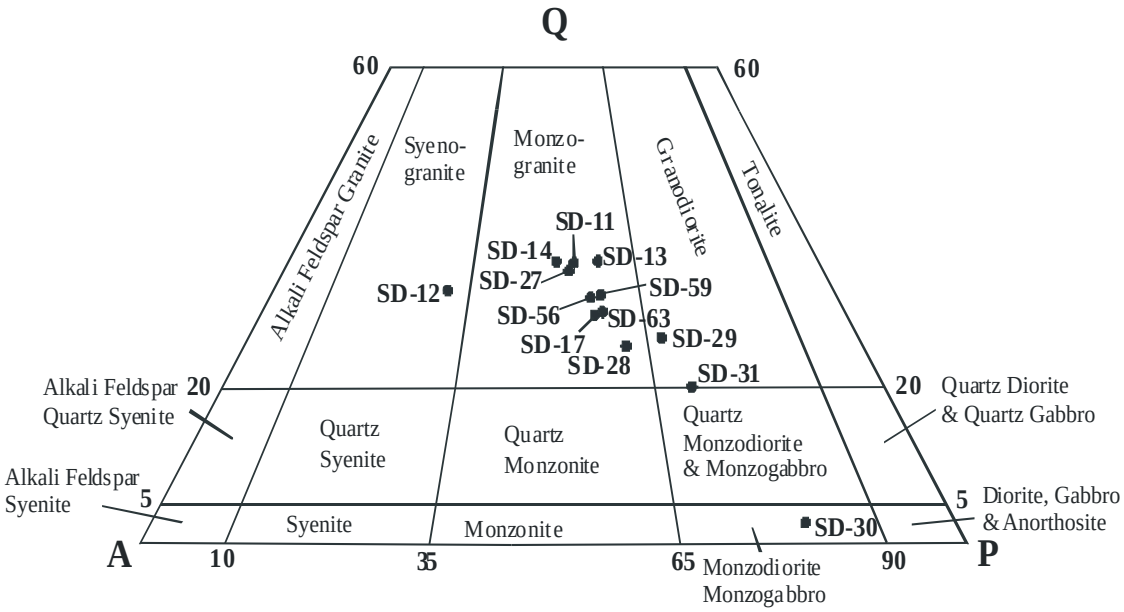
Q
60
60
Alkali Feldspar Granite
Syeno-granite
Monzo-granite
Granodiorite
Tonalite
SD-11
SD-14
SD-13
SD-27
SD-12
SD-59
SD-56
SD-63
SD-17
SD-29
SD-28
SD-31
Alkali Feldspar Quartz Syenite
20
20
Quartz Diorite & Quartz Gabbro
Quartz Syenite
Quartz Monzonite
Quartz Monzodiorite & Monzogabbro
Alkali Feldspar Syenite
5
5
Diorite, Gabbro & Anorthosite
Syenite
Monzonite
SD-30
A
10
35
65
90
P
Monzodiorite Monzogabbro

FIG. 2.12

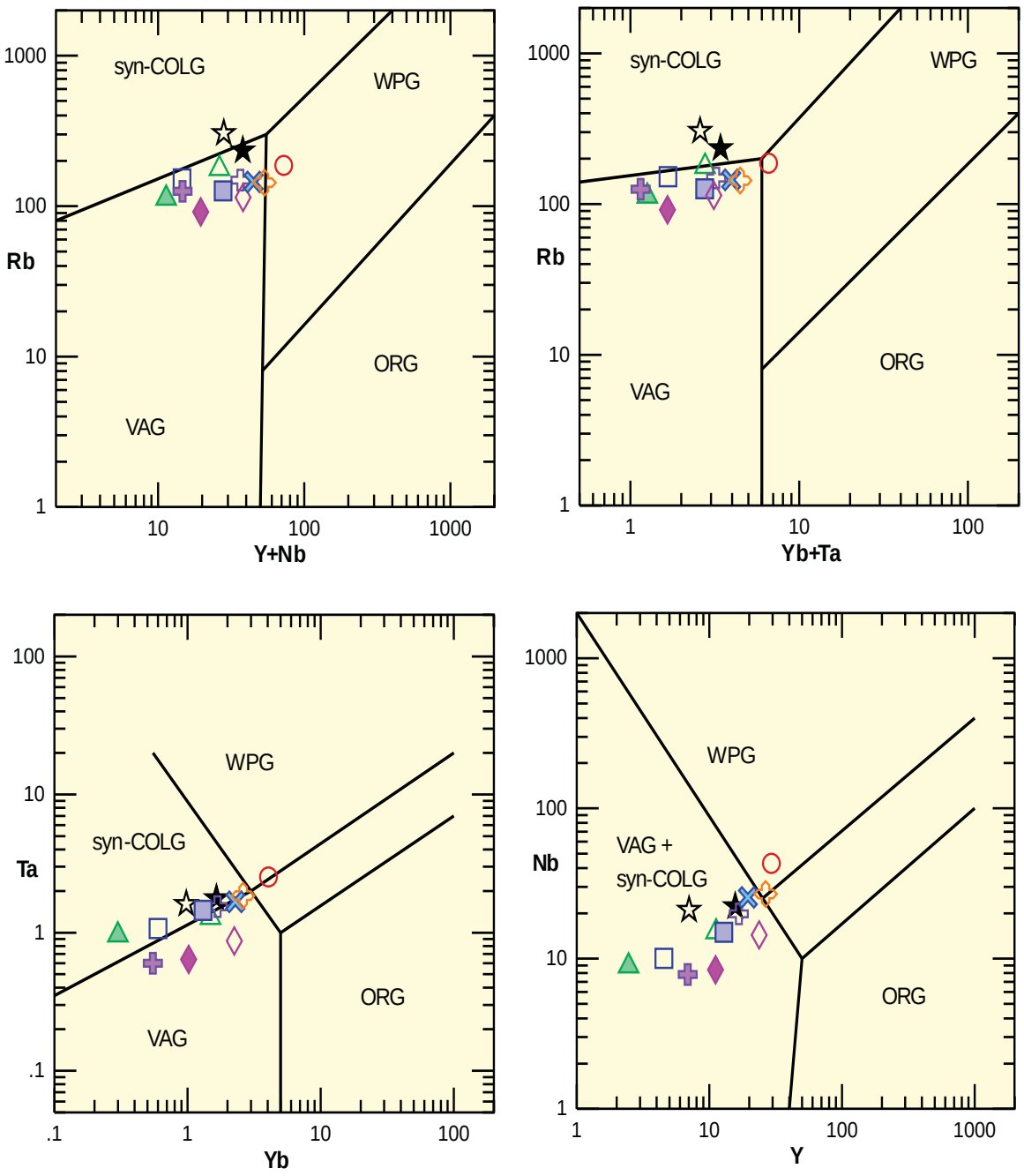
1000
100
10
1
Rb
syn-COLG
WPG
ORG
VAG
10
100
1000
Y+Nb
1000
100
10
1
Rb
syn-COLG
WPG
VAG
ORG
1
10
100
Yb+Ta
100
10
1
.1
Ta
WPG
syn-COLG
ORG
VAG
.1
1
10
100
Yb
1000
100
10
1
Nb
WPG
VAG +
syn-COLG
ORG
1
10
100
1000
Y

FIG. 2.13

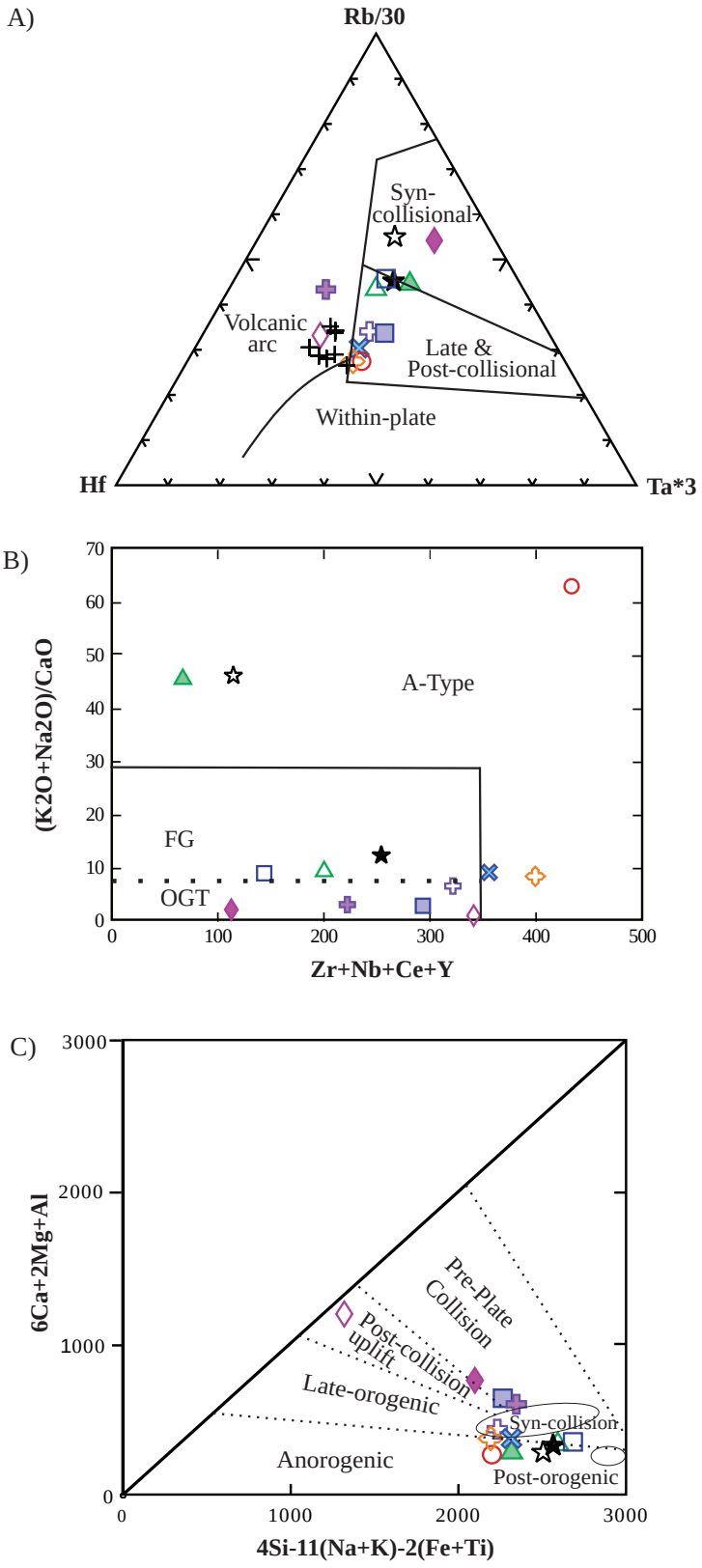
A)
Rb/30
Hf
Ta*3
Syn-
collisional
Volcanic
arc
Late &
Post-collisional
Within-plate
B)
(K2O+Na2O)/CaO
Zr+Nb+Ce+Y
A-Type
FG
OGT
0
10
20
30
40
50
60
70
0
100
200
300
400
500
C)
6Ca+2Mg+Al
4Si-11(Na+K)-2(Fe+Ti)
Pre-Plate
Collision
Post-collision
uplift
Late-orogenic
Syn-collision
Anorogenic
Post-orogenic
0
1000
2000
3000

CHAPTER 3

This chapter has been temporarily removed to prevent public access.

CHAPTER 4

4.1 TECTONIC MODEL

The new precise SHRIMP U-Pb zircon geochronological and detailed geochemical data presented here when combined with previously published data allow the following regional tectonic model to be developed.

During the Early Jurassic the eastern NCC was under a compressional tectonic regime that was the result of subduction of the Pacific Plate westwards beneath the NCC (Qiu et al., 2002b; Kusky et al., 2007; Menzies et al., 2007; Xu, 2007). This tectonic regime changed to one of extension in the Late Jurassic and this continued into the Early Tertiary (Menzies and Xu, 1998; Meng, 2003; Zhang et al., 2003a; Xu, 2007).

The subduction of the Pacific Plate resulted in two effects that would ultimately lead to the eastern NCC undergoing large-scale lithospheric extension and thinning in the Cretaceous. Firstly, as subduction took place, fluids released from dehydration melting of the down-going oceanic slab rose upwards into the overlying subcontinental lithospheric mantle (SCLM) of the eastern NCC. These fluids caused hydration and weakening of the SCLM, which made the lithosphere susceptible to subsequent thinning or partial delamination (Niu, 2005; Niu et al., 2005). Secondly, on-going subduction of the Pacific Plate resulted in slab roll-back and retreat of the trench to the east. This process induced extension in the overriding plate, which was the eastern NCC.

The effects of lithospheric extension have been widely documented over the whole of East Asia extending from the Central Asian Orogenic Belt (CAOB) and Mongolia in the far north, through the eastern and central NCC and into the Yangtze Craton and South China Craton (SCC) (Zhou and Li, 2000; Fan et al., 2003; Zhang et al., 2003d; Wu et al., 2005a; McKenzie and Priestley, 2008). It is difficult to attribute such a broad ranging effect directly to subduction of the Pacific Plate which would not have been able to reach so far inland and nor would it affect all areas at a similar

time. Instead it is proposed that the extension resulting from Pacific Plate subduction led to asthenospheric upwelling, elevation of the lithospheric geotherm and subsequent partial melting of the lithospheric mantle. This would ultimately lead to thinning of the lithosphere followed by partial delamination. This would explain the widespread effects seen over an extensive area of East Asia.

In terms of how the magmatic activity in the eastern NCC that was the focus of my research, fits in with this model I propose the following. In summary, the asthenospheric upwelling and partial melting of the lithosphere led to generation of basaltic magmas. Due to previous subduction events in the area, such as the subduction of the SCC beneath the NCC at ~240-220 Ma, the lithospheric mantle became enriched and this geochemical signature is seen in all the magmatic rocks sampled here. The basaltic magmas were either emplaced in the lower crust with differing degrees of magma mixing and fractional crystallization to produce the dykes and widespread volcanics, or they were underplated beneath the crust causing partial melting, granitoid generation and subsequent intrusion. These parental magmas of the granitoids similarly underwent varying degrees of fractional crystallization and magma mixing. The slightly older, more typical, Late Yanshanian granitoids resulted from predominantly lower crustal melting, however the younger Late Yanshanian granitoids sampled in this thesis demonstrate that as subduction, basaltic magma underplating, lithospheric thinning and partial delamination continued, crustal melting became more extensive as seen by the more anorogenic geochemical signature in the youngest granitoids.

The Late Cretaceous-Tertiary alkali basaltic volcanism in the eastern NCC from ~95-75 Ma onwards has an asthenospheric source signature, suggesting that lithospheric thinning and delamination were completed by then.

BIBLIOGRAPHY

Here is a list of all the references cited in both of the papers and in the exegesis as a whole. There is the possibility of some inconsistencies in regards to the numbering of multiple references from the same first author and same year between the papers and between them and the exegesis which is unavoidable.

Every reasonable effort has been made to acknowledge the owners of copyright material. I would be pleased to hear from any copyright owner who has been omitted or incorrectly acknowledged.

Aitchison, J.C., Ali, J.R., Davies, A.M., 2007. When and where did India and Asia collide? Journal of Geophysical Research 112, 1-19.

Ames, L., Tilton, G.R., Zhou, G., 1993. Timing of collision of the Sino-Korean and Yangtze cratons: U-Pb zircon dating of coesite-bearing eclogites. Geology 21, 339-342.

Batchelor, R.A., Bowden, P., 1985. Petrogenetic interpretation of granitoid rock series using multicationic parameters. Chemical Geology 48, 43-55.

Bird, P., 1979. Continental delamination and the Colorado Plateau. Journal of Geophysical Research 84, 7561-7571.

Chappell, B.W., White, A.J.R., 1992. I- and S-type granites in the Lachlan Fold Belt. Transactions, Royal Society of Edinburgh Earth Science 83, 1-26.

Chen, B., Zhai, M., 2003. Geochemistry of late Mesozoic lamprophyre dykes from the Taihang Mountains, north China and implications for the sub-continental lithospheric mantle. Geological Magazine 140(1), 87-93.

Chen, J.F., Xie, Z., Li, H.M., Zhou, T.X., Park, Y.S., Ahn, K.S., Chen, D.G., Zhang, X., 2003a. U-Pb zircon ages for a collision-related K-rich complex at Shidao in the Sulu ultrahigh pressure terrane, China. Geochemical Journal 37, 35-46.

Chen, B., Jahn, B.M., Zhai, M., 2003b. Sr-Nd isotopic characteristics of the Mesozoic magmatism in the Taihang-Yanshan orogen, North China Craton

and implications for Archaean lithosphere thinning. Journal of the Geological Society, London 160, 963-970.

Clemens, J.D., Holloway, J.R., White, A.J.R., 1986. Origin of an A-type granite; experimental constraints. American Mineralogist 71, 317-324.

Darby, B.J., Davis, G.A., Zhang, X.H., Wu, F.Y., Wilde, S.A., Yang, J.H., 2004. The newly discovered Waziyu metamorphic core complex, YiwuluShan, western Liaoning Province, northwest China. Earth Science Frontiers 11, 145-155.

Davies, J.H., von Blanckenburg, F., 1995. Slab breakoff: a model of lithospheric detachment and it's test in the magmatism and deformation of collisional orogens. Earth and Planetary Science Letters 129, 85-102.

Davies, G.S., Zhang, Y.D., Wang, C., B.J., D., Zhang, C., Gehrels, G., 2001. Mesozoic tectonic evolution of the Yanshan fold and thrust belt, with emphasis on Hebei and Liaoning Provinces northern China. Geological Society of America Memoir 194, 171-197.

de la Roche, H., Leterrier, J., Grandclaude, P., Marchal, M., 1980. A classification of volcanic and plutonic rocks using R1-R2 diagram and major element analyses, its relationship with current nomenclature. Chemical Geology 29, 183-210.

Deng, J.F., Mo, X.X., Zhao, Z.D., Wu, Z.X., Luo, Z.H., Su, S.G., 2004. A new model for the dynamic evolution of Chinese lithosphere: 'continental roots-plume tectonics'. Earth Science Reviews 65, 223-275.

Deng, J.F., Su, S.G., Niu, Y., Liu, C., Zhao, G.C., Zhao, X., Zhou, S., Wu, Z.X., 2007. A possible model for the lithospheric thinning of North China Craton: evidence from the Yanshanian (Jura-Cretaceous) magmatism and tectonism. Lithos 96, 22-35.

Fan, H.R., Zhai, M.G., Xie, Y.H., Yang, J.H., 2003a. Ore-forming fluids associated with granite-hosted gold mineralization at the Sanshandao deposit, Jiaodong gold province, China. Mineralium Deposita 38, 739-750.

Fan, Q., Zhang, H.F., Sui, J., Zhai, M., Sun, Q., Li, N., 2005. Magma underplating and Hannuoba present crust-mantle transitional zone composition: Xenolith

petrological and geochemical evidence. Science in China, Series D Earth Sciences 48, 1089-1105.

Fan, W.M., Zhang, H.F., Baker, J., Jarvis, K.E., Mason, P.R.D., Menzies, M.A., 2000. On and Off the North China Craton: Where is the Archaean Keel? Journal of Petrology 41, 933-950.

Fan, W.M., Guo, F., Wang, Y.J., Lin, G., Zhang, M., 2001. Post-orogenic bimodal volcanism along the Sulu Orogenic Belt in Eastern China. Physics and Chemistry of the Earth, Part A: Solid Earth and Geodesy 26, 733-746.

Fan, W.M., Guo, F., Wang, Y.J., Lin, G., 2003. Late Mesozoic calc-alkaline volcanism of post-orogenic extension in the northern Da Hinggan Mountains, northeastern China. Journal of Volcanology and Geothermal Research 121, 115-135.

Gao, S., Luo, T.C., Zhang, B.R., Zhang, H.F., Han, Y.W., Zhao, Z.D., Hu, Y.K., 1998. Chemical composition of the continental crust as revealed by studies in East China. Geochimica et Cosmochimia Acta 62, 1959-1975.

Gao, S., Rudnick, R.L., Carlson, R.W., McDonough, W.F., Liu, Y.S., 2002. Re-Os evidence for replacement of ancient mantle lithosphere beneath the North China craton. Earth and Planetary Science Letters 198, 307-322.

Gao, S., Rudnick, R.L., Yuan, H.L., Liu, X.M., Liu, Y.S., Xu, W.L., Ling, W.L., Ayers, J., Wang, X.C., Wang, Q.H., 2004. Recycling lower continental crust in the North China Craton. Nature 432, 892-897.

Goss, S.C., Wilde, S.A., Wu, F.Y., Yang, J.H., (in review). The age, isotopic signature and significance of the youngest Mesozoic granitoids in Shandong Province, North China Craton Lithos.

Green, T.H., 1995. Significance of Nb/Ta as an indicator of geochemical processes in the crust-mantle system. Chemical Geology 120, 347-359.

Griffin, W.L., Zhang, A., O'Reilly, S.Y., Ryan, C.G., 1998. Phanerozoic evolution of the lithosphere beneath the Sino-Korean Craton. In: Flower, M.F.J., Chung, S.L., Lo, C.H., Lee, T.Y. (Editors), Mantle Dynamics and Plate Interactions in East Asia. American Geophysics Union Geodynamics, pp. 107-126.

Griffin, W.L., Pearson, N.J., Belousova, E., Jackson, S.E., O'Reilly, S.Y., van Achterberg, E., Shee, S.R., 2000. The Hf isotope composition of cratonic mantle: LAM-MC-ICPMS analysis of zircon megacrysts in kimberlites. Geochimica et Cosmochimia Acta 64, 133-147.

Griffin, W.L., Wang, X., Jackson, S.E., Pearson, N.J., O'Reilly, S.Y., Xu, X., Zhou, X., 2002. Zircon chemistry and magma mixing, SE China: In-situ analysis of Hf isotopes, Tonglu and Pingtan igneous complexes. Lithos 61, 237-269.

Guan, K., Luo, Z.K., Miao, L.C., Huang, J.Z., 1998. SHRIMP in zircon chronology for Guojialing suite granite in Jiaodong district. Scientia Geologica Sinica 33, 318-328.

Guo, F., Fan, W.M., Wang, Y.J., Lin, G., 2001. Late Mesozoic mafic intrusive complexes in North China Block: constraints on the nature of subcontinental lithospheric mantle. Physics and Chemistry of the Earth, Part A: Solid Earth and Geodesy 26, 759-771.

Guo, F., Fan, W., Wang, Y., Zhang, M., 2004. Origin of early Cretaceous calc-alkaline lamprophyres from the Sulu orogen in eastern China: implications for enrichment processes beneath continental collisional belt. Lithos 78, 291-305.

Guo, F., Fan, W., Wang, Y., Li, C., 2005a. Petrogenesis and tectonic implications of Early Cretaceous high-K calc-alkaline volcanic rocks in the Laiyang Basin of the Sulu Belt, eastern China. The Island Arc 14, 69-90.

Guo, J.H., Chen, F.K., Zhang, X.M., Siebel, W., Zhai, M.G., 2005. Evolution of syn- to post-collisional magmatism from north Sulu UHP belt, eastern China: zircon U-Pb geochronology. Acta Petrologica Sinica 21, 1281-1301.

Harris, N.B.W., Pearce, J.A., Tindle, A.G., 1986. Geochemical characteristics of collision-zone magmatism. In: Coward, M.P., Reis, A.C. (Editors), Collision tectonics. Special Publication of Geological Society, pp. 67-81.

Hodges, K.V. 2000. Tectonics of the Himalaya and southern Tibet from two perspectives. Geological Society of America Bulletin 112, 324-350.

Hu, F., Fan, H., Yang, J.H., Wan, Y., Liu, D., Zhai, M.G., Jin, C., 2004. Mineralizing age of the Rushan lode gold deposit in the Jiaodong Peninsula: SHRIMP U-Pb dating on hydrothermal zircon. Chinese Science Bulletin 49, 1629-1636.

Hu, F.F., Fan, H.R., Zhai, M.G., Jin, C.W., 2006. Fluid evolution in the Rushan lode gold deposit of Jiaodong Peninsula, eastern China. Journal of Geochemical Exploration 89, 161-164.

Jahn, B.M., Wu, F.Y., Chen, B., 2000. Massive granitoid generation in Central Asia: Nd isotope evidence and implication for continental growth in the Phanerozoic. Episodes 23, 82-92.

Kusky, T.M., Li, J., 2003. Paleoproterozoic tectonic evolution of the North China Craton. Journal of Asian Earth Sciences 22, 383-397.

Kusky, T.M., Windley, B.F., Zhai, M., 2007. Tectonic evolution of the North China Block: from orogen to craton to orogen. Geological Society of London, Special Publication 280, 1-34.

Le Bas, M.J., Le Maitre, R.W., Streckeisen, A.L., Zanettin, B., 1986. A chemical classification of volcanic rocks based on the total alkali-silica diagram. Journal of Petrology 27, 745-750.

Le Maitre, R.E. (Editor), 1989. A classification of the igneous rocks and glossary of geological terms. Blackwell.

Le Maitre, R.W., 1976. Some problems of the projection of chemical data into mineralogical classifications. Contributions to Mineral Petrology 56, 181-189.

Lee, C.Y., Tsai, J.H., Ho, H.H., Yang, T.F., Chung, S.L., Chen, C.H., 1997. Quantative analysis in rock samples by an X-ray fluorescence spectrometer, (I) major elements. Annual Meetings of the Geological Society of China 418-420.

Li, J.W., Paulo, V., Zhou, M.F., Zhao, X.F., Ma, C., 2006. Geochronology of the Pengjiakuang and Rushan Gold Deposits, Eastern Jiaodong Gold Province, Northeastern China: implications for regional mineralization and geodynamic setting. Economic Geology 101, 1023-1038.

Li, S., Mooney, W.D., 1998. Crustal structure of China from deep seismic sounding profiles. Tectonophysics 288, 105-113.

Liu, D.Y., Nutman, A.P., Compston, W., Wu, J.S., Shen, Q.H., 1992. Remnants of ≥ 3800 Ma crust in the Chinese part of the Sino-Korean craton. Geology 20, 339-342.

Liu, D., Wilde, S.A., Wan, Y., Wu, J.S., Zhou, H., Dong, C., Yin, X., 2008b. New U-Pb and Hf isotopic data confirm Anshan as the oldest preserved segment of the North China Craton. American Journal of Science 308, 200-231.

Liu, J., Zhang, H.F., Sun, J., Ye, J., 2004. Geochemical research on C-O and Sr-Nd isotopes of mantle-derived rocks from Shandong Province, China. Science in China, Series D Earth Sciences 47, 171-180.

Liu, J., Davis, G.A., Lin, Z., Wu, F.Y., 2005. The Liaonan metamorphic core complex, Southeastern Liaoning Province, North China: A likely contributor to Cretaceous rotation of Eastern Liaoning, Korea and contiguous areas. Tectonophysics 407, 65-80.

Liu, J., Davis, G.A., Ji, M., Guan, H., Bai, X., 2008d. Crustal detachment and destruction of the keel of North China Craton: constraints from Late Mesozoic extensional structures. Earth Science Frontiers 15(3), 72-81.

Liu, S., Zou, H., Hu, R.Z., Zhao, J., Feng, C.X., 2006. Mesozoic mafic dikes from the Shandong Peninsula, North China Craton: petrogenesis and the tectonic implications. Geochemical Journal 40, 181-195.

Liu, S., Hu, R.Z., Gao, S., Feng, C.X., Qi, L., Zhong, H., Xiao, T.F., Qi, Y.Q., Wang, T., Coulson, I.M., 2008a. Zircon U-Pb geochronology and major, trace elemental and Sr-Nd-Pb isotopic geochemistry of mafic dykes in western Shandong Province, east China: constraints on their petrogenesis and geodynamic significance. Chemical Geology 255, 329-345.

Liu, S., Hu, R., Gao, S., Feng, C.X., Qi, Y.Q., Wang, T., Feng, G., Coulson, I.M., 2008c. U-Pb zircon age, geochemical and Sr-Nd-Pb-Hf isotopic constraints on age and origin of alkaline intrusions and associated mafic dikes from Sulu orogenic belt, Eastern China. Lithos 106, 365-379.

Liu, S., Hu, R., Gao, S., Feng, C.X., Yu, B., Feng, G., Qi, Y.Q., Wang, T., Coulson, I.M., 2009. Petrogenesis of Late Mesozoic mafic dykes in the Jiaodong Peninsula, eastern North China Craton and implications for the foundering of lower crust. Lithos 13, 621-639.

Liu, X.S., Jin, W., Li, S.X., Xu, X.C., 1993. Two types of Precambrian high-grade metamorphism, Inner Mongolia, China. Journal of Metamorphic Geology 11, 499-510.

Ludwig, K.R., 2001a. SQUID 1.02: A user's manual. Special Publication, volume 2. Berkeley Geochronology Centre, Berkeley.

Ludwig, K.R., 2001b. Users manual for Isoplot/Ex (rev. 2.49): a geochronological toolkit for Microsoft Excel, Special Publication 1a. Berkeley Geochronology Center, Berkeley, CA (2001).

Luo, Z.K., Guan, K., Miao, L.C., 2001. Discussion on relationship between lamprophyre veins and mineralisation in the Linglong gold field, eastern Shandong. Gold Geology 7, 15-21 (in Chinese with English abstract).

Maniar, P.D., Piccoli, P.M., 1989. Tectonic discrimination of granitoids. Geological Society of America Bulletin 101, 635-643.

Mao, J., Wang, Y., Li, H., Pirajno, F., Zhang, C., Wang, R.C., 2008. The relationship of mantle-derived fluids to gold metallogenesis in the Jiaodong Peninsula: Evidence from D-O-C-S isotope systematics. Ore Geology Reviews 33, 361-381.McKenzie, D.M., Priestley, K., 2008. The influence of lithospheric thickness variations on continental evolution. Lithos 102, 1-11.

Meng, Q.R., 2003. What drove late Mesozoic extension of the northern China-Mongolia tract? Tectonophysics 369, 155-174.

Menzies, M.A., Fan, W., Zhang, M., 1993. Palaeozoic and Cenozoic lithoprobes and the loss of >120 km of Archaean lithosphere, Sino-Korean craton, China. Geological Society of London, Special Publication 76, 71-81.

Menzies, M.A., Xu, Y.G., 1998. Geodynamics of the North China Craton. In: Flower, M.F.J., Chung, S.L., Lo, C.H., Lee, T.Y. (Editors), Mantle Dynamics and Plate Interactions in East Asia. American Geophysical Union, pp. 155-165.

Menzies, M.A., Xu, Y.G., Zhang, H.F., Fan, W.M., 2007. Integration of geology, geophysics and geochemistry: A key to understanding the North China Craton. Lithos 96, 1-21.

Middlemost, E.A.K., 1985. Magmas and magmatic rocks: an introduction to igneous petrology. Longman, New York.

Middlemost, E.A.K., 1994. Naming materials in the magma/igneous rock system. Earth Science Reviews 37, 215-224.

Nelson, D.R., 1997. Compilation of SHRIMP U-Pb zircon geochronological data. In: Australia, G.S.o.W. (Editor). Geological Survey of Western Australia, Perth.

Niu, Y., 2005. Generation and evolution of basaltic magmas: some basic concepts and a new view on the origin of Mesozoic-Cenozoic basaltic volcanism in Eastern China. Geological Journal of China Universities 11, 9-46.

Niu, Y., Song, S., Zhang, L., Deng, J.F., Mo, X.X., Su, S.G., Guo, Z., Liu, J., 2005. Slab dehydration, subcontinental lithospheric thinning and Mesozoic/Cenozoic volcanism in eastern China: A special consequence of plate tectonics, IUGS-SECE Conference, Peking University, Beijing, pp. 27-29.

Nomade, S., Pouclet, A., Chen, Y., 2002. The French Guyana doleritic dykes: geochemical evidence of three populations and new data for the Jurassic Central Atlantic Magmatic Province. Journal of Geodynamics 34, 595-614.

Nowell, G.M., Kempton, P.D., Noble, S.R., Fitton, J.G., Saunders, A.D., Mahoney, J.J., Taylor, R.N., 1998. High precision Hf isotope measurements of MORB and OIB by thermal ionisation mass spectrometry: insights into the depleted mantle. Chemical Geology 149, 211-233.

O'Reilly, S.Y., Griffin, W.L., Poudjom Djomani, Y.H., Morgan, P., 2001. Are lithospheres forever? Tracking changes in subcontinental lithospheric mantle through time. Geological Society of America Today 11, 4-10.

Pearce, J.A., Harris, N.B.W., Tindle, A.G., 1984. Trace element discrimination diagrams for the tectonic interpretation of granitic rocks. Journal of Petrology 25, 956-983.

Pei, S., Zhao, J., Sun, Y., Xu, Z., Wang, S., Liu, H., Rowe, C.A., Toksoz, M.N., Gao, X., 2007. Upper mantle seismic velocities and anisotropy in China determined through Pn and Sn tomography. Journal of Geophysical Research 112.

Pidgeon, R.T., Furfaro, D., Kennedy, A.K., Nemchin, A.A., van Bronswijk, W., Todt, W.A., 1994. Calibration of zircon standards for the Curtin SHRIMP II (abstract), Eighth International Conference on Geochronology, Cosmochronology and Isotope Geology, Berkeley, University of California, pp. 251.

Qiu, J., Wang, D., Zeng, J., McInnes, B., 1997. Study on trace element and Nd-Sr isotopic geochemistry of the Mesozoic K-rich volcanic rocks and lamprophyres in Shandong Province. Geological Journal of China Universities 3, 384-395 (in Chinese with English abstract).

Qiu, J., Xu, X., Lo, C.H., 2002a. Potash-rich volcanic rocks and lamprophyres in western Shandong Province: ^{40}Ar-^{39}Ar dating and source tracing. Chinese Science Bulletin 47(2), 91-99.

Qiu, Y.M., Groves, D.I., McNaughton, N.J., Wang, L.G., Zhou, T., 2002b. Nature, age and tectonic setting of granitoid-hosted, orogenic gold deposits of the Jiaodong Peninsula, eastern North China craton, China. Mineralium Deposita 37, 283-305.

Rudnick, R.L., Gao, S., Ling, W.L., Liu, Y.S., McDonough, W.F., 2004. Petrology and geochemistry of spinel peridotite xenoliths from Hannuoba and Qixia, North China Craton. Lithos 77, 609-637.

Santosh, M., Wilde, S.A., Li, J.H., 2007. Timing of Paleoproterozoic ultrahigh-temperature metamorphism in the North China Craton: evidence from SHRIMP U-Pb zircon geochronology. Precambrian Research 159, 178-196.

SBGMR, 1991. Regional Geology of the Shandong Province, Geological Memories. Series 1 (in Chinese) 26. Geological Publishing House, Beijing, 699 pp.

Soderlund, U., Patchett, P.J., Vervoort, J.D., Isachsen, C.E., 2004. The 176Lu decay constant determined by Lu–Hf and U–Pb isotope systematics of Precambrian mafic intrusions. Earth and Planetary Science Letters 219, 311-324.

Song, B., Nutman, A.P., Liu, D.Y., Wu, J.S., 1996. 3800-2500 Ma crustal evolution in the Anshan area of Liaoning Province, northeastern China. Precambrian Research 78, 79-94.

Streckeisen, A.L., 1974. Classification and nomenclature of plutonic rocks. Geologische Rundschau 63 (2), 773-786.

Sun, J., Hu, S., Liu, J., Shen, K., Ling, H., 2001. A study of Sr, Nd and O isotopes of the K-rich melanocratic dykes in the Late Mesozoic gold field in the Jiaodong Peninsula. Acta Geologica Sinica 75(4), 432-444.

Sun, S.S., McDonough, W.F., 1989. Chemical and isotopic systematics of oceanic basalts: implication for mantle composition and processes. In: A.D. Saunders, A.D., Norry, M.J. (Editors), Magmatism in the Ocean Basins Geological Society London, pp. 313-345.

Tang, H.Y., Zheng, J.P., Yu, C.M., 2008. Age and composition of the Rushan intrusive complex in the northern Sulu orogen, eastern China: petrogenesis and lithospheric mantle evolution. Geological Magazine 1, 1-17.

Tatsumoto, M., Basu, A.R., Wankang, H., Junwen, W., Guanghong, X., 1992. Sr, Nd and Pb isotopes of ultramafic xenoliths in volcanic rocks of Eastern China: enriched components EM1 and EM11 in subcontinental lithosphere. Earth and Planetary Science Letters 113, 107-128.

Trap, P., Faure, M., Lin, W., Bruguier, O., Monie, P., 2008. Contrasted tectonic styles for the Paleoproterozoic evolution of the North China Craton: evidence for a ~2.1 Ga thermal and tectonic event in the Fuping Massif. Journal of Structural Geology 30, 1109-1125.

Van der Voo, R., Spakman, W., Bijwaard, H., 1999. Mesozoic subducted slabs under Siberia. Nature 397, 246-249.

Wan, Y.S., Liu, D.Y., Song, B., Wu, J.S., Yang, C.H., Zhang, Z.Q., Geng, Y.S., 2005. Geochemical and Nd isotopic compositions of 3.8 Ga meta-quartz dioritic and trondhjemitic rocks from the Anshan area and their geological significance. Journal of Asian Earth Sciences 4, 563-575.

Wang, L.G., Qiu, Y.M., McNaughton, N.J., Groves, D.I., Luo, Z.K., Huang, J.Z., Miao, L.C., Liu, Y.K., 1998. Constraints on crustal evolution and gold

metallogeny in the Northwestern Jiaodong Peninsula, China, from SHRIMP U-Pb zircon studies of granitoids. Ore Geology Reviews 13, 275-291.

Wang, R.C., Wang, D.Z., Zhao, G.T., Lu, J.J., Chen, X.M., Xu, S.J., 2001. Accessory mineral record of magma-fluid interaction in the Laoshan I- and A-type granitic complex, Eastern China. Physics and Chemistry of the Earth, Part A: Solid Earth and Geodesy 26, 835-849.

Wang, Z., 2009. Tectonic evolution of the Hengshan-Wutai-Fuping complexes and its implication for the Trans-North China Orogen. Precambrian Research 170, 73-87.

Wei, C.S., Zheng, Y.F., Zhao, Z.F., 2000. Hydrogen and oxygen isotope geochemistry of A-type granites in the continental margins of eastern China. Tectonophysics 328, 205-227.

Wei, C.S., Zhao, Z.F., Spicuzza, M.J., 2008. Zircon oxygen isotopic constraint on the sources of Late Mesozoic A-type granites in eastern China. Chemical Geology 250, 1-15.

Whalen, J.B., Currie, K.L., Chappell, B.W., 1987. A-type granites: geochemical characteristics, discrimination and petrogenesis. Contributions to Mineral Petrology 95, 407-419..

Wilde, S.A., Zhou, X., Nemchin, A.A., 2003. Mesozoic crust-mantle interaction beneath the North China craton: A consequence of the dispersal of Gondwanaland and accretion of Asia. Geology 31, 817-820.

Williams, I.S., 1998. U-Th-Pb geochronology by ion microprobe. In: McKibben, M.A., Shanks III, W.C., Ridley, W.I. (Editors), Applications of Microanalytical Techniques to Understanding Mineralizing Processes. Reviews in Economic Geology, vol. 7, pp. 1-35.

Wong, W.H., 1927. Crustal movement and igneous activities in eastern China since Mesozoic time. Bulletin of the Geological Society of China 6, 1.

Wu, C.H., Li, S.X., Gao, J.F., 1986. Archean and Paleoproterozoic metamorphic regions in the North China Craton. In: Dong, S.B. (Editor), Metamorphism and Crustal Evolution of China. Geological Publishing House, Beijing, pp. 53-89.

Wu, F.Y., Lin, J.Q., Wilde, S.A., Zhang, X.O., Yang, J.H., 2005a. Nature and significance of the Early Cretaceous giant igneous event in eastern China. Earth and Planetary Science Letters 233, 103-119.

Wu, F.Y., Zhao, G.C., Wilde, S.A., Sun, D.Y., 2005b. Nd constraints on crustal formation in the North China Craton. Journal of Asian Earth Sciences 24, 523-545.

Wu, F.Y., Yang, J.H., Wilde, S.A., Zhang, X.O., 2005c. Geochronology, petrogenesis and tectonic implications of Jurassic granites in the Liaodong Peninsula, NE China. Chemical Geology 221, 127-156.

Wu, F.Y., Yang, Y.H., Xie, L.W., Yang, J.H., Xu, P., 2006. Hf isotopic compositions of the standard zircons and baddeleyites used in U-Pb geochronology. Chemical Geology 234, 105-126.

Wu, J.S., Geng, Y.S., Shen, Q.H., Wan, Y.S., Liu, D.Y., Song, B., 1998. Archean geological characteristics and tectonic evolution of China-Korea Paleo-continent. Geological Publishing House, Beijing.

Xu, J.W., Zhu, G., 1994. Tectonic models of the Tan-Lu fault zone, eastern China. Geological Review 36, 771-784..

Xu, H., Xu, G.P., 2000. Geochemical characteristics of the lamprophyres from Jiaodong: implications for petrogenesis. Acta Petrologica et Mineralogica 19, 36-43 (in Chinese with English abstract).

Xu, P., Wu, F.Y., Xie, L.W., Yang, Y.H., 2004c. Hf isotopic compositions of the standard zircons for U-Pb dating. Chinese Science Bulletin 49, 1642-1648.

Xu, Y.G., 2001. Thermo-tectonic destruction of the Archaean lithospheric keel beneath the Sino-Korean craton in China: evidence, timing and mechanism. Physics and Chemistry of the Earth, Part A: Solid Earth and Geodesy 26, 747-757.

Xu, Y.G., Ma, J.L, Huang, X.L, Iizuka, Y., Chung, S.L, Wang, Y.B, Wu, X.Y., 2004a. Early Cretaceous gabbroic complex from Yinan, Shandong Province: petrogenesis and mantle domains beneath the North China Craton. International Journal of Earth Sciences 93, 1025-1041.

Xu, Y.G., Huang, X.L., Ma, J.L., Wang, Y.B., Iizuka, Y., Xu, J.F., Wang, Q., Wu, X.Y., 2004b. Crust-mantle interaction during the tectono-thermal reactivation of the North China Craton: constraints from SHRIMP zircon U-Pb chronology and geochemistry of Mesozoic plutons from Western Shandong. Contributions to Mineral Petrology 147, 750-767.

Xu, Y.G., 2007. Diachronous lithospheric thinning of the North China Craton and formation of the Daxin'anling-Taihangshan gravity lineament. Lithos 96, 281-298.

Yang, J.H., Zhou, X.H., 2001. Rb-Sr, Sm-Nd and Pb isotopic systematics of pyrite: Implications for the age and genesis of lode gold deposits. Geology 29, 711-714.

Yang, J.H., Wu, F.Y., Wilde, S.A., 2003. A review of the geodynamic setting of large-scale Late Mesozoic gold mineralization in the North China Craton: an association with lithospheric thinning. Ore Geology Reviews 23, 125-152.

Yang, J., Wu, F.Y., Zhang, Y., Zhang, Q., Wilde, S.A., 2004a. Identification of Mesoproterozoic zircons in a Triassic dolerite from the Liaodong Peninsula, Northeast China. Chinese Science Bulletin 49(18), 1958-1962.

Yang, J.H., Wu, F.Y., Chung, S.L., Wilde, S.A., Chu, M.F., 2004a. Multiple sources for the origin of granites: Geochemical and Nd/Sr isotopic evidence from the Gudaoling granite and its mafic enclaves, northeast China. Geochimica et Cosmochimia Acta 68, 4469-4483.

Yang, J.H., Chung, S.L., Zhai, M.G., Zhou, X.H., 2004b. Geochemical and Sr-Nd-Pb isotopic compositions of mafic dikes from the Jiaodong Peninsula, China: evidence for vein-plus-peridotite melting in the lithospheric mantle. Lithos 73, 145-160.

Yang, J.H., Wu, F.Y., Chung, S.L., Wilde, S.A., Chu, M.F., Lo, C.H., Song, B., 2005. Petrogenesis of Early Cretaceous intrusions in the Sulu ultrahigh-pressure orogenic belt, east China and their relationship to lithospheric thinning. Chemical Geology 222, 200-231.

Yang, J.H., Wu, F.Y., Shao, J.A., Wilde, S.A., Xie, L.W., Liu, X.M., 2006. Constraints on the timing of uplift of the Yanshan Fold and Thrust Belt, North China. Earth and Planetary Science Letters 246, 336-352.

Yang, J.H., Sun, J.F., Chen, F., Wilde, S.A., Wu, F.Y., 2007a. Sources and petrogenesis of Late Triassic dolerite dykes in the Liaodong Peninsula: implications for post-collisional lithosphere thinning of the Eastern North China Craton. Journal of Petrology 48, 1973-1997.

Yang, J.H., Wu, F.Y., Wilde, S.A., Liu, X.M., 2007b. Petrogenesis of late Triassic granitoids and their enclaves with implications for post-collisional lithospheric thinning of the Liaodong Peninsula, North China Craton. Chemical Geology 242, 155-175.

Yang, J.H., Wu, F.Y., Chung, S.L., Lo, C.H., Wilde, S.A., Davis, G.A., 2007c. Rapid exhumation and cooling of the Liaonan metamorphic core complex: Inferences from $^{40}Ar/^{39}Ar$ thermochronology and implications for Late Mesozoic extension in the eastern North China Craton. Geological Society of America Bulletin 119, 1405-1414.

Yang, J.H., Wu, F.Y., Wilde, S.A., Belousova, E., Griffin, W.L., 2008a. Mesozoic decratonization of the North China Block. Geology 36, 467-470.

Yang, J.H., Wu, F.Y., Wilde, S.A., Chen, F., Liu, X.M., Xie, L.W., 2008b. Petrogenesis of an alkali syenite-granite-rhyolite suite in the Yanshan Fold and Thrust Belt, Eastern North China Craton: geochronological, geochemical and Nd-Sr-Hf isotopic evidence. Journal of Petrology 49, 315-351.

Yang, Y.H., Wu, F.Y., Wilde, S.A., Liu, X.M., Zhang, Y.B., Xie, L.W., Yang, J.H., 2009. *In situ* perovskite Sr-Nd isotopic constraints on the petrogenesis of the Ordovician Mengyin kimberlites in the North China Craton. Chemical Geology 264, 24-42.

Ying, J., Zhou, X., Zhang, H., 2006. The geochemical variations of mid-Cretaceous lavas across western Shandong Province, China and their tectonic implications. International Journal of Earth Sciences 95, 68-79.

Ying, J., Zhang, H.F., Kita, N.T., Morishita, Y., Shimoda, G., 2006a. Nature and evolution of Late Cretaceous lithospheric mantle beneath the eastern North

China Craton: constraints from petrology and geochemistry of peridotitic xenoliths from Junan, Shandong province, China. Earth and Planetary Science Letters 244(3-4), 622-638.

Yuan, X.Y., 1996. Velocity structure of the Qinling lithosphere and mushroom cloud model. Science in China, Series D Earth Sciences 39, 233-244

Yuan, H.L., Gao, S., Liu, X.M., Li, H.M., Gunther, D., Wu, F.Y., 2004. Accurate U-Pb age and trace element determinations of zircon by laser ablation-inductively coupled plasma mass spectrometry. Geostandards and Geoanalytical Research 28, 353-370..

Zhai, M., Fan, Q., Zhang, H., Sui, J., Shao, J.A., 2007. Lower crustal processes leading to Mesozoic lithospheric thinning beneath eastern North China: underplating, replacement and delamination. Lithos 96, 36-54.

Zhang, H.F., Sun, M., 2002. Geochemistry of Mesozoic basalts and mafic dykes, southeastern North China Craton, and tectonic implications. International Geology Review 44, 370-382.

Zhang, H.F., Sun, M., Zhou, X.H., Fan, W.M., Zhai, M.G., Yin, J.F., 2002. Mesozoic lithosphere destruction beneath the North China Craton: evidence from major-, trace-element and Sr-Nd-Pb isotope studies of Fancheng basalts. Contributions to Mineral Petrology 144, 241-253.

Zhang, H.F., Sun, M., Zhou, X.H., Zhou, M.F., Fan, W.M., Zheng, J.P., 2003a. Secular evolution of the lithosphere beneath the eastern North China Craton: evidence from Mesozoic basalts and high-Mg andesites. Geochimica et Cosmochimia Acta 67, 4373-4387.

Zhang, H.F., Ying, J.F., Xu, P., Ma, Y.G., 2004. Mantle olivine xenocrysts entrained in Mesozoic basalts from the North China craton: Implication for replacement process of lithospheric mantle. Chinese Science Bulletin 49, 961-966.

Zhang, H.F., Sun, M., Zhou, M.F., Fan, W.M., Zhou, X.H., Guo, Z.M., 2004a. Highly heterogeneous Late Mesozoic lithospheric mantle beneath the North China Craton: evidence from Sr-Nd-Pb isotopic systematics of mafic igneous rocks. Geology Magazine 141, 55-62.

Zhang, H.F., 2005. Transformation of lithospheric mantle through peridotite-melt reaction: A case of Sino-Korean craton. Earth and Planetary Science Letters 237, 768-780.

Zhang, H., Zhai, M., Tong, Y., Peng, P., Xu, B., Guo, J., 2006. Petrogenesis of the Sanfoshan High Ba-Sr granite, Jiaodong Peninsula, East China. Geological Review 52, 43-53.

Zhang, H.F., Ying, J.F., Shimoda, G., Kita, N.T., Morishita, Y., Shao, J.A., Tang, Y.J., 2007. Importance of melt circulation and crust-mantle interaction in the lithospheric evolution beneath the North China Craton: evidence from Mesozoic basalt-borne clinopyroxene xenocrysts and pyroxenite xenoliths. Lithos 96, 67-89.

Zhang, H.F., Goldstein, S.L., Zhou, X.H., Sun, M., Zheng, J.P., Cai, Y., 2008. Evolution of subcontinental lithospheric mantle beneath eastern China: Re-Os isotopic evidence from mantle xenoliths in Paleozoic kimberlites and Mesozoic basalts. Contributions to Mineral Petrology 155, 271-293.

Zhang, M., Zhou, X.H., Zhang, J.B., 1998. Nature of the lithospheric mantle beneath NE China: evidence from potassic volcanic rocks and mantle xenoliths In: Flower, M.F.J., Chung, S.L., Lo, C.H., Lee, T.Y. (Editors), Mantle Dynamics and Plate Interactions in East Asia. American Geophysical Union, Washington, D.C., pp. 197-219.

Zhang, Q., Jian, P., Liu, D.Y., Wang, Q., Qian, Q., Wang, Y., Xue, H.M., 2003d. Zircon SHRIMP dating of volcanic rocks from Ningwu area and its geological implications. Science in China, Series D Earth Sciences 46, 830-837.

Zhang, R.Y., Hirajima, T., Banno, S., Cong, B., Liou, J.G., 1995. Petrology of ultrahigh pressure metamorphic rocks in southern Sulu region, eastern China. Journal of Metamorphic Geology 13, 659-675.

Zhang, X., Cawood, P.A., Wilde, S.A., Liu, R., Song, H., Li, W., Snee, L.W., 2003c. Geology and timing of mineralization at the Cangshang gold deposit, north-western Jiaodong Peninsula, China. Mineralium Deposita 38, 141-153.

Zhang, Y., Dong, S., Shi, W., 2003b. Cretaceous deformation history of the middle Tan-Lu fault zone in Shandong Province, eastern China. Tectonophysics 363, 243-258.

Zhao, G.C., Cao, Q.C., Wang, D., Li, H., 1997. Zirconic U-Pb dating on the Laoshan granitoids and it's significance. Journal of Ocean University of Qingdao 27, 382-387.

Zhao, G.C., Wilde, S.A., Cawood, P.A., Lu, L., 1998a. Thermal evolution of Archaean basement rocks from the Eastern part of the North China Craton and it's bearing on tectonic setting. International Geology Review 40, 706-721.

Zhao, G.C., Wilde, S.A., Cawood, P.A., Lu, L., 1999a. Thermal evolution of two textural types of mafic granulites in the North China craton: evidence for both mantle plume and collisional tectonics. Geological Magazine 136, 223-240.

Zhao, G.C., Wilde, S.A., Cawood, P.A., Lu, L., 1999b. Tectonothermal history of the basement rocks in the western zone of the North China Craton and it's tectonic implications. Tectonophysics 310, 37-53.

Zhao, G.C., Cawood, P.A., Wilde, S.A., Sun, M., Lu, L., 2000. Metamorphism of basement rocks in the Central Zone of the North China Craton: implications for Paleoproterozoic tectonic evolution. Precambrian Research 103, 55-88.

Zhao, G.C., Wilde, S.A., Cawood, P.A., Sun, M., 2001. Archean blocks and their boundaries in the North China Craton: lithological, geochemical, structural and *P-T* path constraints and tectonic evolution. Precambrian Research 107, 45-73.

Zhao, G.C., Sun, M., Wilde, S.A., Li, S.Z., 2005. Late Archean to Paleoproterozoic evolution of the North China Craton: key issues revisited. Precambrian Research 136, 177-202.

Zhao, G.C., Sun, M., Wilde, S.A., Li, S.H., Liu, S., 2006. Composite nature of the North China Granulite-facies Belt: tectonothermal and geochronological constraints. Gondwana Research 9, 337-348.

Zhao, G.T., Wang, D.Z., Cao, Q.C., Yu, L.S., 1998b. Thermal evolution and it's significance of I-A type granitoid complex: The Laoshan granitoid as an example. Science in China, Series D Earth Sciences 41, 529-536.

Zhao, Z.F., Zheng, Y.F., 2009. Remelting of subducted continental lithosphere: petrogenesis of Mesozoic magmatic rocks in the Dabie-Sulu orogenic belt. Science in China, Series D Earth Sciences 52, 1295-1318.

Zheng, J., O'Reilly, S.Y., Griffin, W.L., Lu, F., Zhang, M., 1998. Nature and evolution of Cenozoic lithospheric mantle beneath Shandong Peninsula, Sino-Korean Craton, Eastern China. International Geology Review 40, 471-499.

Zheng, J., Sun, M., Lu, F., Pearson, N., 2003. Mesozoic lower crustal xenoliths and their significance in lithospheric evolution beneath the Sino-Korean Craton. Tectonophysics 361, 37-60.

Zhou, J.B., Wilde, S.A., Zhao, G.C., Zheng, C.Q., Jin, W., Zhang, X.Z., Cheng, H., 2008a. Detrital zircon U-Pb dating of low-grade metamorphic rocks in the Sulu UHP belt: evidence for overthrusting of the North China Craton onto the South China Craton during continental subduction. Journal of the Geological Society, London 165, 423-433.

Zhou, J.B., Wilde, S.A., Zhao, G.C., Zheng, C.Q., Jin, W., Zhang, X.Z., Cheng, H., 2008b. SHRIMP U-Pb zircon dating of the Neoproterozoic Penglai Group and Archaean gneisses from the Jiaobei Terrane, North China, and their tectonic implications. Precambrian Research 160, 323-340.

Zhou, T., Lu, G., 2000. Tectonics, granitoids and Mesozoic gold deposits in East Shandong, China. Ore Geology Reviews 16, 71-90.

Zhou, X., Sun, M., Zhang, G., Chen, S., 2002. Continental crust and lithospheric mantle interaction beneath North China: isotopic evidence from granulite xenoliths in Hannuoba, Sino-Korean craton. Lithos 62, 111-124.

Zhou, X.H., Yang, J.H., Zhang, L.C., 2003. Metallogenesis of super-large gold deposits in Jiaodong region and deep processes of subcontinental lithosphere beneath North China Craton in Mesozoic. Science in China, Series D Earth Sciences 46, 14-25.

Zhou, X.M., Li, W.X., 2000. Origin of Late Mesozoic igneous rocks in southeastern China: implications for lithospheric subduction and underplating of mafic magmas. Tectonophysics 326, 269-287.

Zhu, G., Evans, J.A., Fitches, W.R., Fletcher, C.J.N., Rundle, C.R., Xu, J., 1994. Isotopic constraints on the Palaeozoic evolution of the Shandong Peninsula, N.E. China. Journal of Southeast Asian Earth Sciences 9, 241a-248